Genetic and Cell Biological studies of Sarm1

in Zebrafish

Dissertation

an der Fakultät für Biologie

der Ludwig-Maximilians-Universität München

Durchgeführt am

Helmholtz Zentrum München

Deutsches Forschungszentrum für Gesundheit und Umwelt

Vorgelegt von

Weili Tian

This work has been done in the laboratory of Dr. Hernán López-Schier at the Research Unit Sensory Biology and Organogenesis, Helmholtz Zentrum München (Munich, Germany) from November 2014 to September 2019.

Abstract

The peripheral nerves that communicate skin, muscle and sensory organs with the brain must maintain functionality throughout life despite frequent stress and injury. Loss of integrity of peripheral neurons and associated glial cells is a common occurrence in severe neurological dysfunctions that include weakness, pain and loss of sensation. Therefore, protecting the nervous system from chronic effects of physical and chemical stress is a pressing clinical challenge. This has sparked intense efforts to exploit molecular inhibitors of axonal and glial destruction. Loss of function of the obligate pro-degenerative protein Sarm1 blocks axon degeneration across species. Thus, Sarm1 is an ideal target for clinical application aimed at reducing axonal degradation in humans. In my thesis, I addressed the impact of Sarm1 deficiency on the development of the peripheral nervous system and glial Schwann cells. Using zebrafish, I show that elimination of Sarm1 is compatible with neural homeostasis, and is glioprotective against chemotherapeutic agents after nerve injury. Specifically, I have discovered that Schwann cells are not essential for the maintenance of severed axons lacking Sarm1, which subsist well beyond the normal timeframe allowed by Sarm1 destructive activity. Moreover, in Sarm1-deficient animals, the axons that regenerate after nerve injury regain connectivity with peripheral synaptic targets to enable sensorimotor recovery, revealing that neural-circuit repair is not contingent upon the clearance of damaged axons. In addition, I discovered that the loss of Sarm1 increases Schwann-cell resistance to toxicity by diverse chemotherapeutic agents after nerve injury. Overall, my findings indicate that pharmacological interventions targeting Sarm1 are promising strategies to reduce chronic consequences of nerve injury.

Abstrakt

Die peripheren Nerven, die Haut, Muskeln und Sinnesorgane mit dem Gehirn verbinden, müssen trotz häufigem Stress und Verletzung lebenslang funktionsfähig bleiben. Der Verlust der Integrität von peripheren Neuronen und assoziierten Zellen, einschließlich Glia, tritt häufig bei schweren neurologischen Funktionsstörungen auf, zu denen Schwäche, Schmerzen und Sensibilitätsverlust gehören. Daher ist der Schutz des Nervensystems vor chronischen Auswirkungen von physischem und chemischem Stress eine dringende klinische Herausforderung. Dies hat intensive Bemühungen ausgelöst, molekulare Inhibitoren der axonalen und glialen Zerstörung einzusetzen. Der Funktionsverlust des pro-degenerativen Proteins Sarm1 blockiert Axondegeneration sowohl in Invertebraten als auch in Vertebraten. Somit ist Sarm1 ein ideales Ziel für die klinische Anwendung, um den axonalen Abbau beim Menschen zu verhindern. In dieser Arbeit untersuchte ich die Auswirkungen von Sarm1-Mangel auf die Entwicklung des peripheren Nervensystems und der Schwannschen Gliazellen. Im Zebrafisch Modellorganismus zeigte ich, dass die genetische Ausschaltung von Sarm1 mit der neuralen Homöostase vereinbar ist und gegen chemotherapeutische Wirkstoffe nach Nervenverletzungen glioprotektiv ist. Insbesondere habe ich herausgefunden, dass Schwann-Zellen, die nach Axonenabtrennung eliminiert werden, aber in Abwesenheit von Sarm1 bestehen bleiben, für die Aufrechterhaltung der abgetrennten Axonen nicht wesentlich sind. Darüber hinaus stellen die Axone, die sich nach einer Nervenverletzung regenerieren, beim Sarm1-defizienten Zebrafisch die Konnektivität mit peripheren synaptischen Zielen wieder her, um die Wiederherstellung der Sensomotorik mus zu ermöglichen. Außerdem entdeckte ich, dass der Verlust von Sarm1 die Toxizitätsresistenz von Schwann-Zellen durch verschiedene Chemotherapeutika nach einer Nervenverletzung erhöht. Insgesamt weisen meine Ergebnisse darauf hin, dass pharmakologische Interventionen gegen Sarm1 vielversprechende Strategien zur Verringerung der chronischen Folgen von Nervenverletzungen darstellen.

Table of Contents

List of Figures

List of Tables

List of Abbreviations

AAD	Acute axon degeneration
ADAM17	A disintegrin and metalloproteinase 17
ADP	Adenosine diphosphate
AKT (PKB)	Protein kinase B
ALL	Anterior lateral line system
ALS	Amyotrophic lateral sclerosis
ASD	Autism spectrum disorders
BACE1	β-secretase1
BDNF	Brain-derived neurotrophic factor
BMP	Bone morphogenetic protein
CADM	Cell adhesion molecules
cAMP	Cyclic adenosine monophosphate
CCCP	Carbonyl cyanide m-chlorophenyl hydrazone
CCL2	C-C Motif Chemokine Ligand 2
CIPN	Chemotherapy-induced peripheral neuropathy
CNS	Central nerve system
CRISPR	Clustered regularly interspaced short palindromic repeats
CSPG	Chondroitin sulfate proteoglycans
DLK	Dual leucine zipper kinase
DR6	Death receptor 6
DRG	Dorsal root ganglion
ECM	Extracellular matrix
EGF	Epidermal growth factor
Erbb2	Erb-b2 receptor tyrosine kinase 2
ERK	Extracellular signal–regulated kinases
FRT	Frontotemporal dementia

FTDP-17	Frontotemporal dementia with parkinsonism-17
GDNF	Glial-derived neurotrophic factor
GFAP	Glial fibrillary acidic protein
GPCR	G protein coupled receptor
HDAC4	Histone deacetylase 4
HR	Homology-directed repair
JAK	Janus kinase
JNK	C-Jun N-terminal kinases
LACV	La Crosse encephalitis
LIF	Leukemia inhibitory factor
MAG	Myelin associated glycoprotein
MAPKK	Mitogen-activated protein kinase kinase
MAVS	Mitochondrial antiviral-signaling protein
MBP	Myelin binding protein
MCP1	Monocyte chemoattractant protein1
MEK4	Mitogen-activated protein kinase kinase 4
MPTP	1-methyl-4-phenyl-1,2,3,6-tetrahydropyridine
mTOR1	Mammalian target of rapamycin complex1
NMNATs	Nicotinamide mononucleotide adenylytransferases
NMN	β-nicotinamide mononucleotide
NAD	Nicotinamide adenine dinucleotide
NCAM	Neural cell adhesion molecule
NHEJ	Non-homologous end-joining pathway
NGS	Next-generation sequencing
NOTCH1	Notch homolog 1, translocation-associated
P75NTR (NGFR)	Nerve growth factor receptor
PARP	Poly (ADP-ribose) polymerase
PINK1	PTEN-induced kinase1

PKA	Protein kinase A
PLL	Posterior lateral line system
PNS	Peripheral nerve system
PTEN	Phosphatase and tensin homolog
ROS	Reactive oxygen species
RTCA	RNA 3'-Terminal Phosphate Cyclase a
SARM1	Sterile Alpha and TIR Motif Containing 1
SDF1α (CXCL12)	Stromal cell-derived factor 1α
SOD1	Superoxide dismutase1
STAT3	Signal transducer and activator of transcription 3
TALEN	Transcription activator-like effector nucleases
TBI	Traumatic brain injury
TDP-43	Transactive response DNA binding protein 43 kDa
TLR	Toll-like receptors
TNFα	Tumor necrosis factor alpha
TSC	Tuberous sclerosis proteins
TRIF	TIR-domain-containing adapter-inducing interferon-β
VEGF	Vascular endothelial growth factor
Wlds	Wallerian degeneration slow
WD	Wallerian degeneration
ZFN	Zinc finger nucleases

1. Introduction

1.1 Zebrafish as a vertebrate model to study developmental neuroscience and neurological disorders

The zebrafish (*Danio rerio*) is a small tropical freshwater fish, which has been used for scientific research since the 1980s (Streisinger et al., 1989; Streisinger et al., 1981). This vertebrate is easy and cheap to maintain. It is translucent, has an external embryonic development, breeds year-round and is amenable to genetic modifications. These advantages have made the zebrafish a powerful experimental system.

The embryonic development of zebrafish, from the fertilized egg to the complete fish, is quite rapid. Briefly, after fertilization, the egg undergoes the following stages: Zygote Period (0-0.75 h), Cleavage Period (0.75-2.25 h), Blastula Period (2.25-5.25 h), Gastrula Period (5.25-10.33 h), Segmentation Period (10.33-24 h), Pharyngula Period (24-48 h), Hatching Period (48-72 h), and Larval Period (72 h-30 d) (**Table 1.1**). During this early development, the embryo is visually accessible because of the transparent membrane and cells. This allows researchers to observe the developmental process from one cell-stage to the free-swimming larva with the high-resolution microscopy.

In the zebrafish larva, all the major organ systems, such as the nervous system, the cardiovascular system, the hematopoietic system, and the immune system are functional at 5 dpf (days post fertilization). In addition, the abundance of offspring provides an advantage for genetic mapping and phenotype screening. Normally, one female fish can lay 100-200 eggs per mating and the fish can breed weekly. The zebrafish shares approximately 70 percent of genes with mammals as shown by genome sequencing (Buggs et al., 2012; Howe et al., 2013). It bridges the gap between invertebrate and mammalian model systems for studies, such as development, neuronal circuits, and behavior. Moreover, most of the cellular and physiological mechanisms of organs in zebrafish and mammals are conserved (Hsu et al., 2007; Williams and Hong, 2011).

Periods of zebrafish early development

Duration time (h)	Period Name	Discription
0-0.75	Zygote	fertilized egg, 1-cell, and 2-cell
0.75-2.25	Cleavage	Rapidly cell division 2 to 7 cycles (from 4-cell to 64-cell)
2.25-5.25	Blastula	from 128-cell to 2K-cell, epiboly starts
5.25-10.33	Gastrula	form the epiblast, hypoblast and axis of the embroy
10.33-24	Segmentation	Somites, neuromeres develop, organogenesis
24-48	Pharyngula	Phylotypic-stage embryo, body axis straightens, circulation, fin development
48-72	Hatching	Completion primary organ systems
72-	Larval	larval to adult

Table 1.1 The development of zebrafish. The information is from *Stages of embryonic development of the zebrafish, Kimmel CB, 1995.*

1.1.1 Genetic modification of zebrafish

The Tol2 and Sleeping Beauty transposon systems enable scientists to generate transgenic lines easily. Combine with the UAS-GAL4 and Cre-loxP recombinases systems, researchers can obtain the specific fluorescence labeling transgenic or conditional gene modification lines (Kawakami, 2007; Kwan et al., 2007; Yant et al., 2005).

To generate loss of function mutants or insert nucleotides/sequences in zebrafish, ZFN (zinc finger nucleases), TALEN (transcription activator-like effector nucleases), or CRISPR (clustered regularly interspaced short palindromic repeats) are widely used. The efficiency of the tools for gene editing dependents on their nuclease activity and cell autonomous repair pathways, such as non-homologous end-joining pathway (NHEJ) or homology-directed repair (HR). The difference of these nucleases is the way to recognize the specific site of the gene. ZFN and TALEN have a DNA binding domain which is used to recognize the interested gene, and a nuclease domain that introduces a double-strand DNA break at the location where the DNA binding domain is targeting (Doyon et al., 2008; Miller et al., 2011; Sander et al., 2011; Urnov et al., 2005). For CRISPR/Cas9, the single

guide RNA (sgRNA) works together with Cas9 nuclease to modify the DNA. The single guide RNA consists of a targeting sequence (crRNA: CRISPR RNA) to recognize the gene of interest and a Cas9 nuclease-recruiting sequence (tracrRNA: trans-activating crRNA) to allow Cas9 binding. When the crRNA recognizes the targeting site, the crRNA part recruits Cas9 protein to the site to cleave the DNA sequence (Cong et al., 2013; Hwang et al., 2013). In the DNA repair stage, these three genome-modify tools share the same double-strand DNA break repair mechanisms, the homology or non-homology mediated repairs. Both of these two repair ways are cell autonomous (Gaj et al., 2013; Wyman and Kanaar, 2006). During the DNA repair, some nucleotides are deleted or inserted randomly, which introduces a frameshift to generate a gene knockout line; the simultaneously injected oligonucleotides or short linearized double strand sequences are incorporated into the site of DNA break, which introduces the knock-in line (Chang et al., 2013; Li et al., 2016; Moehle et al., 2007; Ota et al., 2014; Varshney et al., 2015) (**Figure 1.1**).
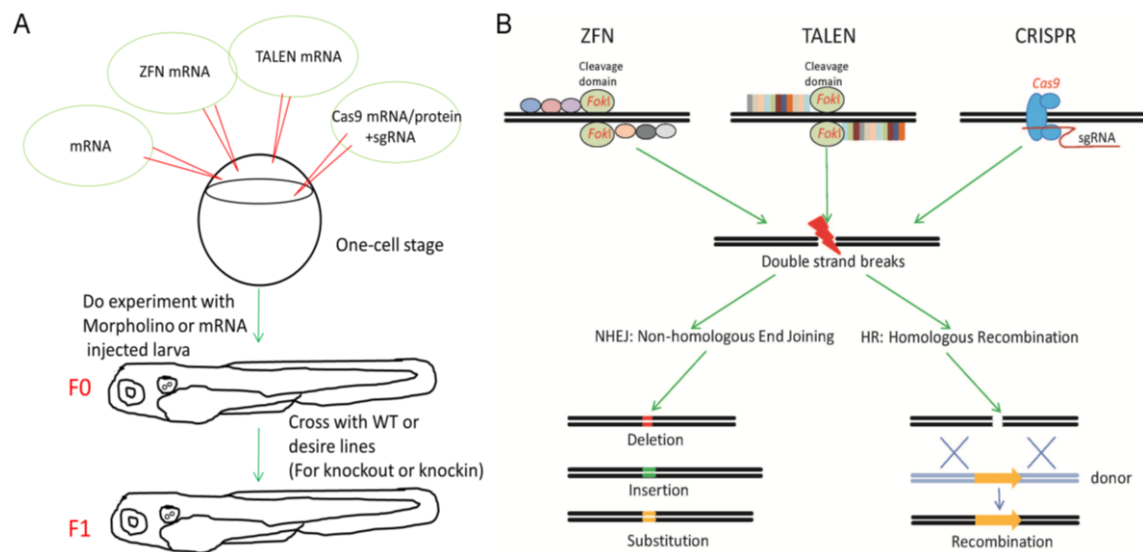
Figure 1.1 Schematic of the genetic methods used in zebrafish research. A)mRNA, ZFN, TALEN and CRISPR are used to modify the gene expression in zebrafish by injection into the one-cell stage embryos. For stable knockout or knock-in lines, the F0 founder fish from ZFN, TALEN and CRISPR is crossed to obtain the F1 stable transgenic line; B) Schematic picture showing the mechanism of how ZFN, TALEN and CRISPR work for knockout or knockin the genes. The designed constructs or RNAs are injected into the one-cell stage embryos. The nucleases break the genome DNA in the target sites, then the NHEJ or HR enables generation of knockout lines by deletion, insertion or substitution of the

nucleotides in the break site, and to make knockin lines by recombination the donor oligonucleotides or constructs.

1.1.2 Zebrafish as a model for neuroscience and neurological disorders research

Zebrafish has similar subdivisions of the nervous system as mammals, including the forebrain, midbrain, hindbrain, and spinal cord, which are formed in around 1 dpf larva. And the thalamus, the optic tectum and the cerebellum of zebrafish share the structural homology with mammals (Kozol et al., 2016). Moreover, the neurons in each subdivision grow and extend their axonal tracts in a stereotyped pattern (Kimmel, 1993). More and more neurotransmitter-expressing neurons and glial cells have been identified in 2-4 dpf larval zebrafish because of similar gene expression pattern in the early development of zebrafish with mammals. For instance, the GABAergic and glutamatergic (Higashijima et al., 2004), monoaminergic (Guo et al., 1999), peptidergic (Kaslin et al., 2004) and glial cells (oligodendrocytes, Schwann cells and astrocytes) (Brösamle and Halpern, 2002; Kawai et al., 2001) are presented in the zebrafish larva. In addition, the anatomical organization of the central and peripheral nervous system is highly conserved from zebrafish to mammals (Mathur and Guo, 2010). Furthermore, the evidence shows that neural circuits controlling the basic behaviors in zebrafish, such as sleep, acoustic startle and arousal (Lovett-Barron et al., 2017; Prober et al., 2006; Schoonheim et al., 2010), are conserved between fish and mammals.

Neurodevelopmental disorders have been investigated using zebrafish. For instance, amyotrophic lateral sclerosis (ALS) and frontotemporal dementia (FTD), are caused by the genetic dysfunction of several ALS an FTD related genes in motor neurons, including SOD1, TARDBP, FUS, and C9orf72 (Armstrong and Drapeau, 2013; Ciura et al., 2013; Hewamadduma et al., 2013; Sakowski et al., 2012; Van Hoecke et al., 2012); autism spectrum disorders (ASD), impairs in social behavior and communication by disrupting the genes shank3, cntnap2, or dyrk1a (Hoffman et al., 2016; Kozol et al., 2016); epilepsy, is mimicked by scn1b or scn1a mutants (Baraban et al., 2013; Grone et al., 2016); intellectual disability, is from stx1b or trappc6b mutants (Marin-Valencia et al., 2018; Schubert et al., 2014) and schizophrenia, is from disc1, cntn4 or mapk2 mutants (De Rienzo et al., 2011; Fromer et al., 2016; Gusev et al., 2018). In addition, models of Parkinson's

4

disease, Alzheimer's disease and Huntington's disease have been reported in zebrafish, including MPTP induced PD model and DJ-1, PINK1 knockdown (Anichtchik et al., 2008; Bretaud et al., 2007; Lam et al., 2005; McKinley et al., 2005), FTDP-17 mutant model of tauopathy (Tomasiewicz et al., 2002), and loss function of HTT in zebrafish (Miller et al., 2005; Schiffer et al., 2007).

In summary, the zebrafish is an optimal complement to mammals in studies of neuronal circuits and neurological disorders.

1.2 Zebrafish lateral line (Sensory nerve system)

The lateral line of zebrafish is a mechanosensory system, which comprises sensory organs, neuromasts and sensory neurons. A neuromast consists of the mechanosensory hair cells and surrounding support cells. Hair cells are named from the hair bundle, a mechanosensory organelle that enables hair cells with vectorial excitability. The sensory neurons innervate the hair cells in the neuromast. Lateral line detects changes of water flow and pressure gradients in the surrounding environment of the zebrafish. It is also involved in large variety of behaviors, including escape, prey detection, detecting and avoiding predators, sexual courtship, tracking hydrodynamic trails, and rheotaxis (Coombs and Conley, 1997; Dehnhardt et al., 2001; Oteiza et al., 2017; Stewart et al., 2013). Furthermore, lateral line can provide sensory feedback to control the movements of the body through afferent and efferent neurons (Akanyeti et al., 2016; Haehnel-Taguchi et al., 2018).

1.2.1 Lateral line development

The lateral line has two separated systems, anterior lateral line system (ALL) and posterior lateral line system (pLL). The ALL comprises the neuromasts on the head and the ganglions which are located between eyes and ears. The pLL comprises a bundle of ganglions which are behind the ear and a line of neuromasts extending from head to tail (Gompel et al., 2001), which develops during the early embryogenesis, around 18 hpf (hours post fertilization), from bilateral cephalic placodes (**Figure 1.2 A**).

The growth of sensory neurites is derived from the primordium (pLLP) which is a cohesive cluster of cells and migrates toward the tail along the horizontal myoseptum under the skin, depositing groups of cells that become neuromasts. The migrating pLLP is a dynamic structure with 100 cells changing in behavior and morphology. The cells in the leading end with the mesenchymal morphology are flatter and displace the proto-neuromast to the trailing position. The trailing part seeds taller cell with apical and basal polarity, which form center-oriented epithelial rosettes with the columnar epithelial morphology, and become the central hair cell progenitor of the nascent proto-neuromast (Lecaudey et al., 2008; Nechiporuk and Raible, 2008). In the maturation stage, the trailing end cells lose their cohesion to the primordium and are deposited to form the neuromasts by incorporating the stable epithelial rosette along the horizontal myoseptum. The rest of the cells are deposited as inter-neuromast cells in the migrating primordium and generate additional neuromasts to the zebrafish (Chitnis et al., 2012). Hair cells of the neuromast are created in pairs by division of progenitors, and sibling hair cells acquire opposing polarities which enables them to be stimulated by water flow from both directions. This functional bi-directional polarity and sensitivity is parallel to the migration of the primordium along the larva rostral-caudal axis in development (López-Schier et al., 2004). As the primordium migrates, axons from the ganglion extend accompanying and are myelinated by the migrating glial cells (Brösamle and Halpern, 2002; Gilmour et al., 2004). In their development, the lateralis afferents project to the hindbrain with central axons and innervate neuromasts with peripheral axons. These bipolar neurons innervate the hair cells of neuromasts and connect them to the hindbrain to establish the lateral line sensory system (Chitnis et al., 2012; Metcalfe et al., 1985).

The posterior lateral line locates superficially along the trunk of the zebrafish, which is formed and becomes functional at the early stage of development. A number of signaling systems regulates the development of the pLL. For instance, neurogenin-1 is involved in the pLL ganglion formation. Loss of ngn1 wipes out the ganglions in pLL, but it does not affect the formation of neuromasts (Andermann et al., 2002; López-Schier and Hudspeth, 2005). Glial-derived neurotrophic factor (GDNF) functions as an attractive cue for axon migration (Schuster et al., 2010). The two chemokine receptors, cxcr4b and cxcr7b, with their ligand SDF1α (CXCL12), regulate the pattern of the anterior-posterior axis (Dambly-

Chaudière et al., 2007; David et al., 2002; Valentin et al., 2007). *Itcha* and *itchb* influence the lateral line development by perturbing the expression pattern of cxcr4 and cxcr7, synchronizing with their function in regulating Wnt signaling pathway. In the *itch* knockdown larva, the failure to down regulate Wnt signaling and cxcr4b overexpression in primordium result in a slower migration of the pLL primordium and abnormal development of the lateral line (Angers and Drapeau, 2014). Moreover, the zinc-finger transcription factor, Insulinoma-associated 1 (Insm1), regulates the Wnt/β-catenin signaling, Fgf target genes, and chemokine signaling genes in the primordium. Loss of insm1a decreases the proliferation of primordium cells and reduces the number of hair cells in neuromasts (He et al., 2017). Hence, the development of lateral line is a highly organized process, enabling the sensory neurons to communicate with their innervating organs (**Figure 1.2 B**).
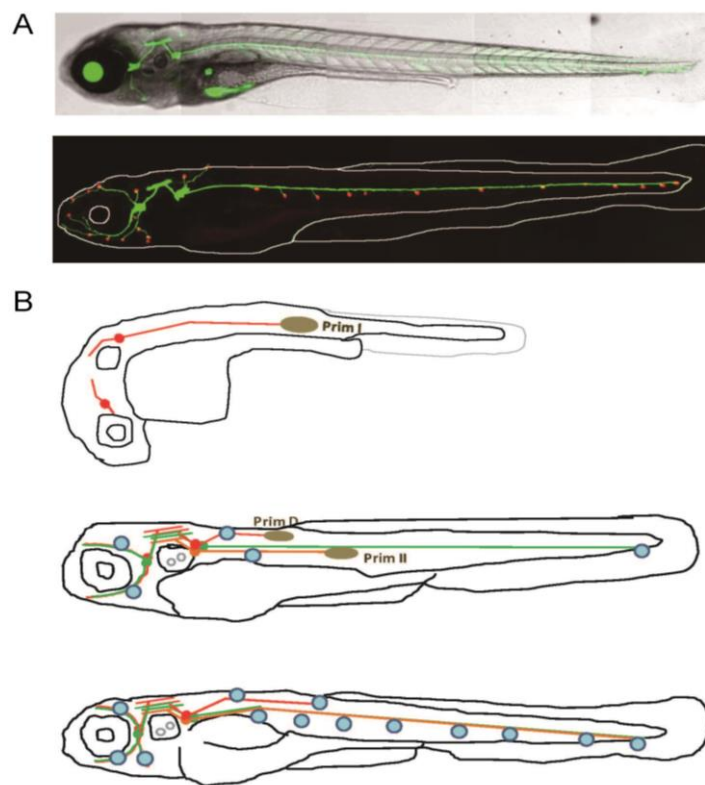
Figure 1.2 The development of the lateral line system in zebrafish. A) Top panel shows the 7dpf larva with bright-field microscope and the whole lateral line neurons with green fluorescence protein label (The line: *Tg[HGn39D]*). Down panel shows the lateral line neurons (Green: *Tg[HGn39D]*) and sensory organs, neuromasts (Red: *Tg[Brn3c-gal4; UAS-RFP]*); B) shows the development of the lateral line. Top panel showing the 2dpf larva with the red ganglions and the brown primI (first primordium)

in the pLL; Middle panel showing the 4 dpf larva with primII (second primodium) and primD (dorsal primordium) and neuromasts in the pLL (posterial lateral line) ; the down panel showing the 7 dpf larva with developed lateral line (Pujol-Martí, J et al., 2013).

1.2.2 Lateral line as a nerve regeneration model for research

The superficially located posterior lateral line (pLL) has the ability to regenerate and to re-innervate its targets (neuromasts) after injury, making the pLL an ideal model for investigating neuron degeneration and regeneration *in vivo*. Axon regeneration has been showed in the posterior lateral line in the *Tg[HuC:GFP]* larva. The extirpated axons regenerate and extend into the trunk, functionally innervating neuromasts within 24 hours (Grant et al., 2005). After axotomy, the distal axon undergoes Wallerian degeneration and the proximal nerve starts to regrow a few hours later. The robust regeneration begins when the axonal debris in the distal part have been cleared. 24 hours after axotomy, the axons regenerate completely to the tip of the tail without difference to the intact pLL in terms of structure and trajectory (Villegas et al., 2012). The transgenic line *Tg[HGn39D]*, which labels the afferent neurons of the lateral line, dramatically improve the ability to record the dynamic events in development (Faucherre et al., 2009). Even in the adult fish, the pLL still has the capacity to regenerate after injury, in which the original branching pattern could be reproduced with the regeneration after axotomy. Thus, the pLL is a convenient *in vivo* system for studying axonal degeneration and regeneration (Graciarena et al., 2014).

1.3 Neuron degeneration and regeneration

In both vertebrate and invertebrate, the peripheral nerves can regenerate functionally by regrowth of axons which reinnervate their target cells after injury. In mammals, the central nervous system has lost the capacity to regenerate after trauma; however, zebrafish can regenerate injured central nerves (Alunni and Bally-Cuif, 2016).

1.3.1 Axon degeneration (Wallerian degeneration)

Axonal degeneration occurs during normal neuron development, pathology of neurodegenerative disorders and nerve damage. After injury, there are two types of axonal degeneration with the damaged axons, acute axonal degeneration (AAD) and Wallerian degeneration (WD) (Knöferle et al., 2010; Waller, 1850).

AAD occurs in minutes following severing, which causes short-distance axonal fragmentation in both the proximal and the distal axonal stumps and leads to retraction of the proximal axonal stump. After AAD, distal portions of the severed axons are in the first stage of WD, called the latent phase. This phase lasts one or two days in the severed nerve in mouse, or 2-6 hours in zebrafish. Then, the severed axons undergo the initiation phase and degenerate quickly upon axon fragmentation, neurofilaments breakdown, swelling of mitochondria in the execution phase. Finally, the debris is eradicated by phagocytes (Martin et al., 2010).

WD is thought to be a protective response for nerve functional recovery from injury. It is a cellular degradation process and is different from apoptosis (Deckwerth and Johnson Jr, 1994). In the initiation phase, the most important factors are NMNATs (nicotinamide mononucleotide adenylytransferases). They catalyse the production of NAD (Nicotinamide adenine dinucleotide), which affects the axonal degeneration. NAD involved in many biological reactions as a co-substrate of sirtuins, ADP (Adenosine diphosphate) polymerases, ADP transferase, and cyclin ADP-ribose processes (CD38). *In vitro* experiments show that the level of NAD significantly decreases around 3 or 4 hours post axotomy; however, the morphology of axons remains intact. The decline of NAD can be delayed by overexpression of NMNATs in the transected axons (Gerdts et al., 2015; Wang et al., 2005). In detail, NMNAT2 knockdown triggers intact axon degeneration, whereas other isoforms (NMNAT1/3) fail to compensate this process (Conforti et al., 2011; Gilley and Coleman, 2010; Yamamoto et al., 2016). New studies suggest that NMN (β-nicotinamide mononucleotide) accumulation in the NMNAT2 null promotes axon degeneration after injury. FK866, an inhibitor of NAMPT (nicotinamide phosphoribosyltransferase) that catalyzes NAM to NMN, delays the axonal degeneration by decreasing the levels of NAD and NMN and accelerating the depletion of ATP (Di Stefano et al., 2015). NMN deamidase decreases NMN accumulation in injured nerves preserving the axons for three weeks. It also rescues the axonal outgrowth and death in the NMNAT2 null mice (Di Stefano et al., 2017; Loreto et al., 2015). Furthermore, Ca^{2+} influx is detected in distal axons after axotomy. In zebrafish, there are two waves of calcium influx during axon degeneration. The first wave occurs during axotomy. The second one takes place 4-6 hours later (Loreto et al., 2015; Vargas et al., 2015). In addition, Sarm1

(Sterile Alpha and TIR Motif containing 1) and DR6 (death receptor 6) have been reported in regulating of WD. Loss of Sarm1 blocks axon degeneration in fruit flies and mice (Osterloh et al., 2012). More details about Sarm1 in axon degeneration will be introduced in the following section (**Section 1.5**). The orphan receptor, DR6, promotes axon degeneration by JNK (C-Jun N-terminal kinases) signaling pathway *in vitro* and *in vivo* (Gamage et al., 2017). In the execution phase, calcium influx activates calpain to fragment the cytoskeleton in distal axons. The calpain inhibitors and methyl pyruvate can block the axonal fragmentation. Moreover, ATP depletion is upstream of calpain activation, because rescuing ATP depletion can block the calpain activation induced-fragmentation (Ma et al., 2013; Yang et al., 2015a; Yang et al., 2013). During the axon degeneration, glia cells and macrophages are involved in clearing the axonal debris (Lyons and Talbot, 2015; Wang et al., 2012).

In zebrafish, distal axons undergo three stereotyped phases of WD, lag phase, fragmentation phase, and clearance phase. The overexpression of Wlds or inhibitors of ubiquitylation dramatically elongates the lag phase, but do not influence the fragmentation (Martin et al., 2010). In the fragmentation phase, the Schwann cells and leukocytes regulate the amount of axon debris and the clearance process in the pLL (Villegas et al., 2012) (**Figure 1.3 A** & **B**).

1.3.2 Axon regeneration

Axon regeneration varies across species as well as in the central and peripheral nervous systems (CNS and PNS) in mammalians. In adult mammals, the injured CNS fails to repair and to rebuild the functional re-innervation of original targets, while the PNS retains the ability to recover functionally after injury. However, zebrafish possess the ability to restore the nerve functionally from injury in both central and peripheral nervous systems (Becker and Becker, 2014; Dias et al., 2012).

The regenerative process requires orchestrating the intrinsic factors which include transcriptional factors, epigenetic modifier and protein regulation, as well as extrinsic events which include tissue repair, interaction with glia cells and immuno-response (Mahar and Cavalli, 2018). In regenerating axons, the injury activates several signal pathways to

promote axonal regeneration. For instance, the conversion of Na^+/Ca^{2+} pumps enhances calcium influx after injury. The calcium wave is involved in axonal membrane resealing, mRNAs and proteins translocation, proteins synthesis, growth cone assembly, transcriptional factors regulation, and epigenetic modification (Bradke et al., 2012; Rishal and Fainzilber, 2014). In the injured axons, the calcium actives cAMP at the near side of injury to promote PKA activation. The activated PKA facilitates DLK (Dual leucine zipper kinase) activation to phosphorylate STAT3 (Signal transducer and activator of transcription 3) to activate the expression of pro-regeneration factors (Hao et al., 2016; Pérez-Cadahía et al., 2011; Shin et al., 2012). Simultaneously, STAT3 mRNA that is near the injury site of the axon is translated into protein which is phosphorylated by JAKs (Janus kinase) and MAPKKs (Mitogen-activated protein kinase kinases). The phosphorylated STAT3 forms strong interactions with stathmin, which inhibits the microtubule destabilizing activity of stathmin and promotes axon regeneration (Selvaraj et al., 2012; Verma et al., 2009). Moreover, the cytosolic ERK1 (Extracellular signal–regulated kinases) and ERK2 are activated by phosphorylation, and bind to vimentin and importin-β to promote retrograde transport (Perlson et al., 2005). The mammalian target of rapamycin (mTOR) is also a key factor for axon regeneration. Directly activating mTOR or deleting its upstream negative factors TSC1 (Tuberous sclerosis proteins 1), TSC2 and PTEN (Phosphatase and tensin homolog) increases the ability of injury axons to regenerate (Abe et al., 2010; Berry et al., 2016; Liu et al., 2010; Park et al., 2008). The transcription factors ATF3 (activating transcription factor 3) activated by cAMP and SMAD (Mothers Against Decapentaplegic Homolog) activated by GSK3 (glycogen synthase kinase 3) or BMP2 (Bone morphogenetic protein 2) or BMP4, promote axon growth in DRG (Dorsal root ganglion) neurons *in vitro* (Seijffers et al., 2007; Zou et al., 2009). In addition, more and more transcription factors, such as HIF1α (hypoxia inducible factor 1 subunit alpha), p53 (tumor protein P53), SOX11 (Sex Determining Region Y – Box 11), MYC (MYC Proto-oncogene, BHLH Transcription Factor) and SRF (Serum Response Factor), play roles in axon regeneration (Belin et al., 2015; Cho et al., 2015; Di Giovanni et al., 2006; Norsworthy et al., 2017; Stern et al., 2013). About the epigenetic dynamics in axon regeneration, the acetylation of histones by KAT2B (lysine acetyltransferase 2B) which is activated by ERK and their oxidization of 5mC to 5hmC by TET3 (Tet methylcytosine

dioxygenase), promotes the transcription of pro-regenerative genes (Puttagunta et al., 2014; Weng et al., 2016). Moreover, HDAC4 (Histone deacetylase 4) translocated from the nucleus deacetylates the microtubules at the injury site increases the dynamic of growth cone and promotes axon growth (Chawla et al., 2003). In contrast to the pro-regenerative factors, there are some axon regeneration inhibitory molecules, such as RTCA (RNA 3'-terminal phosphate cyclase A), RTCB (RNA 3'-terminal phosphate cyclase B), NogoA, MAG, CSPGs (chondroitin sulfate proteoglycan a), PARP1 (poly (ADP-ribose) polymerase), and myelin-derived Nogo (Brochier et al., 2015; Kosmaczewski et al., 2015; Mahar and Cavalli, 2018; Schwab and Strittmatter, 2014; Song et al., 2015; Yiu and He, 2006) (**Figure 1.3 C**).

In zebrafish, a successful CNS regeneration combines a number of intrinsic and extrinsic factors allowing a functional recovery. For instance, ECM (extracellular matrix) components, CSPGs (chondroitin sulfate proteoglycans), form the scar to inhibit axon regrowth in mammals. But the CSPGs are not expressed in the lesion site in zebrafish optic nerve (Becker and Becker, 2002). The inhibitory molecule, NogoA, is shown missing the N-terminal inhibitory domain in zebrafish, which inhibits axon regeneration in mammals (Abdesselem et al., 2009). Additionally, zebrafish oligodendrocytes increase pro-regeneration molecules expression, such as P0 (Schweitzer et al., 2003), L1-related molecules (Bernhardt et al., 1996) and contactins (Haenisch et al., 2005; Schweitzer et al., 2007) after CNS injury; however, the oligodendrocytes in mammals do not.
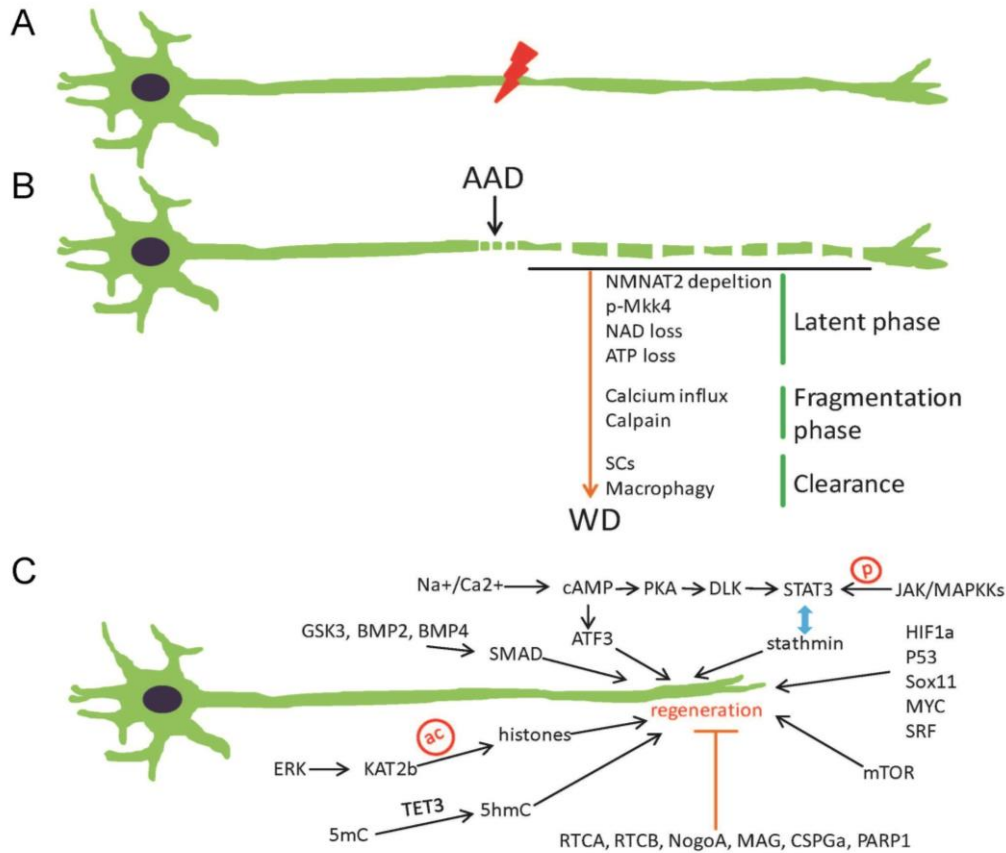
Figure 1.3 The mechanisms of axon degeneration and regeneration after injury. A) & B) The injury axon undergoes the acute axonal degeneration (AAD) and Wallerian degeneration (WD) after injury. The AAD happens at the injury sites, where the axon is quickly fragmented and degrades. The WD consists three phases, latent phase with NAD and ATP loss, fragmentation phase with calcium influx and calpain induced cytoskeleton distruction and clearance phase with Schwann cells and macrophages engulf and clear the debris of axons; C) The network showing the signalling pathways and molecules are involved in axon regeneration by promoting the axon regrowth after injury and molecules which inhibit axon regeneration. NMNAT, nicotinamide mononucleotide adenylyltransferase; NAD, nicotinamide adenine dinucleotide; ATP, adenosine triphosphate; JAK, Janus kinase; MAPK, mitogen-acticated protein kinase; STAT3, signal transducer and activator of transcription 3; DLK, dual leucine zipper kinase; PKA, protein kinase A; cAMP, cyclic adenosine monophosphate; ATF3, activating transcription factor 3; HIF1α, hypoxia inducible factor 1 subunit alpha; GSK3, glycogen synthase kinase 3; BMP, bone morphogenetic protein; ERK, extracellular signal-regulated kinases; RTCA, RNA 3'-terminal phosphate cyclase A; RTCB, RNA 3'-terminal phosphate cyclase B; MAG, myelin associated glycoprotein; CSPGa, chondroitin sulfate proteoglycan a; PARP1, poly (ADP-ribose) polymerase; mTOR, mammalian target of rapamycin complex; KAT2b, lysine acetyltransferase 2B; TET3, Tet methylcytosine dioxygenase.

1.4 Schwann cells

1.4.1 Schwann cell development

Schwann cells (SCs) are the glial cells ensheathing the peripheral nervous system. They supply the myelin that isolates axons from the outside environment, enhances the action potential conduction, and maintains the nerve fasciculation.

Schwann cells are derived from neural crest cells and are sorted into mature myelinating and non-myelinating types in development. The development of Schwann cells consists of several stages, such as neural crest cell, Schwann cell precursors, immature Schwann cells, pro-myelinating Schwann cells and non-myelination Schwann cells or mature myelinating Schwann cells. Several signal pathways are involved in induction of the initial neural crest cells. For instance, activation of BMP (Bone morphogenetic) and FGF (fibroblast growth factor) combining with the Wnt pathway is essential for neural crest induction. After the neural crest cells successfully become the precursors, they are migrating and developing with the growing axons which supply survival signals. In addition, the NRG1 (Neuregulin 1) and Erbb2/3 (Erb-b2 receptor tyrosine kinase 2/3) signaling pathways play pivotal roles in the successful development of Schwann cell precursors (Raphael and Talbot, 2011). In the next stage, the Notch signaling helps the Schwann cell precursors to develop into immature Schwann cells which lose the migratory capacity. When migration finishes, the immature Schwann cells start a process of radial sorting, in which the caliber of the axons determines whether the axons are myelinated or not. The large diameter axons are associated with the pro-myelinating Schwann cells and are wrapped by the compact myelin sheath. Specifically, the immature Schwann cells remodel their cytoskeleton and extend filipodia and lamellipodia, which facilitates pro-myelinating Schwann cells to wrap the axon for further myelination. Simultaneously, the non-myelinating Schwann cells form the Remak bundles with small diameter axons (Feltri et al., 2016; Salzer, 2015). Furthermore, several extracellular matrix adaptors with their receptors, such as laminin, collagen XV, integrins $\alpha6\beta1$, dystroglycan and Rho family kinases, activate their downstream intracellular pathways to control the process of radial sorting (Monk et al., 2015). Besides the above factors, the following transcription factors, Sox10, Brn2, Oct6 and Krox20, are involved in the Schwann cells development and myelination (Jessen and Mirsky, 2005;

Nave and Salzer, 2006; Pereira et al., 2012). Recently, more receptors have been reported in myelination, such as G protein coupled receptors 44 (GPR44), GPR126, P2X7 and the gamma aminobutyric type B receptor (Faroni et al., 2014; Procacci et al., 2013) (**Figure 1.4 A**).

1.4.2 Schwann cells in neuron injury

During the peripheral nerve injury, Schwann cells undergo different stages, including dedifferentiation, demyelination, activation and remyelination. That means the state of the promyelinating Schwann cells is dynamic in response to nerve injury.

A significant phenomenon of Schwann cells after nerve injury is that the Schwann cells bridge the gap for guiding the regenerating axons across the injury area. On both sides of the injury site, filopodia-like structures of Schwann cells which obtain a bipolar elongated morphology migrate and contact each other. This reflects the plasticity of the Schwann cells providing essential cues and structures for axon regeneration (Glenn and Talbot, 2013; Ide, 1996). The migratory behavior of the filopodia-like structure is controlled by ephrin B which is secreted by fibroblasts, EphB2, Sox2 and N-cadherin which are expressed by the Schwann cells. The EphB2 is activated by ephrin B and triggers the N-cadherin redistribution to the junction of Schwann cells by Sox2 signal pathway. This induces the repulsive behavior and causes the formation of the migratory structure for bridging the gap (Clements et al., 2017; Parrinello et al., 2010). In the proximal part of the distal stump of the injury nerves, the Schwann cells which lose the contact with axons (degenerate automatically), lose the capacity of myelin production and proliferate to present the daughter Schwann cells to the injury site. In this case, some of the Schwann cells migrate into the injury gap to facilitate the axons to get over this region. However, the far-side Schwann cells in the distal stump dedifferentiate and lose their original cellular morphology. This pro-regenerative feature of the repairing Schwann cells are from the myelinating Schwann cells which undergo several components upregulating p75NTR (Nerve growth factor receptor), NCAM (Neural cell adhesion molecule), GFAP (Glial fibrillary acidic protein) and mTOR1 (Mammalian target of rapamycin complex1)) and decreasing the expression of MBP (Myelin binding protein), MAG (Myelin associated glycoprotein) and P0 (Myelin protein zero) (Boerboom et al., 2017; Norrmén et al., 2018).

The activating of c-Jun transcription factor and modification of the DNA are also involved in this conversion. When the new axons regrow to their targets, the repairing Schwann cells are activated and gain the capacity to myelinate the new axons again. Many factors are participating in this process. For instance, IL-1α (Interleukin 1 alpha), IL-1β (Interleukin 1 beta), LIF (Leukemia inhibitory factor) and MCP1 (Monocyte chemoattractant protein1) which recruit the neutrophils and macrophages to the injury axons are upregulated in the repairing Schwann cells (Martini et al., 2008; Rotshenker, 2011), accelerate the clearance of the fragment axons. Moreover, Schwann cells activate the breakdown process of myelin, which is beneficial for new axons regrowth. It should be mentioned that several factors in the extracellular space of Schwann cells or axons contribute to the nerve repair. For example, the neurotrophic factors, GDNF (Glial-derived neurotrophic factor), BDNF (Brain-derived neurotrophic factor), VEGF (Vascular endothelial growth factor), and artemin, promote the axons regrowth and elongation (Brushart et al., 2013; Eggers et al., 2010; Fontana et al., 2012) (**Figure 1.4 B**).
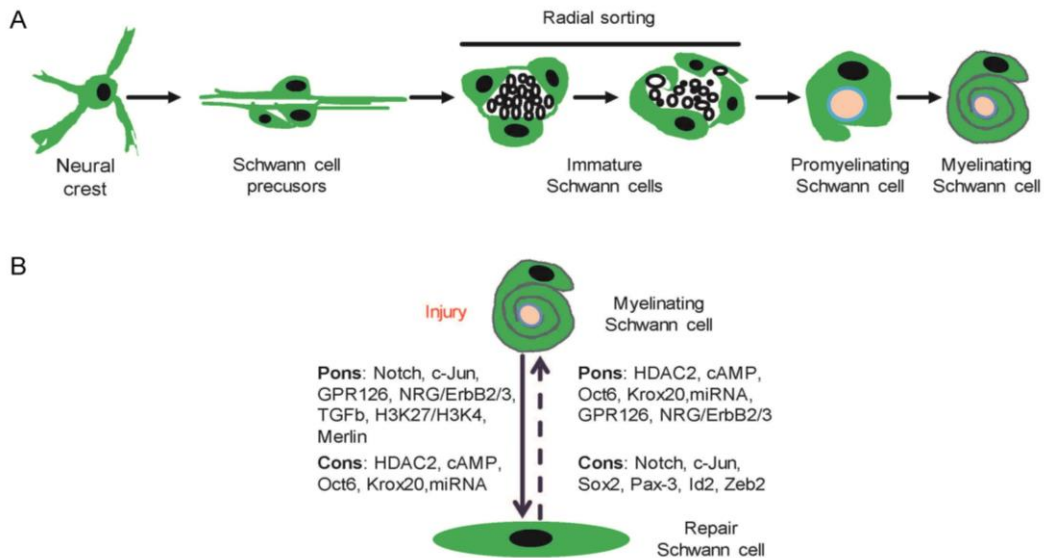
Figure 1.4 The development of Schwann cells (SCs) and Schwann cells response to injury. A) Illustration shows the development of Schwann cells from neural crest cells to Schwann cell precursors, radial sorting immature Schwann cells, promyelinating and myelinating Schwann cells; B) shows the SCs response to injury. The myelinating SCs are converted reversibly into repair SCs under the control of the indicated factors. These factors are separated into Pons for promoting the process and Cons for inhibiting the process of transfer between myelinating and repair SCs. GPR126, G-protein coupled receptor 126; NRG1, neuregulin 1; ErbB, Erb-B2 receptor tyrosine kinase; TGF, Transforming growth

factor; HDAC2, histone deacetylase 2; cAMP, cyclic adenosine monophosphate; Oct6, octamer-binding protein 6; Sox2, SRY (sex determining region Y)-box 2; Pax3, paired box 3; Id2, inhibitor of DNA binding 2; ZEB2, zinc finger E-box binding homeobox 2.

1.4.3 Communication between Schwann cells and axons

Neuregulin is important for development of the normal neuronal connectivity. Its EGF-like domain is for interaction with ErbB receptors which are expressed on the Schwann cells. The Nrg1-Erbb signaling is involved in myelination, synaptic transmission and survival of neurons and glial cells. Nrg1-TypeIII, expressed by Schwann cells, induces Schwann cells dedifferentiation and Remak formation. The activation of Nrg1 is by cleavage of the extracellular part. Nrg1 is positively regulated by β-secretase (BACE1) which cleaves Nrg1 and releases the N-terminal fragment (Nrg1-ntf). Moreover, ADAM17 (A disintegrin and metalloproteinase 17) has been reported to be involved in BACE1 (β-secretase1) cleavage of Nrg1. The Nrg1-ntf binds erbb4 and increases ERK (Extracellular signal-regulated kinases) and AKT (Protein kinase B) phosphorylation, which plays a role in cell survival, synaptic development and remyelination. The C-terminal fragment of Nrg1 participates in enhancing the synaptic plasticity (Krivosheya et al., 2008; Luo and Park, 2012; Zhang et al., 2017).

Neurogenic locus notch homolog protein (Notch) controls Schwann cell proliferation and Schwann cell-axon interaction in development. It promotes Schwann cell maturation from Schwann cell precursors and maintains myelin as a negative regulator. Downregulation of Notch leads to premature myelination, while the overactivation of Notch delays myelin formation (Boerboom et al., 2017; Woodhoo et al., 2009).

Neurotrophin is involved in Schwann cell-axon interaction in both directions: from axons to Schwann cells and *vice versa*. It has two members, BDNF and NT3. BDNF can bind to the p75 from Schwann cells, promoting myelination in the early stages (Brushart et al., 2013; Piirsoo et al., 2010). However, it also binds to TrkB, which inhibits myelination at later stages (Zhang et al., 2016). NT3 promotes SC migration, but it inhibits myelination in *in vitro* experiments. Deficient NT3 mice have shown hypomyelination axons in development (Sahenk et al., 2008).

Nectin-like proteins are expressed in the Schwann Cell-axon interactions, known as cell adhesion molecules (CADM). Indeed, SC-derived Necl-1/Cadm3 and axonal Necl-4/Cadm4 regulate PNS myelination *in vitro* (Maurel et al., 2007; Monk et al., 2015).

GPR126 is required for myelination of the peripheral neurons. Schwann cells secreted collagen IV is an ECM (Extracellular matrix) protein that modulates and activates GPR126. The Gα subunit of GPR126 increases cAMP (Cyclic adenosine monophosphate) level and activates PKA for initiating myelination (Mogha et al., 2013; Paavola et al., 2014). Laminin, another ECM protein, is a new ligand for GPR126 that controls the early and late stages of Schwann cell development by modulating the receptor signaling via a tethered agonist (Petersen et al., 2015). GPCR44 promotes peripheral nervous system myelination by activating the Nfact4 (Nuclear Factor Of Activated T Cells 4) which is in the downstream of NRG1 signaling (Trimarco et al., 2014).

1.5 Sarm1

Sarm1 is conserved from *Caenorhabditis elegans*, *Drosophila* and mammals. It contains the HEAT/Armadillo domain, unique sterile alpha (SAM) motifs, and a Toll-interleukin-1 receptor (TIR) domain. Sarm1 is highly expressed in neurons, astrocytes and the liver, which localizes to the cytoplasm and the mitochondria (Mink et al., 2001; Murata et al., 2013; Pan and An, 2018). In human neuronal cell line SH-SY5Y, the protein level of sarm1 is enhanced after mitochondrial depolarization (Murata et al., 2013). In human PBMC (a peripheral blood mononuclear cell), LPS (lipopolysaccharide) treatment dramatically increased sarm1 protein, but Sarm1 mRNA was suppressed coincidentally, suggesting that Sarm1 mRNA and protein are regulated independently (Carty et al., 2006). In addition, the angiotensin II receptor antagonist and kainic acid can enhance the expression of Sarm1 in brain or retinal ganglion cells (Balaji et al., 2015; Massoll et al., 2013).

1.5.1 Sarm1 in immunology

The *C.elegans* ortholog of Sarm1, Tir-1, is involved in worm development and innate immunity. The expression of two peptides, NLP (neuropeptide-like protein)-29 and NLP-31, is regulated by Tir-1 when *C. elegans* is infected by fungi or bacteria (Couillault et al.,

2004). In mammals, Sarm1 negatively regulates TRIF (TIR-domain-containing adapter-inducing interferon-β)-dependent Toll-like receptor signaling. Knockdown of SARM by RNAi enhances TRIF-dependent chemokine and cytokine induction (Carty et al., 2006). Additionally, Sarm1 regulates TLR signaling when *Burkholderia pseudomallei* infect murine macrophages. Then, the expression of Sarm1 is increased in macrophages, which inhibits TRIF and reduces IFN-β (Interferon beta) production, indicating that Sarm1 is a negative regulator in TLR signaling (Baral and Utaisincharoen, 2013; Pudla et al., 2011). However, some reports show positive roles of Sarm1 in TLR signaling. For instance, in neurons, Sarm1, not the MyD88 (myeloid differentiation primary response 88), is reported to mediate TLR7 and TLR9-induced apoptosis (Mukherjee et al., 2015). In the non-alcohol fatty acid liver disease (NAFALD), Sarm1 deletion reduces inflammation via reduction of TLR2/7/9 responses. Moreover, Sarm1 induces the expression of TLR and proinflammatory cytokine in response to HFD (high fat diet) in the liver and hypothalamus (Pan and An, 2018). Recently, it has been reported that activation of Sarm1 dependent JNK pathway is required for neurons responding to traumatic injury by chemokines (Ccl2, Ccl7, Ccl12 and Csf1) production. Deletion of genes in the Sarm1-JNK-C-Jun pathway effectively blocks immune cells from being recruited into the injury of neural tissues (Wang et al., 2018).

1.5.2 Sarm1 in neurobiology

The role of Sarm1 in neurons was first uncovered in *C. elegans*. Tir-1 activates NSY-1/ASK1 kinases to regulate diversifies odorant receptors expression (Chuang and Bargmann, 2005). In mammals, MyD88-5/Sarm1 is highly expressed in the brain, which interacts with and recruits JNK3 to mitochondria. The hippocampal neurons from Sarm1-null mice resist cell death after oxygen and glucose deprivation (Kim et al., 2007). In La Crosse virus (LACV) inducted neuronal cell death, the expression of SARM1 is upregulated by MAVS (mitochondrial antiviral signaling protein) which induces the cell death upon mitochondrial damage or oxidative stress response (Mukherjee et al., 2013). In addition, Sarm1 plays an important role in neuronal morphology. Specifically, Sarm1 binds to syndecan-2 which is a synaptic heparin sulfate proteoglycan in mouse brain, where Sarm1 transfers signals from syndecan-2 to ASK-MEK4/7-JNK signaling pathway to

regulate neuron dendritic arborization. However, the expression of Sarm1 precedes the expression of syndecan-2 in the brain, indicating that Sarm1 also has a syndecan-2 independent way to control axonal outgrowth and neuronal polarity formation (Chen et al., 2011). In the sensory neurons, Sarm1 functions downstream of ROS (reactive oxygen species) generation inducing cell death. Deletion of Sarm1 blocks cell death but not ATP deletion, ROS accumulation under CCCP treatment (Summers et al., 2014).

1.5.3 Sarm1 in neuron degeneration

In flies and mice, deletion of dSarm1 or Sarm1 prevents the Wallerian degeneration in axotomy (Osterloh et al., 2012). The SAM domain of Sarm1, which mediates the multimerization of proteins, is not essential for triggering axon degeneration. However, the TIR (Toll-interleukin receptor) domain is important for activating downstream signaling pathway to execute axon degeneration and non-apoptotic neuronal death. In addition, the N-terminal mitochondrial targeting sequence is not required for the function of Sarm1, but ablation of the N-terminal armadillo domain actives axonal degeneration and cell death without injury, suggesting that the armadillo domain is a negative regulator of Sarm1 (Gerdts et al., 2013). The evolutionary study suppose that Sarm1 likely develops from bacterial TIR proteins but not from animal TIR protein in the phylogenetic trees. It is possible that the gene transfers between the bacteria and the ancestor of ecdysozoa and deuterostomes (Malapati et al., 2017; Zhang et al., 2011). Moreover, bacterial TIR proteins, TirS, possess the NADase activity and effect the macrophage response to infection (Patot et al., 2017). The Sarm1-TIR has the NADase activity that is necessary for pathological axon degeneration, which cleaves NAD+ into Nam, ADP-ribose (ADPR), cyclin ADPR, and nicotinamide (Essuman et al., 2017).

TIR domain dimerization can promote axon degeneration directly both *in vitro* and *in vivo*, indicating that the dimerization of TIR domains is required for axonal degeneration. Dimerization of TIR triggers the consumption of NAD and ATP in a short period, and the decrease of NAD is much faster than depletion of ATP. However, in Sarm1 deficient nerve, the decline of NAD and ATP is retarded, which maintains the transected axons stable. In addition, increasing NAD synthesis can partly block the axonal degeneration which is induced by TIR dimerization (Di Stefano et al., 2015; Gerdts et al., 2015). Enhancing the

NAD consumption can execute the axonal degeneration in Sarm1 null axons, indicating that NAD loss is required for axon degeneration but not the outcomes. Additionally, poly (ADP-ribose) polymerase and CD38 deletion do not block the Sarm1 induced NAD loss, axon fragmentation, and cell death (Gerdts et al., 2015). However, in another study, deletion of Sarm1 does not prevent the decline of NAD and NMN in the transected neurite (Gilley et al., 2015).

Sarm1 is required for NMN induced Wallerian degeneration, because NMN requires Sarm1 to stimulate Ca^{2+} influx. Inhibition of NMN synthesis and Sarm1 deficiency block Ca^{2+} influx and remain axonal integrity (Loreto et al., 2015). Genetic ablation of NMNAT2 is embryonic lethal with dramatic defects of axon extension in the embryos in mouse. The double mutant animals, NMNAT2$^{-/-}$Sarm1$^{-/-}$, are able to develop into adult. Sarm1 knockout rescues the defects induced by NMNAT2 deficiency. NMNAT2 is the upstream component of Sarm1 in axon degeneration by inhibiting the activity of Sarm1 (Gilley et al., 2015). More studies show that Sarm1 activates mitogen-activated protein kinase (MAPK) signaling pathway in the axon, including the MAPK kinase kinase (MAPKKK), MAPK kinase (MAPKK), and MAPK members, c-Jun N-terminal kinase (JNK1/JNK2/JNK3). In addition, axotomy induces Sarm1 dependent MKK4 phosphorylation in mammalian optic nerves. This phosphorylation event can be diminished by overexpression of NMNAT1 (Yang et al., 2015a). The injury activating Sarm1-MAPK pathway promotes axonal degeneration, but it can be antagonized by AKT which inhibits the activation of JNKs (Yang et al., 2015a). This suggests that the AKT is an inhibitor of axon degeneration after axotomy. The kinase AKT phosphorylates MKK4 directly at Ser78 to preserve the axons after injury. The protein level of AKT is regulated by ZNRF1 mediated proteasomal degradation following axon injury (Wakatsuki et al., 2011), which accelerate the axon degeneration by removing the inhibitor of MAPK signaling (Gerdts et al., 2016; Yang et al., 2015a). Sarm1 interacts with JNK3 which participates in mitochondrial apoptosis pathways (Kuan et al., 2003), and Sarm1 recruits JNKs to mitochondria to regulate cell apoptosis under glucose deprivation and hypoxia (Kim et al., 2007). Recent study shows that phosphorylated SARM1 at serine 548 by JNK under oxidative stress conditions, results in NAD+ cleavage activity enhancement and mitochondrial respiration inhibition. In Parkinson's disease (PD) patient, the

phosphorylation of Sarm1 is increased and the neurons are more sensitive to oxidative stress, comparing to the neuronal cells from a healthy person (Murata et al., 2018). The Sarm1-MAPK pathway induces calpain activation and axon morphological degeneration by triggering energy deficit in the injured axons, which precedes proteolysis of axonal cytoskeletal proteins degradation and axon degeneration. Either depletion of Sarm1, MKK4/MKK7, or JNKs, maintains the ATP levels in the injured axons (Yang et al., 2015a) (**Figure 1.5**).
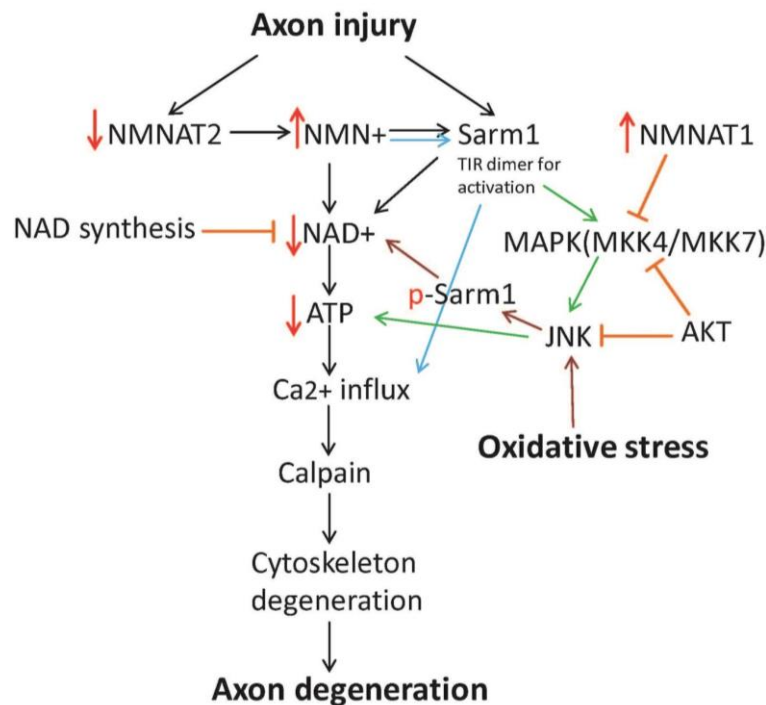
Figure 1.5 The network of Sarm1 in axon degeneration. This network shows the molecules and signalling pathways in Sarm1 induced axon degeneration. The central axis is the NAD^+, ATP, Ca^{2+}, and cytoskeleton breakdown for axon degeneration. Activation of Sarm1 (TIR dimerization) and phosphorylation of Sarm1 increased the consumption of NAD^+ which triggers axon degeneration. Axotomy can active Sarm1 directly or through down regulation of NMNAT2. The oxidative stress promotes JNK to phosphorate Sarm1 in axon degeneration. NMNAT, nicotinamide mononucleotide adenylyltransferase; NMN, β-nicotinamide mononucleotide; NAD, nicotinamide adenine dinucleotide; MAPK, mitogen-activated protein kinase; AKT, Protein kinase B; JNK, C-Jun N-terminal kinase; ATP, adenosine triphosphate.

1.5.4 Sarm1 in neuron pathology

Lack of Sarm1 improves traumatic brain injury (TBI) associated phenotypes after injury. Sarm1 knockout mice have less β-amyloid precursor protein aggregation in the axons of the corpus callosum, comparing to the wild type mice in TBI. In addition, the behavioral deficits in the wild type mice after TBI is attenuated in the Sarm1 KO mice (Henninger et al., 2016). Peripheral neuropathy is the major side effect in clinical trials, especially in chemotherapy. Sarm1 deletion preserves nerve fibers following vincristine treatment in mice, indicating that genetic ablation of Sarm1 inhibits the vincristine-induced peripheral neuropathy in mice (Geisler et al., 2016). Moreover, Sarm1 participates in the development of Amyothrophic lateral sclerosis (ALS). In the *C.elegans* ALS model, tir-1 deletion suppresses the motor neuron degeneration via the regulation from UNC-13 and UNC-31. The components in this pathway may be the new targets sites for ALS therapy (Carty and Bowie, 2019; Vérièpe et al., 2015).

1.6 Chemotherapy and neuropathy

Chemotherapy–induced peripheral neuropathy (CIPN) is the main adverse effect associated with chemotherapeutic agents in patients (Starobova and Vetter, 2017). The most popular reagents include the vinca alkaloids (vincristine), taxanes (paclitaxel, docetaxel), platinum-based antineoplastics (oxaliplatin, cisplatin), immunomodulatory drug (thalidomide), and the proteasome (bortezomib). These drugs increase the survival rates of patients, but the side-effect makes numbers of survivors suffering from the pain of neuropathy (Seretny et al., 2014) (**Tabel 1.2**). The damages to peripheral sensory and motor neurons are dose dependent and progressive (Kautio et al., 2011). Additionally, the conditions of patients, such as pre-existing nerve damage or diabetes, also relate to the development of CIPN (Starobova and Vetter, 2017). CIPN shows the deficits in sensory nerves, motor nerves, and autonomic function with the agent specific manner (Park et al., 2013b). Specifically, sensory symptoms develop in the sensory neurites, including the sense to touch, temperature, vibration and pain. The severe cases present the loss of sensory perception (Bernhardson et al., 2007; Postma et al., 1993; Sahenk et al., 1994; Strumberg et al., 2002). Motor symptoms display impaired fine movements and balance disturbances. It can progress to paralysis and loss of motor functions which are more severe than the deficits in sensory nerves (Mols et al., 2016). About the autonomic symptoms, which occur

in the compound specific manner and less frequent. The symptoms involve constipation, orthostatic and urinary function (Mols et al., 2016). Strikingly, CIPN can cause irreversible sensory neuron deficit in severe cases (Starobova and Vetter, 2017). Due to inadequate efficacy or adverse effects of the agents, it is urgent to find novel and systematic approaches to quickly evaluate the drugs and their side effect. Zebrafish could be a powerful model system to promote novel drugs discovery and evaluate the drug toxicity and efficacy (Holloway et al., 2016).

1.6.1 Mechanism of CIPN

The mechanism of chemotherapeutic agents resulting in CIPN has been studied for many years. The potent effects of these agents on cell proliferation and cell death are relatively well understood. For instance, disrupting axonal transport, axonal degeneration, and mitochondrial function have been reported to contribute to CIPN. But the additional side-effects are not clear (Starobova and Vetter, 2017) (**Table 1.2**).

Chemotherapeutic drugs implicated in CIPN

Type of Drug	Names	Mechanisms in therapy	Side effect
Taxene	Paclitaxel	Inhibit microtuble depolymerization, mitotic arrest	Sensory
Platinum	Oxalplatin Cisplatin	DNA binding, cell cycle arrest	Sensory
Vinca	Vincristine	Inhibit microtuble depolymerization, mitotic arrest	Sensory, motor nerve
Proteasome inhibitor	Bortezomib	Inhibit proteasome degeradation, cell cycle arrest	Sensory

Table 1.2 Chemotherapeutic drugs implicated in CIPN. This table shows a brief description of the chemotherapeutic drugs and the mechanisms of the drugs for therapy, and the side-effect for the patients.

The platinum agents (Oxaliplatin and Cisplatin), side-effect in nephrotoxicity and neurotoxicity, lead to cell cycle arrest and apoptosis by forming platinum-DNA adducts (Johnstone et al., 2014; Suchánková et al., 2012). Besides the DNA level damage, they also affect transmembrane receptors and ion channels (Cavaletti et al., 2001; Grolleau et al., 2001; McDonald and Windebank, 2002). For instance, oxaliplatin which causes sensory

neuropathy, affects axonal excitability by ion channel dysfunction and dysregulation of calcium homeostasis, and alters the function of potential channels of transient receptors. Moreover, oxaliplatin induces neuronal and glial cell dysfunction and death by activating the caspases, mitogen-activated protein kinases (MAPK) and protein kinase C (PKC) (Carozzi et al., 2015; Cersosimo, 2005). However, cisplatin reduces loss of large myelinated fibers and sensory nerve action potentials (Krarup-Hansen et al., 2007). In addition, it interferes in cell division and transcription of messenger ribonucleic acid (mRNA) and affects the calcium signaling pathway related kinase proteins (MAPK, JNK, PKC and AKT) (Dasari and Tchounwou, 2014).

Paclitaxel, one agent of taxanes, targets the microtubules during the cell cycle and causes sensory neuropathy with axonal degeneration (Jordan and Wilson, 2004). The study in zebrafish showed that paclitaxel accumulates in the basal keratinocytes and enhances the expression of epidermal matrix-metalloproteinase-13. Moreover, paclitaxel promotes sensory axon degeneration and weakens the touch response in the distal caudal fin (Lisse et al., 2016).

Vincristine from vinca alkaloids, has the high affinity to α-tubulin, leading to mitotic arrest and cell death in sensory and motor neurons (Gan et al., 2010). In the rat model, vincristine decreases the expression of endomorphin-2, which attenuates allodynia and central sensitization in the spinal cord (Yang et al., 2015b). Vincristine disrupts calcium homeostasis and membrane remodeling of peripheral neurons, causes loss of large myelinated fibers, and activates immune system and subsequent neuroinflammation in the CIPN mice (Boehmerle et al., 2014; Carozzi et al., 2015).

Thalidomide causes peripheral neuropathy in sensory or sensorimotor secondary to microvascular changes as its anti-angiogenic properties. It decreases the expression of tumor necrosis factor alpha (TNF-α), which protects neurons avoiding death in an inhibitory manner (Addington and Freimer, 2016; Coutsouvelis and Corallo, 2004; Dimopoulos et al., 2007).

Proteasome inhibitor, bortezomib, inhibits the 26s ribosome subunit, preventing protein degradation, and affects the polymerization of α-tubulin, leading to cell cycle arrest and

apoptosis (Curran and McKeage, 2009; Poruchynsky et al., 2008). In the Wistar rat study, the bortezomib induces satellite cell intracytoplasmic vacuolization by damaging the mitochondria and endoplasmic reticulum. It also causes moderate pathological changes in Schwann cells, myelin, and axonal degeneration in DRG, but the morphology of spinal cord is normal (Cavaletti et al., 2007).

1.6.2 CIPN and Axon transport, axonal degeneration

Platinum, vinca alkaloids and bortezomib inhibit the processes of tubulin polymerization and depolymerization, which affects the microtubule dynamics. Microtubule dynamics is important for both of the anterograde and the retrograde transport which is relying on axon. Disrupting microtubule dynamics induces dysfunction of the axonal cytoskeleton, which contributes to the development of neuropathy. In addition, axon degeneration, either directly or indirectly caused by the chemotherapeutic agents, is a significant phenotype in neuropathy. The axonal response to injury linked to CIPN has been reported in several studies. Axonal degeneration with myelinated fibers was revealed with electron microscopy in peripheral nerves in patients treated with cisplatin. In addition, vincristine, paclitaxel, and oxaliplatin were also reported to induce sensory axon degeneration and loss of nerve fibers (Argyriou et al., 2008; Boehmerle et al., 2014; Boyette-Davis and Dougherty, 2011; Sahenk et al., 1994).

Blocking axon degeneration could be a way to attenuate the neuropathy. The initial experiments show that the cultured dorsal root ganglion neurons from Wlds mouse have relative resistance to vincristine induced neuropathy (Wang et al., 2001). Recently, Sarm1 deficient mice have been shown to be resistant to vincristine or paclitaxel induced axon degeneration (Geisler et al., 2016; Turkiew et al., 2017). Sarm1 has the NADase activity which depletes NAD+ in axon degeneration. In the vincristine induced neuropathy experiments, Sarm1 intrinsic NADase activity is required for axon degeneration. Inhibiting the NADase activity, vincristine induced axon degeneration can be significantly blocked (Essuman et al., 2017). More evidences show that constitutive expression NMNAT1 or NMN deaminase is involved in protecting animals against by vincristine induced peripheral neuropathy (Di Stefano et al., 2017; Sasaki et al., 2009). Both of NMNAT1 and MNM play roles in the Sarm1 mediated axon degeneration. Therefore, inhibition of the pro-

degeneration cellular pathway for axon degeneration, such as Sarm1, or enhancing the anti-degeneration molecules, such as NMNAT1 or NMN deaminase, could be a useful strategy to attenuate the side adverse of chemotherapeutic agents (Fukuda et al., 2017).

2. Aims

Upon peripheral nerve injury, Schwann cells dedifferentiate to promote the clearance of axon fragments ahead of axonal re-growth from the proximal stump which remains associated to the neuronal perikaryon (Jessen et al., 2015). Expeditious axonal regeneration is important because sustained Schwann cell denervation leads to protracted loss of glial terminal phenotype and eventual death of neuron. In turn, glial cell loss impairs regenerating nerve myelination and circuit repair, transforming acute neuropathies into irreversible chronic neurological dysfunction. Therefore, inhibiting or delaying axon destruction has been hypothesized as an effective strategy to counter heightened Schwann cell vulnerability to additional stressors that include metabolic imbalance and drugs (Jortner, 2000; Morell and Toews, 1996). This idea has sparked intense academic and commercial efforts to identify specific molecular inhibitors of axon degeneration for clinical applications (Koeppen, 2004; Simon and Watkins, 2018). Sarm1 has been reported in regulating axon degeneration after injury. In *Drosophila* and mouse, loss of *dSarm1* or Sarm1 prevents the Wallerian degeneration of transected nerves (Osterloh et al., 2012). Sarm1-deficient mouse has been reported to attenuate axonal injury and to improve functional outcome after traumatic brain injury. Thus, Sarm1 could be a possible target for clinical application. However, in case of the Sarm1 inhibition which causing axonal degeneration blocking, the potentially deleterious effect and the recovery ability of the injury nerve remain unknown. In addition, the influence of Sarm1 deficiency on Schwann cells, on the macrophages response to axon degeneration, and on behavioral performance is still unclear.

Zebrafish is a small vertebrate whose nervous system is anatomically simpler but structurally and functionally similar to that of mammals (Friedrich et al., 2013). Crucially, zebrafish larva is ideal to study axonal degeneration and regeneration, and Schwann-cell biology in the natural context of the behaving animal (Bin and Lyons, 2016; Rosenberg et al., 2014; Xiao et al., 2015a). Moreover, its nervous system is as functionally sophisticated as that of adult zebrafish. Yet, it is anatomically simpler, rendering it ideal for high-resolution observation and controllable experimental manipulations.

The aim of my study was to answer a number of seminal questions about the roles of Sarm1 in sensory neurons and glial cells, axon degeneration and regeneration; the effect of Sarm1 deficiency on the development and behavioral performance of zebrafish; the possibility of clinical applications by inhibiting Sarm1. The specific aims of my thesis are following:

1) To generate the loss of Sarm1 zebrafish. There is no report about Sarm1-deficient zebrafish until now. The Sarm1-knockout fish is the fundamental tool to exploit the role of Sarm1 in zebrafish.

2) To investigate the role of Sarm1 in axon degeneration and regeneration in zebrafish. Taking the advantage of zebrafish, it is possible to study the process of axonal degeneration and regeneration by taking long-time live imaging with high-resolution microscopy.

3) To reveal the role of Sarm1 in the development of Schwann cells and the role of Schwann cells in axon degeneration and regeneration. With the Sarm1-deficient zebrafish, I can furtherly study the dynamics of Schwann cells in axon degeneration and regeneration and the role of Sarm1 in Schwann cells.

4) To assess the role of Sarm1 in macrophage response to injury and fragmented axons. With the transparent zebrafish larva, it is possibly to assess the behavior of the macrophages *in vivo*.

5) To evaluate the possibility of targeting on Sarm1 as the clinical application to reduce chronic consequence of nerve injury systemically. Here, I combine microsurgery, multicolor high-resolution intravital microscopy, electrophysiology, pharmacology and behavioral tests to provide novel insights of Sarm1 into the cellular basis of axon degradation, nerve repair, and the possibility of Sarm1 inhibition for clinical application.

3. Materials and Methods

3.1 Zebrafish strains and husbandry

a. The zebrafish lines for my experiments were the following strains:

AB	(Faucherre et al., 2009)
Casper	(Faucherre et al., 2009)
Tg[UAS:EGFP]	(Faucherre et al., 2009)
Tg[HGn39D]	(Faucherre et al., 2009)
Tg[SILL:mCherry]	(Faucherre et al., 2009)
Tg[Brn3c]	(Faucherre et al., 2009)
Tg[gSAGFF202A]	(Xiao et al., 2015a)
Tg[UAS:GCaMP7a]	(Muto et al., 2013),
Tg[MBP:tgRFP]	(Auer et al., 2018),
Erbb2 mutants	(Lyons et al., 2005; Xiao et al., 2015a)
Tg[Sarm1-/-]	(in this thesis)
Tg[mfap4:EGFP-CAAX]	(in this thesis)
Tg[SILL:ratTRPV1-tgRFP]	(in this thesis)

b. The zebrafish (*Danio rerio*) were maintained in a centralized facility in accordance to guidelines by the Ethical Committee of Animal Experimentation of the Helmholtz Zentrum München, the German Animal Welfare act Tierschutzgesetz §11, Abs. 1, Nr. 1, Haltungserlaubnis, to European Union animal welfare, and to protocols number Gz.:55.2-1-54-2532-202-2014 and Gz.:55.2-2532.Vet_02-17-187 from the "Regierung von Oberbayern", Germany.

The facility keeps 14/10 h light/dark cycle at 28.5 °C. The embryos for experiments were kept with E3 or 30% Danieau's solution in incubator at 28.5°C. All the experiments were performed strickly in accordance with the protocols.

3.2 List of chemicals and reagents

Paraformaldehyde (PFA*)*	Sigma-Aldrich, P6148
Tricaine (MS-2222)	PharmQ, UK
Sodium chloride (NaCl)	Merck, 1.06404.5000
Potassium chloride (KCl)	Sigma-Aldrich, P9541-500G
Calcium chloride dihydrate (CaCl2·2H2O)	Sigma-Aldrich, C3306-250G
Magnesium sulfate (MgSO4)	Sigma-Aldrich, M5921 500G
Trizma (TRIS base)	Sigma-Aldrich, G8898
Sodium dodecyl sulfate (SDS)	Sigma-Aldrich, L3771
Glycine	Sigma-Aldrich, T1503-1KG
HCl	Sigma-Aldrich, H1758-500ML
Ammonium persulphate (AP)	Sigma-Aldrich, 215589
Tetramethylethylenediamine (TEMED)	Sigma-Aldrich, T7024
Kanamycin sulfate	Sigma-Aldrich, 60615
Ampicillin	Sigma-Aldrich, 10835242001
capsaicin	Sigma-Aldrich, M2028
10-Hydroxycamptothecin (10-HCT)	Sigma-Aldrich, H3148
Blotto, non-fat dry milk	Santa Cruz, sc-2324
Paclitaxel	Cayman CHEMICAL, 10461
Docetaxel	Cayman CHEMICAL, 11637
Oxaliplatin	AdipoGen, AG-CR1-3592-M005
Cisplatin	Cayman CHEMICAL, 13119
Vincristine	Santa Cruz, sc-201434
QIAquick Gel Extraction kit	Cat.no.28706
DH5α Competent Cells	Thermo Scientific™, 18263012
TOP10 competent cells	Invitrogen™, C404010
DraI	Thermo Scientific™, FD0224)
BsaI	Thermo Scientific™, FD0294
PmeI	Thermo Scientific™, ER1341

NotI	Thermo Scientific™, FD0595
REDExtrac-N-AmpTM Tissue PCR Kit	Sigma-Aldrich
Extraction Solution	Sigma-Aldrich, E7526
Tissue Preparation Solution	Sigma-Aldrich, T0373
Neutralization Solution B	Sigma-Aldrich, N3910
DreamTaq	Thermo Scientific™, EP0702
T4 ligase	NEB, M0202
poly (A) tailing kit	Ambion™, AM1350
MEGA shortscript T7	Ambion™, AM1334
mMESSAGE mMACHINE T7 kit	Ambion™, AM1344
mMESSAGE mMACHINE SP6 kit	Ambion™, AM1340
BP Clonase™ Enzyme Mix	Invitrogen™, 11789-013
LR Clonase™ Enzyme Mix	Invitrogen™, 11791-019
RIPA lysis buffer	Thermo Scientific™, 89900
BCA Protein Assay Kit	Pierce™, 23227
Protease inhibitor cocktail	Roche, 04693159001
30% Acrylamide/Bis solution, 29:1	BioRad, 1610156
PVDF membrane	Thermo Scientific™, LC2005
Prestained Protein Ladder	Thermo Scientific™, 26619
Mouse anti-acetylated tubulin	Sigma-Aldrich, T7251
Rat anti-Claudin-k	(Münzel et al., 2012)
Mouse anti-6D2	(López-Schier and Hudspeth, 2005)
Rabbit anti-Sarm1	ANASPEC, 55381
Mouse anti-β-Tubulin	Sigma-Aldrich, T5168
Donkey anti-Mouse Alexa Fluor® 555	Abcam, ab150106
Pierce™ ECL Western Blotting Substrate	Thermo Scientific™, 32109
UltraPure™ Low Melting Point Agarose	Invitrogen™, 16520100)
VectaMount® Permanent Mounting Medium	VECTOR, Cat. NO: H-5000

Donkey anti-Rat IgG H&L (Alexa Fluor® Abcam, ab150155
647) pre-adsorbed

Peroxidase-Affini Pure Goat Anti-Mouse IgG Jackson ImmunoResearch, 115035003
(H+L)

Peroxidase-Affini Pure Goat Anti-Rabbit IgG Jackson ImmunoResearch, 115035144
(H+L)

3.3 List of plasmids and primers

1   List of plasmids

pMLM3613	Addgene, 42251
pDR272	Addgene, 42250
SILL:mCherry	(Faucherre et al., 2009)
SILL:Gal4	(Faucherre et al., 2009)
pCS^{2+}-Tp Transposase	(Faucherre et al., 2009)
mbp:EGFP-CAAX	(Auer et al., 2018; Czopka and Lyons, 2013)
UAS: ratTRPV1-tagRFP	(Tim Czopk lab)
pDONR221	(Faucherre et al., 2009)
pDONRP2R-P3	(Faucherre et al., 2009)
pDestTol2pA2	(Faucherre et al., 2009)
p3E-mCherry	(Faucherre et al., 2009)
p3E-polyA	(Faucherre et al., 2009)
SILL:Sarm1-v2a-mCherry	(in this thesis)
SILL:Sarm1△TIR-v2a-mCherry	(in this thesis)
SILL:mito-mCherry	(in this thesis)
SILL:Kaede	(in this thesis)
Sill:Synapsin1-mCherry	(in this thesis)
mfap4:EGFP-CAAX	(in this thesis)

SILL:mitoRGECO   (in this thesis)

SILL:erGCaMP3   (in this thesis)

SILL:ratTRPV1-tagRFP   (in this thesis)

The plasmids were generated using Tol2 kit (Kwan et al., 2007). Mitochondria in lateralis neurons were marked by expressing the mitochondria targeting sequence from the Cytochrome-C oxidase subunit 8A fused to mCherry. The plasmids containing mito-RGECO and er-GCaMP3 (Esterberg et al., 2016) were gifts from David W. Raible (University of Washington).

2 List of primers (sequence 5'-3')

sgRNA (sarm1) oligonucleotides:

oligo1_TAGGGACTTGGAAGAGACCCGC

oligo2_AAACGCGGGTCTCTTCCAAGTC

Genotyping primers for Sarm1 mutants:

Forward_GATTTGCCGTTATCTCTCCA

Reverse_TCAAGCAGTTTGGCAGACTC

pMiddle-Sarm1-v2a-mCherry:

Forward_GGGGACAAGTTTGTACAAAAAAGCAGGCTCAGCCACCATGTT
TTTGTCCCTCGTCGT

Reverse_GGGGACCACTTTGTACAAGAAAGCTGGGTACTACTTCTTTTGT
GGCTCTTTTT

overlap of mCherry and the v2A sequence:

Forward_TCATCTCAGAAGAGGATCTGGGAAGCGGAGCTACTAACTTCA
GCCTGCTGAAGCAGGCTGGAGACGTGGAGGAGAACCCTGGACCTATG
GTGAGCAAGGGCGAGGA

Reverse_TCCTCGCCCTTGCTCACCATAGGTCCAGGGTTCTCCTCCACGT
CTCCAGCCTGCTTCAGCAGGCTGAAGTTAGTAGCTCCGCTTCCCAGAT
CCTCTTCTGAGATGA'

pMiddle- Sarm1△TIR-v2a-mCherry:

Forward_CCCTGCTTAACCGATTCCCAGGATAACTTTGTGTGGCCTGA

Reverse_TCAGGCCACACAAAGTTATCCTGGGAATCGGTTAAGCAGGG

pMiddle-mito-mCherry:

Forward_GGGGACAAGTTTGTACAAAAAAGCAGGCTTTATGTCTGGACT
TCTGAGGGGA

Reverse_GGGGACCACTTTGTACAAGAAAGCTGGGTACTACTTCTTTTGT
GGCTCTTTTT

Overlap of mitochondria and mCherry:

Forward_GCCACCGCGGCCGCCATGGTGAGCAAGGGC

Reverse_GCCCTTGCTCACCATGGCGGCCGCGGTGGC

pMiddle-Kaede:

Forward_GGGGACAAGTTTGTACAAAAAAGCAGGCTCAGCCACCATGGT
GAGTCTGATTAAACCAG

Reverse_GGGGACCACTTTGTACAAGAAAGCTGGGTACTACTTACTTGA
CGTTGTCCGGCA'

pMiddle-Synapsin1:

Forward_GGGGACAAGTTTGTACAAAAAAGCAGGCTCAGCCACCATGA
ATTACCTGCGACGTCGA

Reverse_GGGGACCACTTTGTACAAGAAAGCTGGGTACTACTTCCACGG
AGAAGAGGCTTG

p5E-mfap4:

Forward_GGGGACAACTTTGTATAGAAAAGTTGTTGCGTTTCTTGGTACA
GCTGGA

Reverse_GGGACTGCTTTTTTGTACAAACTTGCCACGATCTAAAGTCATG
AAG

pMiddle-mitoRGECO:

Forward_GGGGACAAGTTTGTACAAAAAAGCAGGCTTTATGTCTGGACT
TCTGAGGGGA

Reverse_GGGGACCACTTTGTACAAGAAAGCTGGGTTCTACTTCGCTGTC
ATCATTTG

pMiddle-erGCaMP3a:

Forward_GGGGACAAGTTTGTACAAAAAAGCAGGCTTTATGGAACACAG
CGGGATTCTG

Reverse_GGGGACCACTTTGTACAAGAAAGCTGGGTTCTACTTCGCTGTC
ATCATTTG

pMiddle-ratTRPV1-tgRFP:

Forward_GGGGACAAGTTTGTACAAAAAAGCAGGCTCAGCCACCATGG
AACAACGGGCTA

Reverse_GGGGACCACTTTGTACAAGAAAGCTGGGTACTACTTCTTTTGT
GGCTCTTTTT

3.4 Plasmids construction

BP reaction for cloning the PCR products into the pDonors: (Dilute the PCR products and pDonor vectors to 50 fentmole with TE buffer, pH 8.0)

50 fentmole (fm) = 1000 bp / 33 ng

For 10 μL BP reaction:

pDonor middle (5'E), 50 fm	1 μL
PCR product, 50 fm	1 μL
TE buffer, pH 8.0	6 μL
BP enzyme	2 μL

The reaction was incubated at 25°C for 1 hour. Then, the reaction was stopped by incubating with 1 μL Proteinase K for 15 mins at 37°C. Afterwards, 2 μL of BP

reaction was transformed into DH5α competent cells, which were cultured in kanamycin resistant plate.

The positive pMiddle-target gene vectors were confirmed by sequencing with M13 Fwd or/and M13 Rev primers.

Next, the LR reaction was performed to get the Tol2 constructs: (Dilute all the needed vectors to 20 fentmole with TE buffer, pH 8.0)

For 10 μL LR reaction:

Destination vector, pDonor, 20 fm   1 μL

Entry vector 1, p5E (SILL, UAS, or mfap4), 20 fm   1 μL

Entry vector 2, p3E (poly (A) or mCherry or RFP), 20 fm   1 μL

Entry vector 3, pMiddle (for example: Sarm1-v2a-mCherry or   1 μL
mitoRGECO), 20 fm

TE buffer, pH 8.0   4 μL

LR clonase™ II enzyme   2 μL

The LR reaction was incubated at 25°C for 1 hour. Then, the reaction was added 1 μL Proteinase K for digestion 15 mins at 37°C. Afterwards, 2 μL of reaction was transformed into TOP10 competent cells. Then, the cells were cultured in kanamycin resistant plate.

The positive colonies were confirmed by restriction enzyme digestion.

3.5 Sarm1 mutagenesis

1. Prepare the sgRNA and Cas9

    1) sgRNA

        a. Clone the sgRNA construct

        The oligonucleotides of sgRNA were designed on the website. First, I screened the first exon of sarm1 with the on-line tool "ZiFiT Targeter software package" (http://zifit.partners.org) (Wright et al., 2006). The target sequence

5'-GGGACTTGGAAGAGACCCGC-3' was selected to clone into the sgRNA transcription construct, pDR274.

The oligonucleotides were annealed at 95°C for 10 mins. Then the oligonucleotides were kept at room temperature for 2 hours. Before ligation, the annealed oligonucleotides were digested with BsaI for 30 mins at 37°C. The vector, pDR274 had already been linearized with BsaI and was purified with QIAquick Gel Extraction kit. After 10 mins ligation with the T4 ligase, 5 μL of the ligated product was transformed into DH5α Competent Cells, and was cultured in Ampicillin resistance plate. The correct constructs were confirmed by sequencing.

The reaction for restriction enzyme digestion:

2-5 μg DNA or 20 μL annealed oligos, 5 μL 10x buffer, 10 units Fast digestion
  Enzyme, ddH$_2$O up to 50 μL.

The digestion was incubated at 37°C for 0.5-1 hour. Then, the enzyme was
  inactivated at 85°C for 10 mins. The digested DNA was purified by gel
  electrophoresis.

T4 ligation system (10 μL):

1 μL annealed oligos, 1 μL linearized pDR274, 1 μL 10x T4 buffer, 0.5 μL T4 ligase, 6.5 μL ddH$_2$O, incubated at room temperature for 10 mins.

b. *In vitro* transcript, sgRNA

The constructs which had already incorporated the sgRNA target sequence were linearized with DraI for 3-4 hours at 37°C. Then, the purification was done with the QIAquick Gel Extraction kit. For *in vitro* transcript, 200 ng linearized plasmid was used for the T7 promotor transcription system.

In vitro transcript system (20 μL):

2 μL T7 10x buffer, 2 μL T7 ATP, 2 μL T7 CTP, 2 μL T7 GTP, 2 μL T7 UTP, 200 ng linearized plasmid, 2 μL T7 Enzyme mix, up to 20 μL with Nuclease-Free water, and incubated at 37°C for 2 hours.

Next, the template DNA was digested with 1 μL TURBO DNase at 37°C for 15 mins. Finally, the sgRNA was purified with the RNA easy kit and was kept at -80°C.

2) Cas9 mRNA or Protein

    a. Cas9 mRNA

The vector for producing Cas9 mRNA, pMLM3613, was linearized with PmeI and was purified with QIAquick Gel Extraction kit. The linearized pMLM3613 was used as the template to transcript the Cas9 mRNA with mMESSAGE mMACHINE T7 kit.

The reaction system for mRNA transcription (20 μL):
2 μL 10x T7 reaction buffer, 10 μL T7 2x NTP/ARCA, 2 μg Linearized template, 2 μL T7 Enzyme mix, up to 20 μL with Nuclease-Free water, and incubated at 37°C for 2 hours.

Next, the template DNA was digested with 1 μL TURBO DNase at 37°C for 15 mins.

Then, poly (A) tailing reaction was used to add poly (A) to the mRNA.

The reaction system for adding poly (A) (100 μL):
20 μL mMESSAGE mMACHINE reaction, 20 μL 5XE-PAP buffer, 10 μL MnCl$_2$ 25 mM, 10 μL ATP 10 mM, 4 μL E-PAP, up to 100 μL with Nuclease-Free water, incubated at 37°C for 1 hour.

The mRNA was purified with the RNA easy kit and was kept at -80°C.

    b. Cas9 protein

The Cas9 protein was the commercial one from the company, PNA Bio, cat.no. CP01.

2. Microinjection

1) Mixture RNA: Cas9 mRNA 1500 ng, sgRNA 70 ng, added Nuclease Free water to 10 μL.

       1-2 nL of mixture was injected into one-cell stage embryos.

2) Mixture Cas9 protein: Cas9 protein 200 ng, sgRNA 100 ng, added Nuclease Free water to 10 µL.

       1-2 nL of mixture was injected into one-cell stage embryos.

3. Screen the sarm1 mutants

When the injected fish grew up to 2-3 months old, I did fin-cut and extracted the genome with REDExtrac-N-Amp^{TM} Tissue PCR Kit, including the following buffers: Extraction Solution, Tissue Preparation Solution, Neutralization Solution B.

The procedure was following: suspended the samples with 50 µL Extraction Solution, then added 12.5 µL Tissue Preparation Solution and mixed well, incubating at 95°C for 10 mins. Next, added 50ul Neutralization Solution B and mixed well for centrifuging the samples at room temperature with 12000 rpm for 5 mins. Then, 2 µL of the medium was taken as the template for PCR (Polymerase chain reaction).

The PCR system (50 µL):

5 µL 10x buffer, 3 µL 2.5mM dNTP, 1 µL genotyping forward primer, 1 µL genotyping reverse primer, 2 µL template, 0.2 µL Taq Enzyme, 37.5 µL ddH2O up to 50 µL.

Setup for the PCR steps:

95°C   3 mins for initial denaturation

95°C   30 sec for denaturation
60°C   30 sec for annealing   35 cycles
72°C   35 sec for elongation

72°C   10 mins for final elongation
4°C   Holding

Purified the PCR product and sequenced the PCR fragment with the forward primer. The positive fish with mutations was crossed with wild type ones or desire lines for the next generation.

Finally, I obtained germ-line transmission of two independent alleles: sarm1[hzm13] and sarm1[hzm14].

3.6 Transgenic lines

1. Prepare the transposase mRNA and Tol2 constructs

   1) transposase mRNA

   The vector for transposase mRNA, pCS^{2+}-Tp Transposase, was linearized with NotI and was purified with QIAquick Gel Extraction kit.

   The transcription was done with mMESSAGE mMACHINE SP6 kit.

   The reaction system for mRNA transcription (20 µL):
   2 µL 10x SP6 reaction buffer, 10 µL SP6 2x NTP/ARCA, 2 µg Linearized template, 2 µL SP6 Enzyme mix, up to 20 µL with Nuclease-Free water, and incubated at 37°C for 2 hours.

   Next, the template DNA was digested with 1 µL TURBO DNase at 37°C for 15 mins.

   The mRNA was purified with the RNA easy kit and was kept at -80°C.

   2) Tol2 constructs

   The details of these two constructs, mfap4:EGFP-CAAX and SILL:ratTRPV1-tagRFP were section **3.3**.

2. Microinjection

   The concentration was 12.5 ng/µL of both DNA and mRNA, diluting in RNase-free water.

   To make transgenic lines, 25 pg of Tol2 donor plasmid and 25 pg of transposase mRNA were injected into one-cell stage embryos.

3. Screen the transgenic fish

   30-60 embryos (F0) were selected with correct expression of the desire constructs, then the embryos were maintained in the fish facilities;

   F1 founders were getting by outcrossing the F0 ones with the *Tg[Casper]* strain;

   F2 embryos from F1 adults were used to do experiments. The F2 inherited stable transposons in a Mendelian fashion. This helped to evaluate for proper expression based on the promoter used within the injected transposon.

3.7 Immunostaining

Procedure of immunostaining

1) Fixed the larvae with fresh 4% PFA which was dissolved in PBS (phosphate-buffered saline buffer);

   The larvae with indicated dpf (days post fertilization) were anesthetized with Tricaine (MS-222) (0.016% M/V) in Danieau's (1X, 5 mM NaCl, 0.17 mM KCl, 0.33 mM $CaCl_2$, 0.33 mM $MgSO_4$, dissolved in 1 L deionized water). Then, the larvae were fixed with 4% PFA and incubated at 4°C overnight.

2) Penetrated the sample with pre-cold acetone or digested with Proteinase K;

   For samples which were stained with Claudin-k (diluted 1:500) and 6D2 antibodies (diluted 1:5);

   > The samples were washed at room temperature (RT) with PBST (0.2% Tween 20) three times (10mins per wash) after fixation. Then, the samples were incubated in pre-cold acetone 6-10 mins at -20°C. Next, the samples were transferred into ddH_2O at RT for 5 mins. Finally, the samples were washed with PBST for 10 mins at RT.

   For samples which were stained with Acetylated tubulin antibody (diluted 1:1000);

   > The samples were washed at RT with PBST (0.2% Tween 20) three times (10 mins per wash) after fixation.

Firstly, the samples ware dehydrated with gradient solutions (RT, 5 mins per step): 25% methanol (in PBST), 50% methanol (in PBST), 75% methanol (in PBST), and 100% methanol with twice. Then, the samples should be kept at -20°C for at least 1 hour;

Secondly, the samples were rehydrated with the gradient solutions (RT, 5 mins per step): 75% methanol (in PBST), 50% methanol (in PBST), 25% methanol (in PBST), and PBST with twice. Then, the samples were digested with 10 μg/mL final concentration of Proteinase K solution. For 3 dpf larva, the digestion time was 20 mins. For 4 dpf larva, the time was 30 mins. For 5 dpf or 6 dpf, the digestion time was 30 mins with 20 μg/mL final concentration of Proteinase K;

Thirdly, the digested reaction was stopped by incubating the samples in 4% PFA at RT for 20 mins;

Finally, the samples were washed with PBST for three times (5 mins per wash).

3) Blocking the samples with 10% bovine serum albumin (BSA, Sigma A4612) which was diluted with PBST at RT for 2 hours or longer;

4) Incubated the samples with indicated primary antibodies overnight at 4°C;

The antibodies were diluted in the blocking buffer (10% BAS in PBST). When the incubating was done, the samples were washed with PBST for 2 hours (changing the PBST every 30 mins).

5) Incubated the samples with secondary antibodies (diluted 1:200) at 4°C overnight (avoiding light);

The secondary antibodies were diluted in the blocking buffer (10% BAS in PBST). When the incubating was done, the samples were washed with PBST for 3 times, 20 mins per wash.

6) Kept the samples in VectaMount® Permanent Mounting Medium at 4°C or mounted the samples with 0.8% low melting-point agarose on a 35 mm glass-bottom Petri dish for imaging with the laser-scanning confocal microscope (LSM 510, Carl Zeiss) or the spinning disc confocal microscope (Carl Zeiss).

3.8 Intravital microscopy

1. Samples preparation

   The larvae with indicated fluorescence were screened with a fluorescence stereomicroscope. Then, the samples were anesthetized with Tricaine and were mounted in 0.8% low melting-point agarose on a 35 mm glass-bottom Petri dish. The position of the samples was adjusted by the hair-loop glued to the tip of a glass pipette.

2. Videomicroscopy

   a. The Petri dish was loading on the holder of spinning disc microscope. The holder was keeping at 28.5°C with the heating system (Xiao and López-Schier, 2016). The samples were checked with 40x air objective or 60x water-immersed objective (for time lapse imaging, changed the water with the oil for 60x water-immersed objective).

   b. For the video imaging, the interested region was in the central of focus. Then, I set up the top and down boundaries of the images to scope the whole axons or/and Schwann cells. This was the Z-stacks of the images. When Z-stack was ready, the intervals of one stack were set to 0.8 – 1.5 µm. The exposure time of the 488 nm laser for green or 561 nm laser for red were adjusted to 400 ms or 600 ms. Time intervals were 10 minutes or 15 minutes per frame. The whole video imaging can be 12 hours or 24 hours.

3.9 Western blot assay

1. Buffers and Equipment;

   SDS-PAGE: Hand-made 12%

   (5 mL Separating gel: ddH$_2$O 1.65 mL, 1.5 M Tris pH 8.8 1.25 mL, 30% AB 2 mL, 10% SDS 50 uL, 10% AP 50 uL, TEMED 2 uL;

   2 mL Stacking gel: ddH$_2$O 1.4 mL, 1.0 M Tris pH 6.8 0.25 mL, 30% AB 0.5 mL, 10% SDS 20 uL, 10% AP 20 uL, TEMED 2 uL)

   Running buffer (1 L): Tris 3 g, Glycine 18.8 g, SDS 1 g, dissolved into 1 L ddH$_2$O.

Transfer buffer (1 L): Tris 3.03 g, Glycine 14.3 g, dissolved into 800 mL ddH$_2$O, then added 200 mL methanol to 1 L, kept at 4°C.

Protein electrophoresis equipment: BIO-RAD, Mini-PROTEIN® System

2. Procedure of the Westernblot

1) Prepare the sample:

5 dpf larvae were anesthetized with Tricaine in the tubes. 5 mins later, the Tricaine was aspirated;

200 μL of RIPA buffer (pre-cold on ice, with Protease inhibitor cocktail (one plate for 50mL buffer) was added, then the samples were homogenized carefully with tips;

The tubes were putted on ice for further lysis. 20 mins later, the tubes were centrifuged in the tabletop microcentrifuge at 12000 rpm, 4°C for 10 mins. Then, the supernatant was transferred to a new tube;

The protein was measured with BCA assay;

The supernatant was diluted with loading buffer and boiled at 99°C for 5 minutes.

2) Performed the SDS-PAGE and membrane transfer:

Loaded 20 ng proteins for performing the SDS-PAGE and set the voltage to 50 V for samples through the stacking gel, then set 100 V to the separating gel;

The proteins were transferred into PVDF membrane at 100 V for 90 mins (The PVDF membrane should be pre-soaked with methanol and the whole transferring box should be kept at 4°C).

3) Primary antibody incubation:

The membrane was rinsed with PBST and blocked with 5% skimmed milk (diluted with PBST) for one hour at room temperature;

Then, the membrane was incubated with primary antibodies, (rabbit anti-Sarm1, 1:500; mouse anti-β-tubulin, 1:2000), at 4°C overnight.

4) Secondary antibody incubation:

After the primary incubation, the membrane was quickly washed with PBST at RT, 3 times, 10 mins per wash;

Then, the membrane was incubated with secondary antibodies (Peroxidase-Affini Pure Goat Anti-Mouse IgG (H+L), 1:10000; Peroxidase-Affini Pure Goat Anti-Rabbit IgG (H+L), 1:10000) at RT for 1 hour

5) Developing:

The secondary antibodies were washed quickly with PBST, 3 times, 15 mins per wash;

Then, the membrane was incubated with mixed ECL buffer (Buffer A: peroxide solution; Buffer B: luminol enhancer solution) for 1-2 mins;

Finally, the membrane was put into the equipment for getting the images.

3.10 Laser microsurgery

1. Samples preparation:

The larvae with injected constructs or from crossed directly were anesthetized and were screened for the positive ones. Then, anesthetized larvae were mounted with low melting-point agarose in the Petri dish, which was loaded to the platform of spinning disc microscope for laser microsurgery.

2. Microsurgery:

The laser system for microsurgery is from Roper scientific AS. It is set up with an ultraviolet laser using the iLasPulse system and is compiled into the software, VISION, for further manufacturing. The laser is 350 nm, and with 400 ps/2.5 uJ per pulse (Pujol-Martí et al., 2014; Xiao and López-Schier, 2016; Xiao et al., 2015b)

Then, the samples were checked with 63x water-immersion objective (the laser beam works in 63x objective) and the interesting region for surgery was selected;

Next, the laser pluses were calibrated and adjusted the power to 27 mW with the control panel;

A rectangle region was selected for transection. The pulse was 0.05 ms performing and 3 times/mouse click. To fully sever the axons, the laser pulses should be applied repeatedly until it was a clear gap in the rectangle region. Then, the rectangle region was moved to the next position. The samples were observed again one hour later to confirm that the axons were completely transected.

3.11 Chemogenetic approach

1. Samples preparation:

   For chemogenetic experiments, the UAS: ratTRPV1-tagRFP was used to response the capsaicin for calcium channel control.

   The embryos from *Tg[UAS:GCaMP7a]* were co-injected the two constructs, SILL:Gal4 and UAS : ratTRPV1-tagRFP. The positive larvae were selected under fluorescence stereomicroscope at 4 dpf.

2. Calcium channel manipulating:

   For activating the TRPV1 channel, I used 2 μM capsaicin final concentration in the experiment.

   Then, the larva was mounted in the dish which was loaded on the holder of spinning disc;

   The region for imaging was selected for imaging (the 63x water-immersion objective with an exposure time of 400 milliseconds. The imaging was taken by two channels (488 nm for GCaMP7a and 561 nm for TRPV1-tgRFP labeled axons) and was lasting for one hours with 2 or 3 mins per frame.

   The capsaicin was added into the medium up to 2 μM final concentration at 20 mins after imaging started.

   Ablation the axons in Sarm1 mutant:

   Sarm1 mutant larvae, the HGn39D with SILL-Gal4; UAS: mCherry or SILL-Gal4; UAS: ratTRPV1-tagRFP positive animals were axotomized by the laser.

2 hours after axons transection, the larvae were treated with 10 μM capsaicin or ethanol (1:1000, V/V). 1.5 hours after capsaicin treatment, images were taken by spinning disc microscopy.

3.12 Electrophysiological recordings

(This protocol is from Melanie Haehnel-Taguchi.)

1. Samples preparation:

    4-5 dpf larvae were anaesthetized in 0.03% Tricaine solution and paralyzed in 0.1% α-bungarotoxin (Molecular Probes);

    Samples were rinsed and mounted laterally with tungsten pins on Sylgard lined dishes.

2. Preparation for recording:

    Recordings were performed as previously described in the paper (Haehnel-Taguchi et al., 2014), with some modifications.

    a. Recordings of action potentials in lateralis afferent neurons were made in extracellular solution (NaCl 134 mM, KCl 2.9 mM, $MgCl_2$ 1.2 mM, HEPES 10 mM, Glucose 10 mM, pH 7.8, osmolarity 290 mosM), under an Axioskop microscope (Zeiss) modified to a fixed-stage set-up, using DIC optics;

    b. Action potentials were recorded in loose patch configuration from afferent neurons of the posterior lateral line with borosilicate glass pipettes pulled (Sutter P-2000) to a resistance of 3.5-6 MΩ in extracellular solution.

    c. Data were acquired with a Multiclamp 700 B amplifier and a Digidata 1440 A digitizer using pClamp10 software (Molecular Devices).

3. Electrophysiological recording:

    1) Recordings were made in current clamp mode, sampled at 20 kHz and filtered at 1 kHz. Direct mechanical stimulation of hair cells was achieved using a water jet from a glass micropipette (tip diameter~30 µm) driven by a pressure

pump (ASI MPPI-3) triggered by a voltage output signal from the Digidata 1440 A;

2) The stimulation pipette was positioned parallel to the fish trunk along the midline in proximity to a neuromast. Neuromasts were sequentially stimulated with a test pulse until an evoked response was detected;

3) Once a response was detected, 20 pressure pulses were applied during 5 seconds long sweeps, with one-second delay and 100-millisecond duration;

4) Spontaneous spike rate was recorded before stimulation during 12-120 seconds. Spike rate before each stimulus was calculated during the first 200 milliseconds of a recording sweep and evoked spikes were calculated from spikes during 200 milliseconds after stimulus onset;

5) Latency was measured as the first spike after stimulus onset. Spike rate and latency were averaged from 20 stimulations for each recording;

6) Spike detection from recordings was done in DataView (Version 11.0, W. Heitler, University of St. Andrews) by setting a negative threshold at 4X the standard deviation of the first 1000 milliseconds of the recording;

7) Further data analysis and statistics were performed using Matlab (Version 8.6 R2015b).

3.13 Behavioral assays

1. Touch invoked escape response:

   a. Samples preparation:

   2 dpf embryos were gently dechorionated and were kept in Danieau's solution at 28ºC for at least 1 hour before experiment.

   b. Recording the behavior of larvae under stimulation:

   Embryos were placed into a flat uncovered Petri dish containing Danieau's and were recorded with a high-speed camera (NX4 series, Imaging solution, GmbH);

Video recording was launched and a randomly chosen embryo was touched with a blunt glass needle until it evoked a reaction. Recordings were done under white-light illumination over 150 seconds at a rate of 200 frames per second (fps);

The swimming trajectories were obtained with 3D Particle Tracker plugin, ImageJ software. The further quantification and statistics were performed by Python.

2. Rheotaxis experiments (Asgharsharghi, 2019):

(This setup was designed and was assembled by Amir Asgharsharghi Bonab. I performed the experiments under Amir's supervision. Amir got the data from the recording videos. I plotted the results and performed the statistical test.)

a. Setup for recording the Rheotaxis:

The behavioral rig is designed to evaluate zebrafish orientation to the direction of water flow under laminar conditions in darkness and in isolation from significant environmental noise, as described in Amir' preparing paper, *Mechanosensory Control of Rheotaxis in Larval Zebrafish*. The rig is constructed of a Plexiglas® pipe with inner diameter of 2.4 cm filled with the water. One side of the pipe is connected to the water reservoir and in the other side is the plunger connected to the motor shaft. Movement of the motor shaft displaces the plunger back and forth causing the water flow inside the tube. The rig was illuminated with an infrared light-emitting diode (LED) array (IR: 940 nm). Images of fish movement were captured with a high-speed camera (NX4 series, Imaging solution, GmbH) at 200 frames per second (fps). Captured images were saved on the computer hard drive for further analysis.

b. Samples preparation:

The fish for rheotaxis assay were 7 dpf larvae. Here, I prepared the fish with following groups (for WT and Sarm1$^{-/-}$);

intact 7 dpf larva, sham ablation larva, 3 days recovery larva (ablation at 4 dpf), and one day recovery larva (ablation at 6 dpf).

Ps: ablation group indicated that all the axons of one side lateral line was cut (including the anterior and posterior neurons), following the protocol of laser microsurgery.

c. Recording the larva behavior:

For rheotaxis recording, the fish was placed and was kept in the rig for at least 30 mins prior to do the experiment;

Set the speed of the motor to 6 mm / sec. When the fish was closed to the plunger and was with a long distance for swimming, I started to record and pushed the motor movement;

For each fish, there were 10 trails done with 5-10 mins interval for fish adapting to the environment;

Animal tracking and orientation analysis were done using the Bonsai software;

The orientation of the fish relative to flow direction was used to derive a rheotactic performance.

3.14 Quantification of mitochondrial density and motility

1. Imaging

a. For imaging the mitochondria in the axons, I injected the SILL:mito-mCherry into the embryos from WT or Sarm1$^{-/-}$ to label the single axon with mito-mCherry.

b. The imaging was done with the 63x water immersion objective. Each imaging was 3 mins-long with one second interval.

2. Quantification

a. For density quantification, images were inverted to black and white. Then, I used the Fiji software (*http:fiji.sc*) to calculate the area of the signal.

b. For movement quantification, the plugin, Multi-Kymograph was used to generate kymographs of mitochondrial movement;

The movement of mitochondria was determined by the slope of lines drawn over time, and the direction of movement was determined by the moving mitochondria crossing the time line (vertical) in the kymographs;

The data were analyzed with the Graphpad Prism software.

3.15 Calcium imaging and quantification

1. Imaging

   a. For calcium imaging in lateralis neurons, *Tg[SILL:Gal4; UAS:GCaMP7a]* double-transgenic larvae were anesthetized and were mounted in 0.8% low melting-point agarose on a 35mm glass-bottom Petri dish.

   b. Imaging was acquired through a 63x water-immersion objective with an exposure time of 400 milliseconds. Laser-mediated axon transection was done after the fourth imaging of time series. Next, the videomicroscopy was done for 2 minutes at a frame rate of 400 milliseconds at 28.5°C.

2. Calcium signal quantification

   To quantify the calcium signal, images were processed in ImageJ. The region of interest (ROI) was selected and the density of ROI was measured. GCaMP or RGECO intensity changes were calculated as follows: $\Delta F/F0 = (F–F0)/F0$, where F0 is the value of the fluorescent signal before axons transected, and F is the value of the fluorescent signal with time point after axon severing (Esterberg et al., 2016).

3.16 Statistical analysis

The Student's t-test (two tailed), T-test (Turkey test), ANOVA test, and Wilcoxon rank sum test were applied using Graphpad prism or SigmaPlot software. Error bars in all figures are standard errors of the mean (SEM).

4. Results

4.1 Identification and mutagenesis of Sarm1 in zebrafish

Sarm1 (Sterile Alpha and TIR Motif containing 1) has one MTS (mitochondria target sequence) in the N terminal, followed by two SAM (sterile α motif) domains and one TIR (Toll-interleukin-1 receptor) domain in mouse and human. The amino acid sequence of Sarm1 is conserved across species (Osterloh et al., 2012). To identify Sarm1 orthologous in zebrafish, I screened the publicly accessible genomic data (*Danio rerio reference genome assembly version GRCz11*) by blasting the TIR domain which is present in all known Sarm1 and the Toll-like receptor family proteins. There was only one candidate *sarm1* gene in zebrafish genome, which locates on the chromosome 15 and contains 8 exons that code for a protein consisting of 713 amino acids. Then, I compared the amino acid sequence of zebrafish Sarm1 to the orthologs in human, mouse, and *Drosophila*. The two SAM domains and the TIR domain are conserved in these species. However, I did not find the potential mitochondrial targeting sequence in zebrafish Sarm1 by aligning the N terminal of Sarm1 to mitochondrial located zebrafish proteins, such as COX4I1 (zgc:110058), VDAC1 (zgc:85830) and TOMM20b (zgc:92628). This indicates that Sarm1 lacks an obvious mitochondrial target sequence (**Figure 4.1 A** and **B**).

To study the function of Sarm1 in zebrafish, I generated loss-of-function mutations in Sarm1 gene with CRISPR/Cas9 mediated genome modification. The CRISPR tool is user-friendly and highly efficient for genome editing in zebrafish. A single guide RNA was designed to target the fiftieth amino acid of the sarm1 protein, which is located in the first exon (**Figure 4.1C**). To obtain a mutant zebrafish, I screened the F1 generation fish by sequencing. F1 generations were obtained by crossing the mutation carriers of F0 (injected ones) generation with *Tg[HGn39D]* line, in which lateralis afferent neurons are marked with GFP. I identified germline transmission of two alleles: sarm1[hzm13] and sarm1[hzm14]. The hzm13 allele introduces with 11-base deletion and T/C mutation, resulting in a frame shift and premature stop codon generating a truncated protein lacking all the SAM and TIR domains. The hzm14 harbors a 7-base deletion and AG/GA mutation that generates a frame shift and premature stop codon (**Figure 4.1 D**).

To confirm the absence of Sarm1, I performed Western-Blots with the lysate from 4 dpf (days post fertilization) wild type (WT) and Sarm1[hzm13] larvae, respectively. The commercial Sarm1 antibody recognizes the C terminal of Zebrafish Sarm1. The blots showed one single band approximately to 80KD in the WT that was consistent to the expected size of sarm1 protein in the SDS-PAGE, but I did not detect any band of a comparable size on the lane with the protein extract from Sarm1[hzm13] (**Figure 4.1E**). Taken together, two mutant alleles of Sarm1 have been successfully generated with CRISPR/Cas9 (Tian et al., 2020).
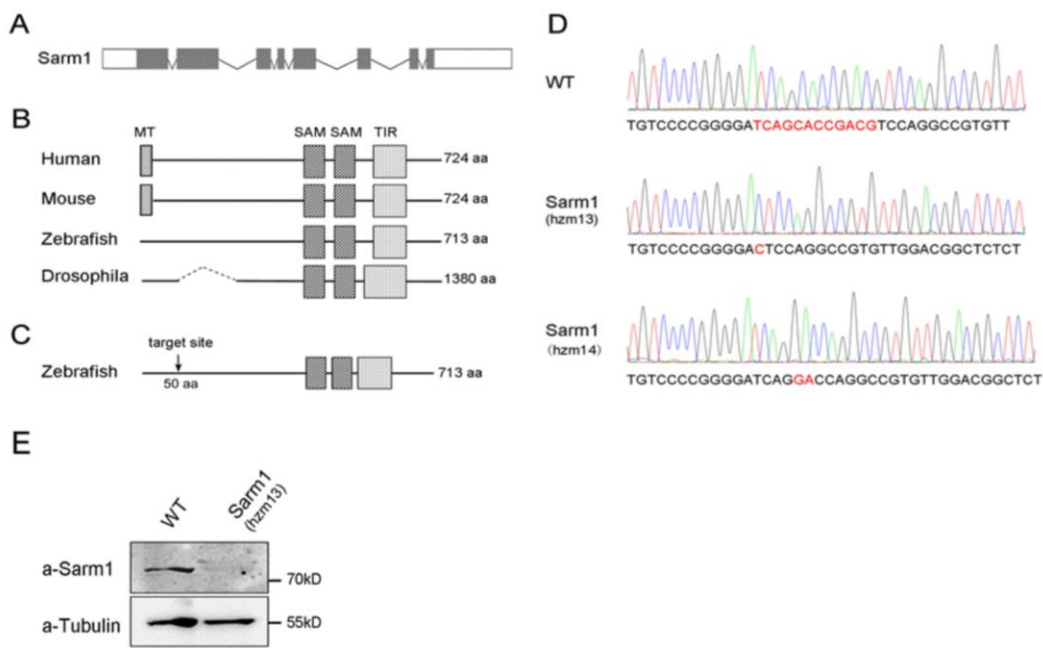

Figure 4.1 Identification and mutagenesis of Sarm1 in zebrafish. A) Genomic structure of *sarm1* gene in *Danio rerio*, indicating 8 exons, with protein coding-regions in grey, non-coding region in white, and introns as bent lines (not in scale). B) Alignment of the Sarm1 functional domains from different species, the MT (mitochondrial targeting sequence) is conserved in mouse and human, the two SAM domains and one TIR domain are conserved in all these species. C) Structure of the zebrafish Sarm1 protein highlighting the two SAM domains (dark grey), the TIR domain (light grey). The downward arrow indicates the region targeted for mutagenesis (sgRNA target site), approximately 50 amino acids from the start codon. D) Sequence of the WT and Sarm1 mutants, the mutagenized region is indicated in red. The hzm13 allele introduces an 11-base deletion and T/C mutation, resulting in a frame shift and premature stop codon. The hzm14 allele is a 7-base deletion and AG/GA mutation that also generates a frame shift and premature stop codon. E) Western blots of protein extracts from WT and Sarm1[hzm13]

fish embryos with a commercial antibody which recognizes the N-terminal of Sarm1, revealing absence of the protein in the Sarm1 mutants. Blot of the expression of tubulin is the loading control (modified from Tian et al., 2020).

4.2 Sarm1 is dispensable for the development and maintenance of a sensorineural pathway

To assess the effects of absence of Sarm1 in the nervous system, I examined several parameters of neuronal structure and circuit function by combining sarm1[hzm13] (hereafter: Sarm1-deficient or Sarm1^{-/-}) with various transgenic lines, expressing fluorescent markers in the afferent neurons of the mechanosensory lateral line, as well as in their associated Schwann cells (Ghysen and Dambly-Chaudière, 2007; Lopez-Schier and Pujol-Martí, 2013). The zebrafish lateral-line system is ideal for *in vivo* studies at high-resolution over extended periods, and for physiological studies under normal and altered conditions (Drerup and Nechiporuk, 2016; Haehnel-Taguchi et al., 2018; Pujol-Martí et al., 2014). It combines the organization of a typical vertebrate sensory system with the amenability for controlled experimental interventions that include microsurgery, pharmacology, and optogenetics (O'Donnell et al., 2013; Vargas et al., 2015; Xiao et al., 2015a). Additionally, the lateral line mediates a robust behavioral reaction to water currents called rheotaxis, which can be easily quantified by measuring the orientation of animals to the direction of water flow (Oteiza et al., 2017).

Firstly, I found there were no obvious anatomical defects in the Sarm1^{-/-}, including the size, shapes and locations of organs from the images of 5dpf wild type and Sarm1^{-/-} zebrafish larvae with bright-field microscopy (**Figure 4.2.1A**). In the adult stage (around 3-4 months), Sarm1^{-/-} zebrafish were viable, normally developed and fertile, as compared to their WT siblings. Next, I performed immunostainings with an antibody that recognizes acetylated tubulin, which can be used to highlight axons and stain the whole nervous system in zebrafish and mammals. The structure of the nervous system showed no anatomical defects in the whole brain in 4 dpf Sarm1^{-/-} larva, comparing to the WT. Moreover, the shape and the connections of neurons in the forebrain and midbrain showed no difference between WT and Sarm1^{-/-} (**Figure 4.2.1B**).

To analyse the function of the nervous system in development, I examined the touch-evoked escape response, a simple assay to monitor sensorimotor function that consists of eliciting the escape response after tactile stimuli (Sztal et al., 2016). The escapes were recorded with a high-speed camera when the 2 dpf larvae were stimulated with a tiny needle. The time-lapse images showed that the larvae escaped quickly when the needle was close to their bodies, and they preferred to swim to the opposite direction of the needle (**Figure 4.2.1C**). The quantification of swimming distance showed that the average of total distance was around 40 mm in both groups and there was no statistical significance (**Figure 4.2.1D**). Acceleration of escape is used to measure the ability to swim immediately after stimulation (Burgess and Granato, 2007). My quantification showed that there was no statistical difference in acceleration between WT and Sarm1$^{-/-}$ (**Figure 4.2.1E**). Taken together, these results demonstrate that loss of function of Sarm1 impacts neither the neural development nor the growth of the zebrafish. Moreover, the neural wiring, especially the innervation between sensory neurons and muscle was not affected in Sarm1$^{-/-}$ zebrafish, as inferred from the normal escape response (Tian et al., 2020).
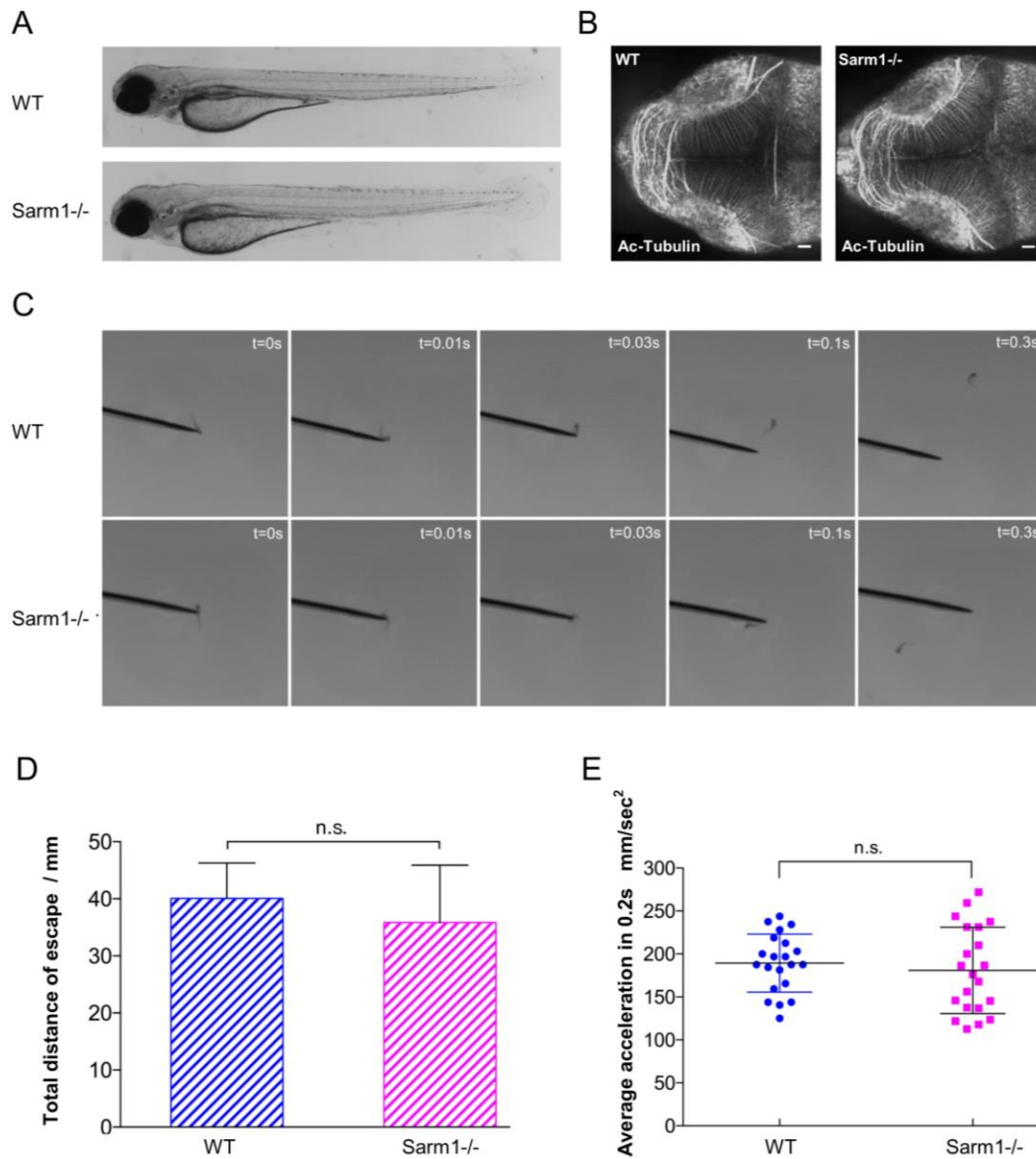
Figure 4.2.1 Overview and touch-evoked escape tests of wild type and Sarm1^{-/-} zebrafish. A) Low-magnification image showing the whole view of a WT 5 dpf zebrafish (top) and a Sarm1^{-/-} (bottom), no overall anatomical differences. B) Confocal image of dorsal view of a WT 5 dpf zebrafish (left) and a Sarm1^{-/-} (right) larva stained with an antibody against acetylated Tubulin to mark neurons in the central nervous system, showing no evident defects in the Sarm1^{-/-}. In this and all figures, rostral is left and caudal is right. Scale bar 20 µm. C) Time lapse images showing the escape response behavior of 2 dpf larva upon stimulus; Up panels showing the escape of WT larva, down panels showing the escape of Sarm1^{-/-} larva. Times are indicated in the upper-right of the images. D-E) Quantification of sensorimotor function in zebrafish; (D) shows the total distance traveled by larvae after touch-trigger escape response in WT (dashed blue bar) and Sarm1^{-/-} (dashed magenta bar). (E) Dot-plot of the average acceleration of WT (blue) and Sarm1^{-/-} (magenta) after tactile touch-induced escape response. Error bar = SEM; n.s.

means no significant difference, Student's t-test. WT n = 21, Sarm1$^{-/-}$ n = 21 (modified from Tian et al., 2020).

Secondly, I examined the development of sensory neurons in Sarm1$^{-/-}$ zebrafish by combining it to the sensory neuron labeled transgenic line *Tg[HGn39D]*. In this transgenic line, all the peripheral sensory neurons which connect the sensory organs of the lateral line to the brain are labeled with green fluorescence protein. The confocal microscopy images showed that lateralis afferent neurons appeared of normal size and localization in the head, and were polarized correctly in WT and Sarm1$^{-/-}$. Additionally, neuronal central projections along the length of the ipsilateral hindbrain in Sarm1$^{-/-}$ are structurally and numerically indistinguishable from age-matched WT controls (**Figure 4.2.2A-B**). High magnification images showed the lateralis neurons are projecting peripheral axons that arborize normally underneath the receptive peripheral organs called neuromasts. There was no difference between WT and Sarm1$^{-/-}$ zebrafish (**Figure 4.2.2C-D**). To explore the central part of sensory neurons, SILL:mCherry and SILL:Synapsin1-GFP were co-expressed to label all the neurons and synaptic vesicles in the lateral line. I observed a normal morphology and consistent distribution of synapsin1 in neurons of WT and Sarm1$^{-/-}$. Quantification of the number of synapsin1 dots in the single neuron showed that there was no statistical significance between WT and Sarm1$^{-/-}$ (**Figure 4.2.2E-G**). These data suggest that the loss of Sarm1 does not affect the development and maintenance of the lateralis afferent neurons (Tian et al., 2020).
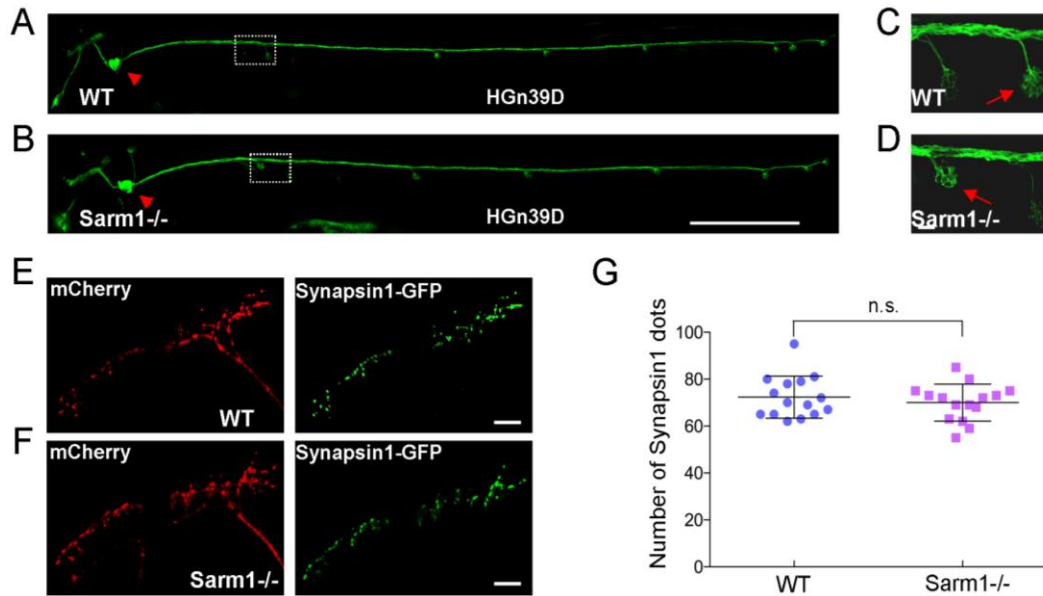
Figure 4.2.2 Sarm1 deficiency does not influence the development of zebrafish lateral line. A-B) Confocal image of a 5 dpf WT (A) and Sarm1$^{-/-}$ (B) larvae carrying the *Tg[HGn39D]* transgene to mark lateralis afferent neurons with GFP. The posterior lateral-line ganglion is indicated with a red arrowhead. The dotted box indicates an innervated neuromast (expanded in C and D). Scale bar 400 μm. C-D) Confocal image of the peripheral arborization of lateralis neurons in 5 dpf WT (C) and Sarm1$^{-/-}$ (D). Red arrows indicate the position of a neuromast from the dotted boxes in (A-B). E-F) Confocal images of the central arborization of lateralis neurons in 5 dpf WT (E) and Sarm1$^{-/-}$ (F). mCherry (red, labeling the branches of axons in central) and Synapsin1-GFP (green, showing the puncta of synapsin1) reveal normal arborization and pre-synaptic puncta in both cases. G) Quantification of the number of synapsin1 puncta. Error bar = SEM; n.s. = no significant difference, Student's t-test. WT n = 15, Sarm1$^{-/-}$ n = 15 (modified from Tian et al., 2020).

Thirdly, the electrophysiological activity of the ganglion cells of sensory nerve under water stimulation was examined by Dr. Melanie Haehnel-Taguchi from University of Freiburg. The loose patch recordings of the lateralis afferent neurons under a 100-millisecond mechanical stimulation of neuromasts with a water jet showed spontaneous and evoked neuronal activity for 5 seconds in Sarm1$^{-/-}$ and control larvae (**Figure 4.2.3A**). Although, the general spontaneous spike rate and spike amplitude of lateralis afferent neurons varied across recording, it appeared that spike amplitude was lower in Sarm1$^{-/-}$ compared to controls. Raster plots from two stimulus protocols in control and Sarm1$^{-/-}$ larvae showed that both groups reliably responded to repeated stimulation (**Figure 4.2.3B**). For each recorded neuron, the stimulus was presented 20 times. The spontaneous spike rates of

lateralis neurons which showed the average records over 12 seconds to 2 minutes was not significantly different when comparing the WT and Sarm1$^{-/-}$ (**Figure 4.2.3C**). Moreover, there was no statistical significance in the latency of response onset upon stimulation between WT and Sarm1$^{-/-}$, although the average latency time was slightly longer in WT (**Figure 4.2.3D**). In addition, both Sarm1$^{-/-}$ and WT responded with a significant increase in the spike rate to mechanical stimulation. The spike rate was around 3-folds increased in evoked condition than no stimulation; however, there was no statistical significance of with or without stimulation between Sarm1$^{-/-}$ and WTs (**Figure 4.2.3E**). Next, I wondered whether these mild differences of neuronal activity would impact the behavioral reaction of the fish to water flow that is mediated by the lateral line. To answer this question, I conducted a rheotactic assay by exposing the larval zebrafish to 6mm/s laminar water flow. For each larva, I performed more than 10 repeats in order to obtain the convincing results. The analysis and statistic quantification of the orientation of the fish to the direction of water flow was performed with the help of my colleague, Mr. Amir Asgharsharghi Bonab. The scope of cosine of orientation was similar in both WT and Sarm1$^{-/-}$, which varied from 0.82 to 1.00. However, the rheotaxis of normal specimens showed no statistical significance with the Sarm1$^{-/-}$ zebrafish from the Wilcoxon rank sum test (**Figure 4.2.3F**).

Taken together, the above results indicate that systemic loss of Sarm1 is compatible with life, normal growth, reproduction, and nervous system development and function in zebrafish.
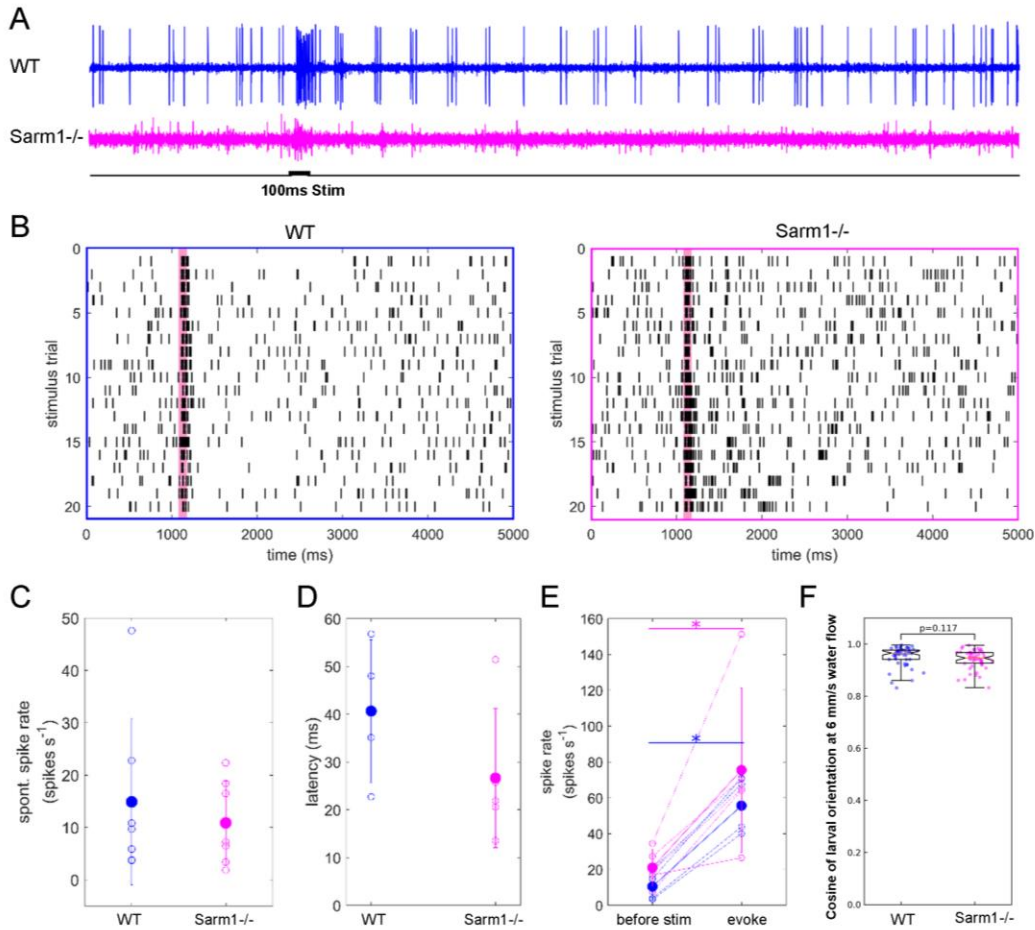
Figure 4.2.3 *In vivo* electrophysiological analysis of lateral neurons in wild type and Sarm1^{-/-} zebrafish. A) Examples of five seconds long loose patch recordings of WT and Sarm1^{-/-} larvae. Stimulus (water jet): 100 ms. B) Raster plots of the recorded response from two stimulus protocols. For each recorded neuron stimulus was presented 20 times. Blue: control, magenta: Sarm1^{-/-}. C) Spontaneous spike rates from recorded neurons, averaged over entire recording (12 seconds to 2 minutes). Data obtained from n = 7 controls, n = 7 Sarm1^{-/-}. No significant difference between control and Sarm1^{-/-}. D) Latency of response onset after stimulus presentation from control and Sarm1^{-/-} larvae. Responses were obtained from n = 4 controls and n = 5 Sarm1^{-/-}. Individual data points represent the average from 20 responses. Filled data points represent mean responses from experimental group. Error bar: standard deviation. No significant difference between control and Sarm1^{-/-} group. E) Spike rates before and in response to stimulus. Significant difference for both groups between spike rate before stimulus and after stimulus presentation (calculated over 200 ms before and after stimulus). F) Rheotaxis (oriented swimming against water-flow direction) shown as cosine of the orientation from WT and Sarm1^{-/-} larva in 6 mm/s water flow, showing a marginal difference between WT and Sarm1^{-/-}. $p = 0.117$ was conducted by Wilcoxon rank sum test. WT n = 7 Sarm1^{-/-} n = 7, 10 trails for each larva (modified from Tian et al., 2018).

4.3 Sarm1 deletion does not affect the number and the movement of mitochondria in the posterior lateral-line sensory neurons

To assess neuronal intracellular dynamics, I marked the mitochondria of sensory neurons with SILL:mitoCherry, in which the mitochondrial targeting sequence was cloned from zebrafish Cytochrome-C oxidase subunit 8A gene (Jung Kim et al., 2008). I chose mitochondria because they produce energy for the neurons and regulate calcium levels, which are critical for the function and viability of the neurons. These intracellular organelles are dynamic and distribute throughout the neurons mediated by molecular motors that move along microtubule tracks. In axons, microtubules are polarized such that their plus ends are directed toward the axon terminals, in turn orienting the movement of distinct molecular motors in the antero- and retro- grade directions (Mandal et al., 2018). Intra-axonal movement direction also reflects mitochondrial fitness because stressed organelles are biased in the retrograde direction (Lin et al., 2017). Therefore, axonal mitochondria represent an optimal proxy for neuronal polarization, intracellular dynamics and overall cellular health. Two types of mitochondria, stable and motile ones, were present in sensory neurons. The stable mitochondria were large and dense than the motile ones which were small but highly dynamic (**Figure 4.3A**). From the kymographic analysis, I discriminated the static mitochondria which were represented by the vertical lines, the moving mitochondria with anterograde movement represented by the red lines and the mitochondria with retrograde movement represented by the green lines (**Figure 4.3B**). Quantification of the density of mitochondria in WT and Sarm1$^{-/-}$ did not show any statistical significance (**Figure 4.3C**). Moreover, neither the anterograde nor the retrograde speed of mitochondria was changed in Sarm1$^{-/-}$, as compared to the WT siblings (**Figure 4.3D**) (Tian et al., 2020). The percentage of stable and motile mitochondria was similar in WT and Sarm1$^{-/-}$, in which stable mitochondria occupied approximately 88% of the total mitochondria in the sensory neurons (**Figure 4.3E**). Furthermore, I visualized the mitochondrial turnover with mitoTimer, in which the fluorescence shifts from green to red over time as the protein mature (Hernandez et al., 2013). To express the Timer into mitochondria, I cloned and injected the construct, SILL:mitoTimer. The images were captured by spinning disc microscopy on 5 dpf mitoTimer positive larvae. However, the

images did not show a difference of the mitochondrial turnover between the WT and Sarm1^{-/-} (**Figure 4.3F**).
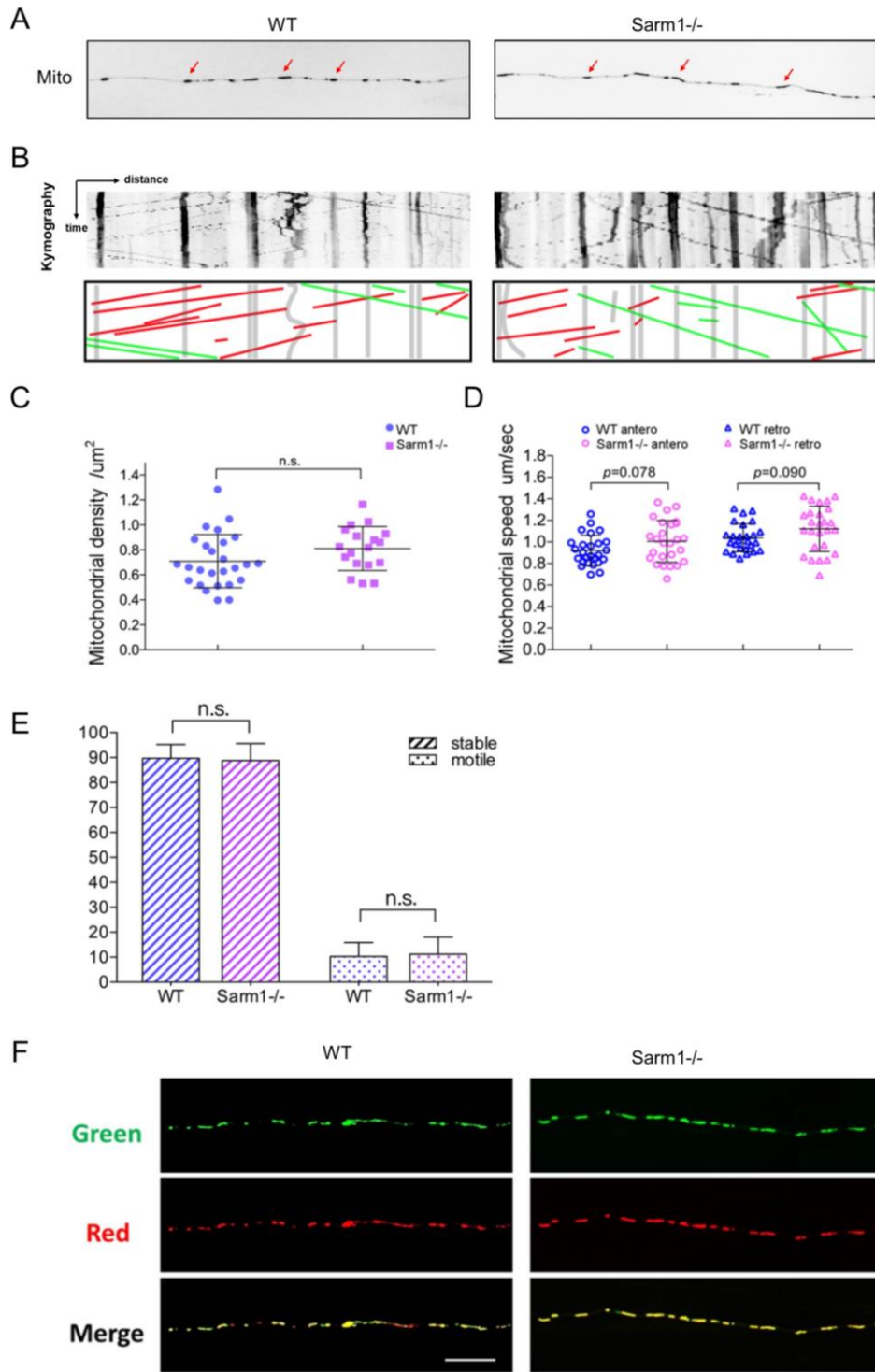
Figure 4.3 Loss of Sarm1 does not influence the number, movement and turnover of mitochondria of the sensory neurons. A-B) Confocal image of axonal mitochondria marked with mito-mCherry in WT and Sarm1^{-/-}. The mCherry signal was changed to grey here. The images were captured with 63x air objective. Red arrows point to prominent mitochondrial groups in axons. B) Upper panels, kymographs from videomicroscopic recording of axonal mitochondria in WT (A) (left panel) and Sarm1^{-/-} (A) (right panel). The video was lasting for 150 seconds with 600 ms intervals. Lower panels show color-coded traces of moving mitochondria in anterograde (green) and retrograde (red) directions, taken from the kymographs shown in the upper panels. C) Quantification of the mitochondrial density in the axons in 5 dpf WT and Sarm1^{-/-}, Error bar = SEM; Student's t-test, n.s. = not significant, WT n = 25, Sarm1^{-/-} n = 19. D) Quantification of the mobility of mitochondria in the whole axons in 5 dpf WT and Sarm1^{-/-}. Circles show the anterograde and triangles the retrograde movement of the mitochondria in the axons. p value from one-way ANOVA, WT n = 26, Sarm1^{-/-} n = 26. E) Quantification of the stable and motile mitochondria in the axons in 5 dpf WT and Sarm1^{-/-}. Rectangles with slash depict the stable mitochondria and the dash rectangles are the motile mitochondria. Error bar = SEM; Student's t-test, n.s. = not significant, WT n = 26, Sarm1^{-/-} n = 26. F) Confocal images show the expression of mitoTimer in the axons in 5dpf WT and Sarm1^{-/-} larva. The red panels show the mature mitochondria and green panels the nascent mitochondria. Scar bar 20 μm (modified from Tian et al., 2020).

4.4 Sarm1 is essential for the degradation of severed axons in zebrafish

Loss of Sarm1 in *Drosophila* or in mice prevents the degradation of injured axons (Osterloh et al., 2012). To test functional conservation of Sarm1 in zebrafish, I used a previously established bioassay of nerve injury in the lateral-line system (Xiao and López-Schier, 2016). The preparation employs intact larval zebrafish, laser-mediated severing of axons individualized by single-cell fluorescent-protein expression, and intravital high-resolution videomicroscopy of axons and their associated Schwann cells (Xiao et al., 2015a). Axotomy was done in fluorescently marked neurons by focusing an ultraviolet laser beam to a discrete region of the peripheral axons. Upon severing, the distal axonal segments quickly degenerated in WT, whereas the proximal segments remained associated with the intact neuronal perikaryon. This proximal part was normal and the regenerating axons would start to grow at 8 hpi (hours-post injury) (**Figure 4.4.1A**). However, the degeneration of distal segment axons was blocked in the severed specimens of Sarm1^{-/-}. Kinetic analysis showed that WT axons degenerated through two phases: a fragmentation of the distal part that started as soon as 2 hpi, and a complete clearance that could complete

as early as 8 hpi (**Figure 4.4.1B**). By contrast, severed Sarm1-deficient axon segments retracked a very short distance and resisted degeneration more than 5 days (**Figure 4.4.1C**). However, the regrowth of proximal parts that starts from 8hpi, was normal in the WT and Sarm1$^{-/-}$ (**Figure 4.4.1A-B**). To confirm the altered axon degeneration is due to absence of Sarm1, I performed the rescue experiment by reconstituting the sarm1 protein in the Sarm1-deficient larvae. SILL:mCherry construct was injected in the WT *Tg[HGn39D]*. The images showed that the axons labeled with GFP and mCherry undergo Wallerian degeneration after axon transection in WT. Next, I injected the SILL:mCherry or SILL:Sarm1-v2a-mCherry in the embryos from *Tg[Sarm1$^{-/-}$; HGn39D]*. The images showed that the distal part of the transected axons degenerate in the Sarm1-v2a-mCherry positive axons which obtain the sarm1 expression but not in the mCherry ones (**Figure 4.4.1D**). The published biochemistry work shows that Sarm1 executes the axon degeneration through dimerization of TIR domains after injury (Gerdts et al., 2015). Thus, I constructed the vectors with the truncated Sarm1 without TIR domain and expressed it in the Sarm1$^{-/-}$ larvae. The result shows that the TIR domain truncated Sarm1 could not rescue the phenotype of Sarm1 in axon degeneration (**Figure 4.4.1E**). Therefore, these data demonstrate that Sarm1 regulates Wallerian degeneration through its conserved TIR domain after transection in zebrafish (Tian et al., 2020).
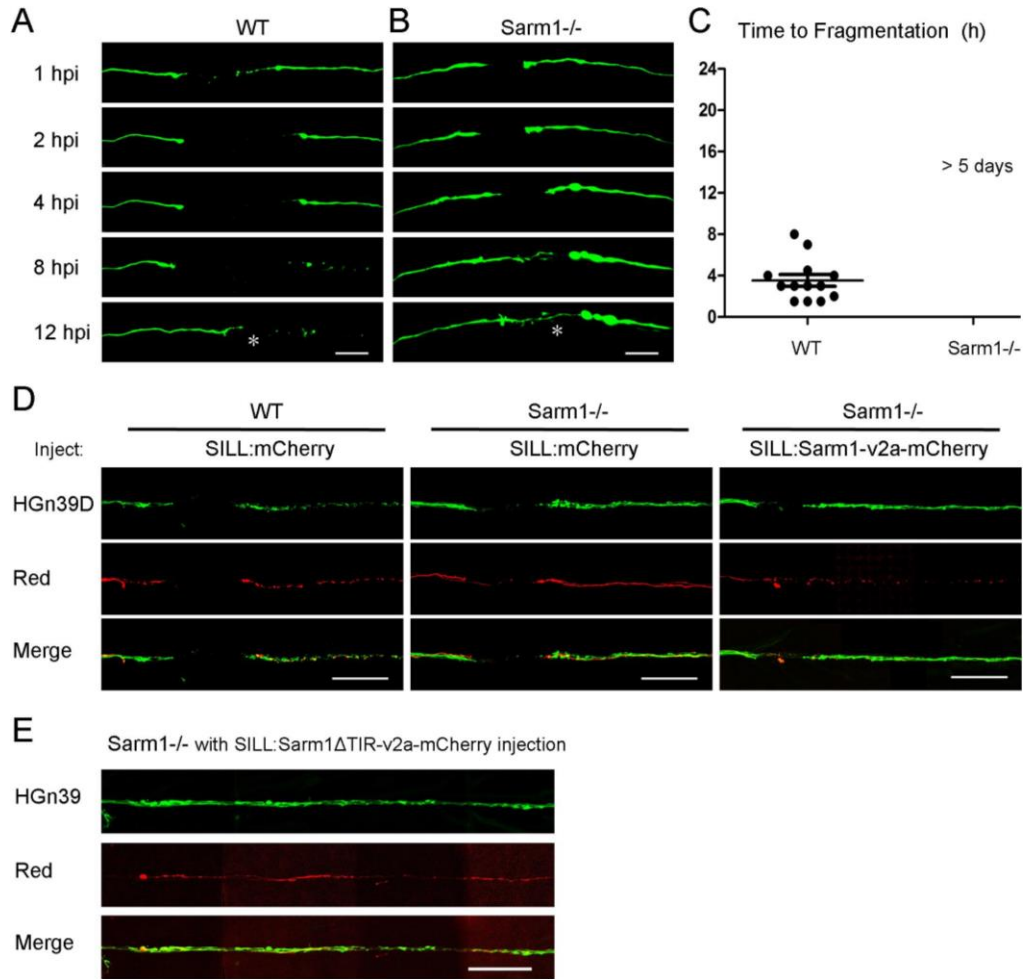
Figure 4.4.1 Sarm1 is required for injury-induced peripheral axon degeneration in zebrafish. A-B) Time-lapse images of axonal degeneration of GFP-labeled lateralis sensory neuron in WT (A) and Sarm1$^{-/-}$ larvae (B). hpi = hours post injury, scale bar 50 μm, white asterisk indicates the regrowing axons from the proximal stump. C) Quantification of the time from axon transection to fragmentation in WT n = 13 and Sarm1$^{-/-}$ n = 13. We observed the degeneration event up to 5 dpi maximum in our experiments. D) Confocal images of a severed lateralis nerve in the *Tg[HGn39D]* transgenic line (green) that also expresses mCherry in a fraction of axons in a WT (left) and a Sarm1$^{-/-}$ larva (center). The images on the right show a Sarm1$^{-/-}$ larva in which the red axons express a fusion between a functional Sarm1 and mCherry, revealing degradation of red axons and maintenance of green axons. Scale bar 100 μm. E) Confocal images of the HGn39D (green) and constituted Sarm1 with TIR domain deletion (red) in Sarm1$^{-/-}$ larva. The images show that TIR domain is essential for Sarm1 conducting axon degeneration after transection. Scale bar 100 μm (modified from Tian et al., 2020).

Next, the central part axonal degeneration was visualized by injection of SILL:mCherry construct. The results were consistent with that of the peripheral axons which showed loss of Sarm1 impedes the degeneration of injured axons. Because of the central part with poor regenerative capacity (Xiao et al., 2015b), I did not observe the regenerative axons in WT and Sarm1$^{-/-}$ (**Figure 4.4.2**). These data suggest that Sarm1 influences the axon degeneration in both central and peripheral parts of the sensory neurons, but it does not affect the capacity of axon regeneration.
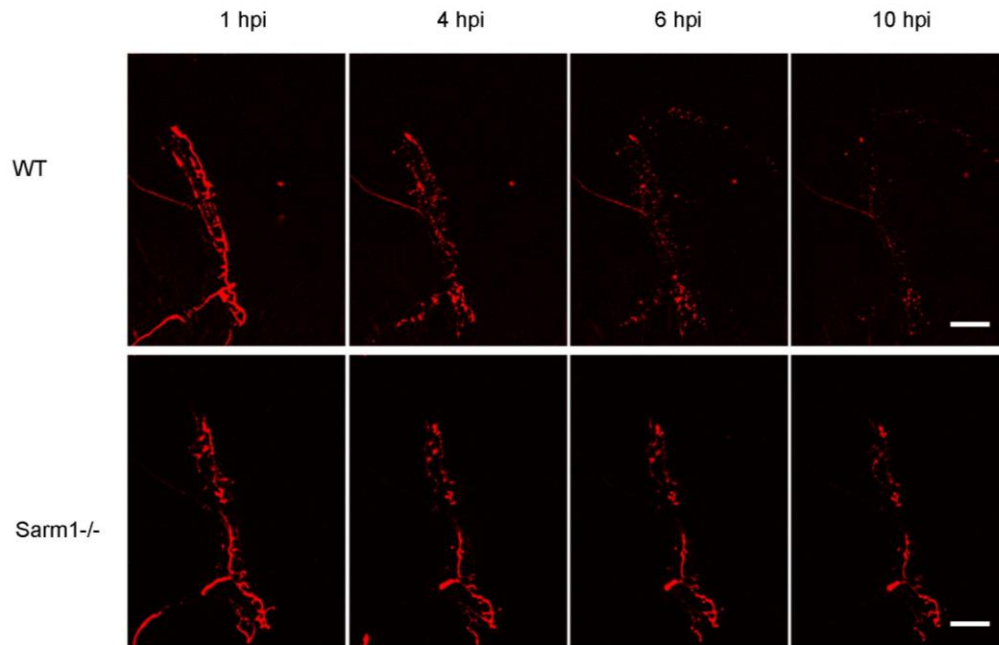

Figure 4.4.2 Loss of Sarm1 blocks central axon degeneration after injury. Time-lapse images of axonal degeneration of mCherry-labeled central part of lateralis sensory neuron in WT (up) and Sarm1$^{-/-}$ larvae (down). The central part degraded quickly after transection in WT, not in Sarm1$^{-/-}$. hpi = hours post injury, scale bar 50 μm.

In *C. elegans*, severed axons can re-seal their proximal and distal stumps and restore the function quickly (Neumann et al., 2015). However, whether axons resealing occurs in other species remains unclear. I assessed this issue in Sarm1-deficient zebrafish, in which the distal part of transected peripheral axons does not degenerate and the proximal part retains regenerative capacity. To recognize the distal and proximal segments of the same axon after severing and during regrowth, I expressed individual lateralis neurons with Kaede, a photoconvertable protein that can be converted from Green into Red after exposing to 405

nm laser pulse (Ando et al., 2002). The positive larvae with Kaede_Green were transected with laser. 6 hours later (6 hpi), the distal parts of the axons were converted into Kaede_Red. Then, the larvae were released into the incubator. All the images were taken at 14 hpi with confocal microscopy (**Figure 4.4.3A**). The representative images showed that the distal axons with Kaede_Red did not reseal with the Kaede_Green labeled regenerative axons (**Figure 4.4.3B**). The high magnification image was the rectangular dash box from Figure 4.4.3B, showing clear detail of the action of these two axonal segments. The regrowing axon did not reseal with the non- degradable distal part. However, the regrowing proximal axon grew bypath the old non-degradable segments and re-innervated neuromasts (**Figure 4.4.3C**). This experiment was reproducible in more than twenty individual larvae. I did not observe the resealing event in the regeneration of sensory neurons. These results indicate that the resealing of transected axons does not occur in Sarm1- deficient zebrafish. The vertebrate might lose the capacity to reseal injured axons.

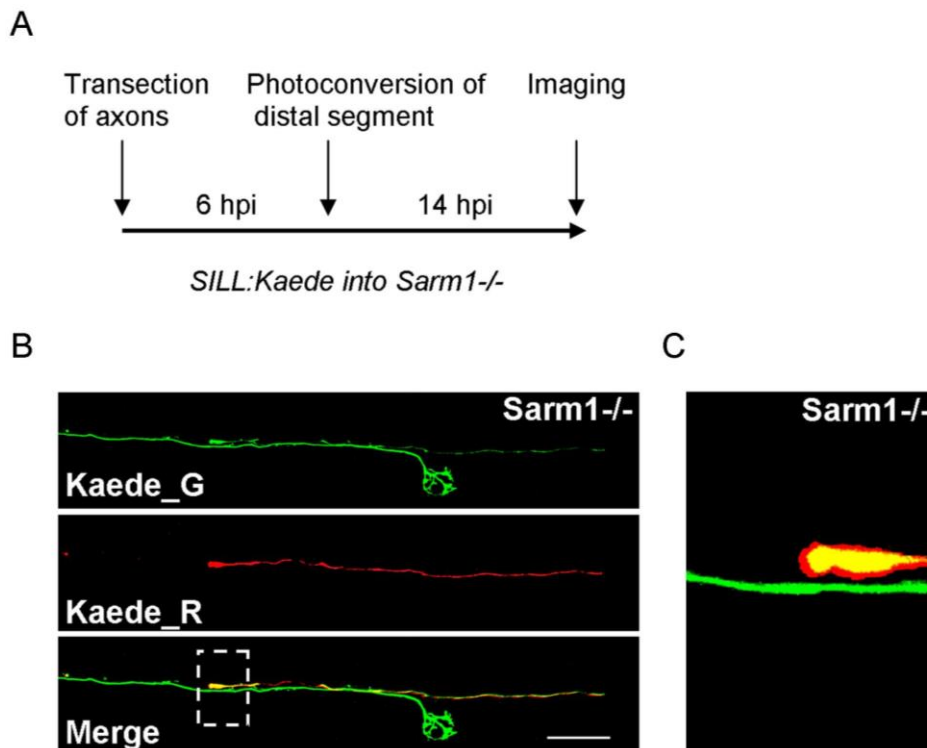**Figure 4.4.3 Regenerating axons do not reseal with non-degradable segments in zebrafish.** A) Schematic representation of the experimental strategy to test the axon resealing in Sarm1^{-/-} transected axons expressing Kaede. Photoconversion of distal segment was performed 6 hours post injury (hpi), and imaging 14 hours afterwards. B) Confocal images of the photoconversion experiment. Kaede_G is

the green (native) form of Kaede, in the proximal (regrowing) axon; Kaede_R is the red (photoconverted) form of Kaede in the non-degradable (distal) axon segment. Scale bar 40 μm. The dotted box indicates the site of transection, which also contains the juxtaposition between the proximal end of the distal axon segment and the passing regenerated axon. Note the arborization of the green axon below a neuromast. C) Zoomed from the dotted box in (B), detailing the interphase between the non-degradable distal axon (orange) and the passing regenerated proximal axons (green) (modified from Tian et al., 2018).

4.5 Synthetic elevation of intracellular calcium suffices to induce the degradation of severed Sarm1-deficient axons

Calcium regulation is critical for neuronal homeostasis because sustained elevation of cytosolic calcium leads to axonal degeneration. This occurs because mitochondria release apoptosis-inducing factors and proteases in a calcium-dependent manner (Ozaki et al., 2009). In addition, calcium influx is essential for axonal microtubule breakdown via calpain activity which cleaves the microtubules and induces the axon fragmentation (Ma et al., 2013; Yang et al., 2013). To understand the role of Sarm1 in calcium influx, I monitored the calcium influx in axoplasm, mitochondria, and endoplasmic reticulum when the axons were severed. To visualize the calcium influx in axoplasm, SILL:Gal4 and UAS:mCherry constructs were co-injected into embryos from the *Tg[UAS:GCaMP7a; Sarm1$^{-/-}$]* or *Tg[UAS:GCaMP7a; WT]* transgenic lines. The calcium signal was captured by spinning disk microscopy with 2.5 Hz (400 ms per frame). Undamaged wild-type and Sarm1-deficient axons showed undetectable levels of axoplasmic fluorescence above background. Upon severing, the fluorescent signal in WT axons distal segments increased immediately and subsequently decayed with a near constant slope, whereas fluorescence remained undetectable in Sarm1-deficient distal axon segments (**Figure 4.5.1A**). The quantification of calcium signals showed that the ΔF/F0 reached 1.4 in WT after transection, indicating that the calcium signal was increased 1.4-fold of the basal level; however, in Sarm1$^{-/-}$, the ΔF/F0 was 0.15 after transection. The statistical analysis showed the difference between WT and Sarm1$^{-/-}$ (**Figure 4.5.1B**). These results show that Sarm1 deletion prevents the calcium influx into the axoplasm in injury.

To monitor the calcium signal in mitochondria, the mitochondrial located RGECO (red calcium channel sensor) (Esterberg et al., 2014), was expressed in the sensory neurons with the construct, SILL:mitoRGECO. The images showed that the RGECO labelled mitochondria are red dots or tubulars along the axons. Upon severing, the signal of RGECO was enhanced in both WT and Sarm1^{-/-} samples (**Figure 4.5.1C**). The quantification result showed that the calcium signal was elevated around 0.2-fold after axon transection. However, there was no statistical significance between WT and Sarm1^{-/-} (**Figure 4.5.1D**). In addition, the calcium activity in ER was examined with the sensor, ER-GCaMP3, which includes the ER target sequence in the N terminal of the GCaMP3. The basal level of calcium signal was stronger in ER than in cytosol, because GCaMP3 is more sensitive than GCaMP7a (Muto et al., 2013). Upon injury, the calcium signal of ER was increased in both groups, WT and Sarm1^{-/-}, but without statistical significance (**Figure 4.5.1E-F**). Taken together, these results demonstrate that loss of Sarm1 attenuates the calcium influx into the axoplasm but not Ca^{2+} uptake in mitochondria and endoplasmic reticulum (Tian et al., 2020).
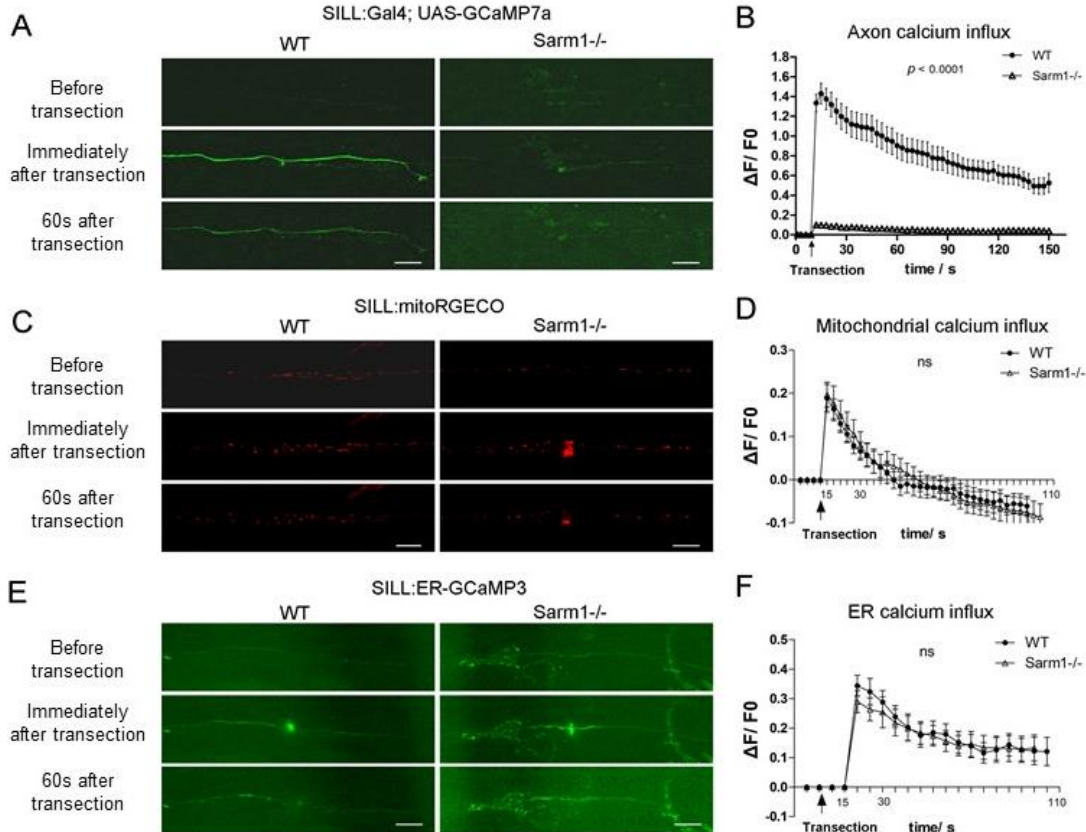
Figure 4.5.1 Loss of Sarm1 attenuates axoplasmic calcium influx but not mitochondrial and ER calcium uptake in injury. A) Confocal image of a single lateralis sensory axon expressing the green-fluorescent calcium sensor GCaMP7a in WT (left column) and Sarm1$^{-/-}$ fish (right column). Rows show the same samples before laser-mediated transection (top), immediately after transection (middle) and 60 seconds after transection (bottom). Scale bar 20 μm. B) Shows quantification of the first wave of axoplasmic calcium. Data are shown as mean ± SEM; *p* from one-way ANOVA, WT n = 16, Sarm1$^{-/-}$ n = 16. C) Shows a confocal image of lateralis sensory axons expressing the red-fluorescent calcium sensor RGECO in WT (left column) and Sarm1$^{-/-}$ zebrafish (right column). Rows show that same samples before laser-mediated transection (top), immediately after transection (middle), and 60 seconds after transection (bottom). D) Quantification mitochondrial calcium influx shows the strong and nearly identical elevation and decay in WT and Sarm1$^{-/-}$ immediately after the cuts. The data is shown as mean ± SEM; *p* from one-way ANOVA, WT n = 16, Sarm1$^{-/-}$ n = 16. E) Shows a confocal image of lateralis sensory axons expressing the green-fluorescent calcium sensor CCaMP3a targeted to the endoplasmic reticulum (ER) in WT (left column) and Sarm1$^{-/-}$ fish (right column). Rows show that same samples before laser-mediated transection (top), immediately after transection (middle), and 60 seconds after transection (bottom). F) Quantification ER calcium influx shows strong and statistical equal elevation and decay in WT and Sarm1$^{-/-}$ after transection. Data are shown as mean ± SEM; *p* from one-way ANOVA, WT n = 16, Sarm1$^{-/-}$ n = 16 (modified from Tian et al., 2020).

Studies in mammalian and zebrafish have shown that neuronal damage triggers two waves of elevation of axoplasmic calcium (Ca^{2+}), and the second wave of calcium activates the Wallerian degeneration through Calpain which facilitates axonal fragmentation by cleaving microtubules and neurofilaments (Park et al., 2013a; Vargas et al., 2015). To observe the calcium changes in the distal segments, I performed live imaging of the transected axons with spinning disc microscopy for 12 hours. The images showed that the second wave of calcium influx occurs at 4 hpi in WT, when the axon has not degenerated yet. 2 hours later, the axon was under fragmentation and the calcium signal was weakened sequentially. By contrast, the second wave of axoplasmic calcium signal did not come up in Sarm1-deficient axons up to 12 hpi (**Figure 4.5.2A-B**).

Moreover, I monitored the calcium signal in mitochondria in the late stage of axonal degeneration. The images showed that the mitochondrial calcium was enhanced at 3 hpi in WT, which is around the same time as the axoplasmic calcium influx; however, the mitochondrial calcium concentration was not changed in the Sarm1$^{-/-}$. It shows that the

axoplasmic calcium influx from the extracellular space increases the mitochondrial calcium uptake before axon fragmentation. It has been reported that the influx calcium is the source of mitochondrial calcium in axon degeneration (Villegas et al., 2014). At later time, the RGECO labelled axons underwent fragmentation, but there was no obvious difference of the calcium signal before and after axon fragmentation in WT. In contrast, although the distal segments were not fragmented in Sarm1$^{-/-}$, the mitochondrial calcium was not changed (**Figure 4.5.2C**). Taken together, absence of Sarm1 impairs the axoplasmic calcium influx which is essential for axonal fragmentation in early and later stages of axonal degeneration after axotomy (Tian et al., 2020).
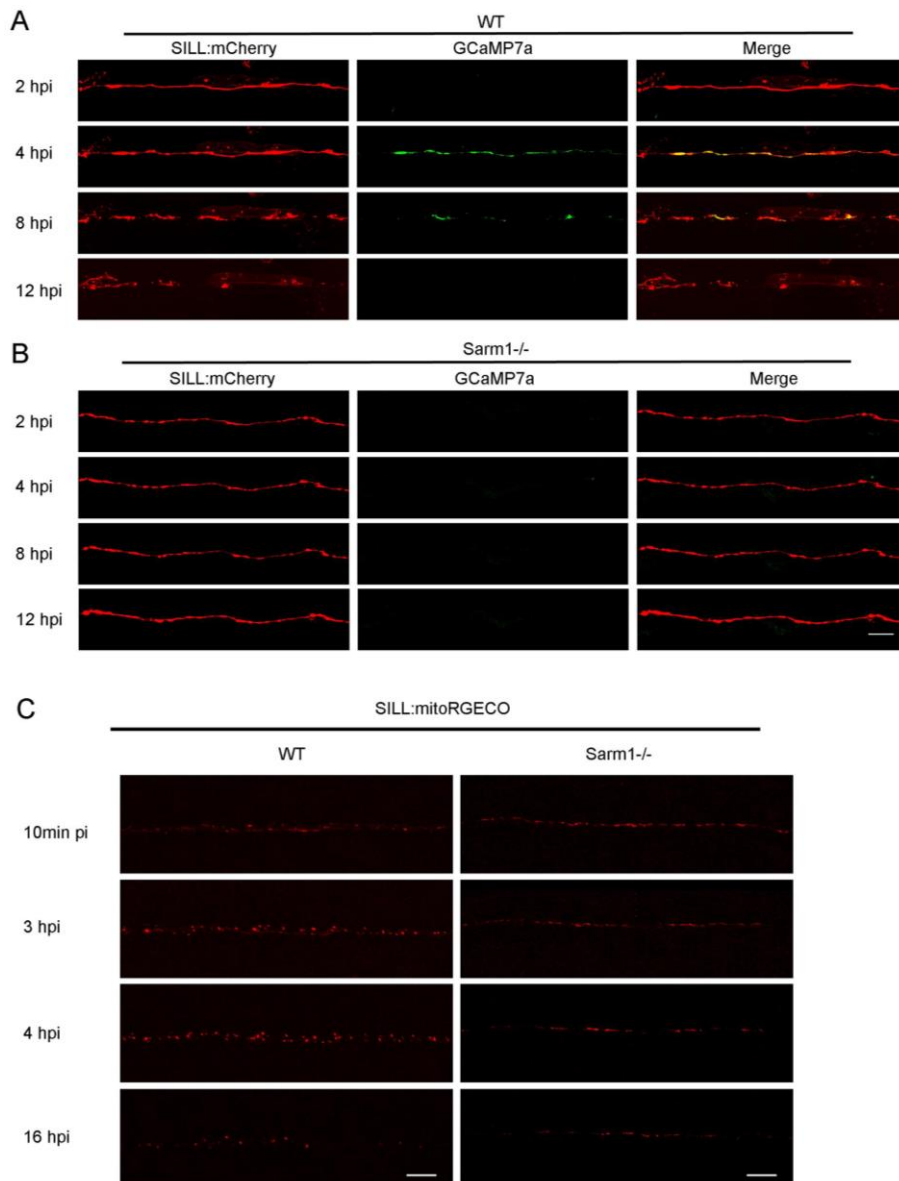
Figure 4.5.2 Second wave of axoplasmic calcium influx triggers axon fragmentation. A) Confocal images of lateralis sensory axons expressing the mCherry (red) and green-fluorescent calcium sensor GCaMP7a (green) in WT zebrafish. Rows show same axons 2, 4, 8 and 12 hours after transection (hours-post-injury = hpi). B) Confocal image of lateralis sensory axons expressing the mCherry (red) and green-fluorescent calcium sensor GCaMP7a (green) in Sarm1$^{-/-}$ zebrafish. Scale bar 20 μm. C) The mitoRGECO was fragmented and become clustered in the WT, but the strength of the calcium signal was not changing. However, the mitoRGECO did not change in the Sarm1$^{-/-}$. Scale bar 20 μm (modified from Tian et al., 2020).

Further, I used the capsaicin/ratTRPV1 (transient receptor potential cation channel subfamily V member 1) system to enforce the axoplasmic calcium influx in Sarm1-deficient axons. The TRPV1 in rat is sensitive to capsaicin, whereas the orthologue TRPV1 in zebrafish is not. Thus, ratTRPV1 has been used to manipulate the calcium activity in zebrafish (Chen et al., 2016; Gau et al., 2013). First, I expressed the ratTRPV1-tgRFP in the GCaMP7a transgenic axons in Sarm1$^{-/-}$. Then, I monitored the calcium signal with or without capsaicin incubation. The results showed that the calcium signal was obviously enhanced in the ratTRPV1 positive neurons in presence of the capsaicin (**Figure 4.5.3A**). Calcium influx is induced by ratTRPV1/capsaicin in the Sarm1-deficient axons, indicating that the calcium activity is downstream of Sarm1 in axon degeneration. Next, I injected the construct SILL: ratTRPV1-tgRFP or SILL: mCherry in the embryos of *Tg[Sarm1$^{-/-}$; HGn39D]* respectively. The positive larvae were the ones with both green fluorescence labeling of all the sensory neurons and red fluorescence labeling of the ratTRPV1-expressing neurons. Then, I transected all the axons and incubated the larvae in vehicle (ethanol) or capsaicin. Finally, the images were taken at 1.5h later by confocal microscopy (**Figure 4.5.3B**). The results show that capsaicin does not affect the transected axons in Sarm1$^{-/-}$, because the HGn39D and SILL:mCherry labelled transected axons did not fragment in presence of capsaicin (**Figure 4.5.3C**). However, ratTRPV1 positive Sarm1-deficient neurons rapidly degraded in the presence of capsaicin. Neither the HGn39D positive ones nor the ratTRPV1 positive neurons degraded with control (ethanol) incubation (**Figure 4.5.3D-E**). Thus, these results confirm that the calcium signal is downstream of Sarm1 for axon degeneration. Elevation of axoplasmic Ca^{2+} is sufficient to trigger the degradation of Sarm1-deficient axons *in vivo* (Tian et al., 2020).
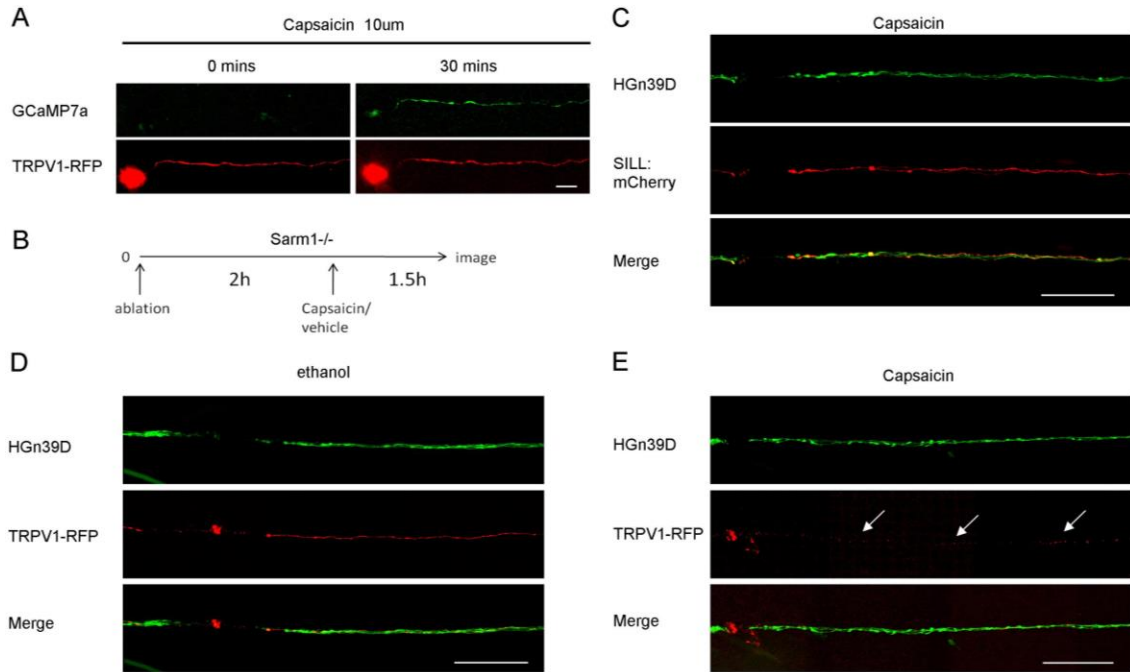
Figure 4.5.3 Synthesis elevated axoplasmic calcium influx induces axon fragmentation in Sarm1$^{-/-}$ zebrafish. A) Confocal images of the GCaMP7a (Green) and TRPV1-tgRFP (red) before and after capsaicin treatment in Sarm1$^{-/-}$ zebrafish, which shows the calcium influx under capsaicin treatment. Scale bar 20 μm. B) Schematic representation of the experimental strategy to synthetically elevate calcium in transected Sarm1$^{-/-}$ axons. Lateralis sensory neurons expressed a transgene coding for the rat transient receptor potential cation channel subfamily V member 1 (ratTRPV1) fused to tgRFP, or mCherry as a control. Two hours after axon transection, zebrafish larvae were bathed in ethanol solution (control), or ethanol containing capsaicin, a natural activator of TRPV1. 90 minutes after treatments, larvae were imaged by confocal microscopy to assess the extent of distal segment degradation. C) Sarm1$^{-/-}$ zebrafish expressing GFP in all lateralis neurons (*Tg[HGn39D]*) and mCherry in a mosaic manner in some neurons. The sample was treated with 10um capsaicin. Scale bars 100 μm. D) Sarm1$^{-/-}$ zebrafish expressing GFP in all lateralis neurons and ratTRPV1-tgRFP in a mosaic manner. The sample was incubated in ethanol solution 1/1000 (vol/vol). Scale bars 100 μm. E) Sarm1$^{-/-}$ zebrafish expressing GFP in all lateralis neurons and ratTRPV1-tgRFP in a mosaic manner. Capsaicin treatment induced transected axon degradation (former location of the axon signaled by three white arrows). Scale bars 100 μm (modified from Tian et al., 2020).

4.6 Equivalent sensorimotor recovery after nerve regeneration in wild type and Sarm1-deficient zebrafish

To know what happens when the regenerating axons get into the neuromast, I generated the transgenic line, *Tg[Sarm1$^{-/-}$; SILL:mCherry; Brn3c:Gal4; UAS:GCaMP7a]*. After axon transection, I took the time-lapse imaging of the neuromasts, which were innervated by the sensory axons. Compared to the non-degradable transected trunks, the axonal branches in neuromasts were divided into two groups, degradable and non-degradable branches. In the degradable ones, the regenerating axons got into the neuromast and innervated the related hair cells around 14 hpi. This was consistent to the WT, in which the old axons degenerated and were eradicated, releasing the space and touching sites for the innervation of regenerative axons and neuromast. In the non-degradable ones, the old axons were maintained in surrounding of the neuromast. But, the terminal of non-degradable axons became small dots and detached from the neuromast, releasing the connected sites to the regenerative axons. Moreover, the non-degradable segments did not repel the regenerative axons to innervate hair cells (**Figure 4.6.1A-B**). These results show that regenerative sensory axons could innervate the neuromasts normally in Sarm1-deficient zebrafish.
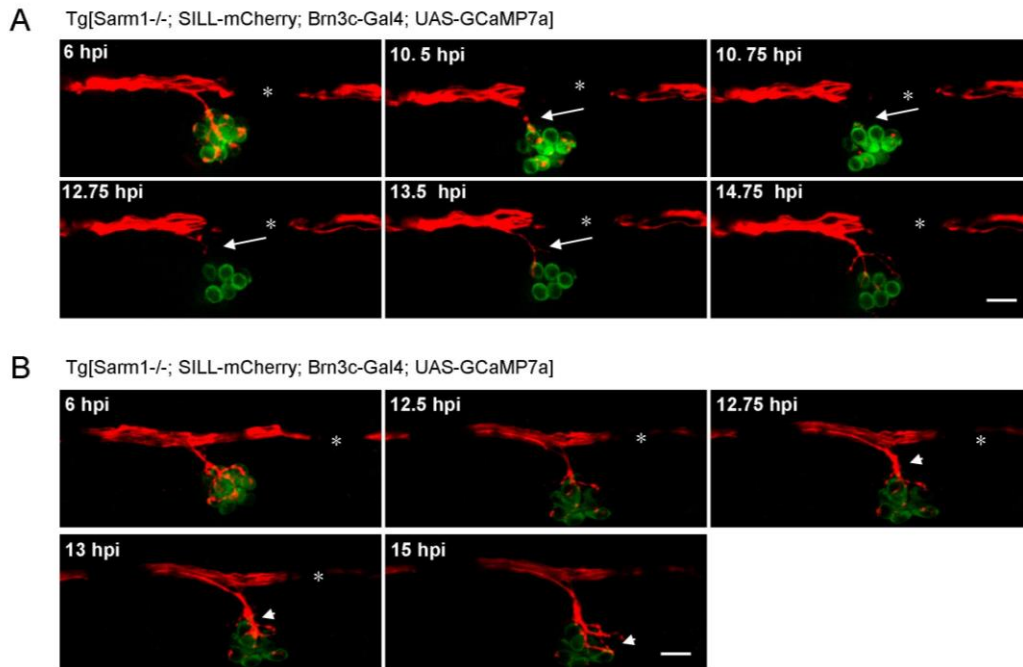

Figure 4.6.1 Regrowth of axons innervate neuromasts in Sarm1$^{-/-}$ zebrafish after axon transection.
A) Confocal images of the regrowing axons towards to the neuromast in Sarm1$^{-/-}$. Time points are indicated in the upper- left of the images. Asterisks indicate the pigment. Arrows show the regrowth site

of new axons towards to neuromast after transection. Scale bar 20 μm. B) Confocal images of the regrowth axons towards to the neuromast in Sarm1^{-/-}. Time series are in the down left of the images. Asterisks indicate the pigment. Arrowheads show the regrowth site of new axons towards to neuromast after transection. Scale bar 20 μm.

To test the impact of systemic loss of Wallerian axon degeneration on sensorimotor recovery after damage, I employed the natural regeneration of the lateralis peripheral nerve. It has been reported that unilateral abrogation of anterior and posterior lateral-line decreases the orienting performance of fish in laminar flow (Oteiza et al., 2017). I performed and quantified the rheotaxis tests on following experimental groups: WT, Sarm1^{-/-}, WT 1 dpi, Sarm1 1 dpi, WT 3 dpi, and Sarm1^{-/-} 3 dpi. The dpi (days post injury) groups had been transected on one-side either at the level of the anterior or posterior lateral-line. Therefore, they had lost all the connection between sensory organs and the central nervous system. The performance of the intact larvae shows no statistical difference between WT and Sarm1^{-/-}. The distribution of quantified performance was in a small range, which varied from 0.8-1 (**Figure 4.6.2**).

In the lateral-line transected groups, the orientation performance of larvae was affected dramatically. From the quantification results, cosines of orientation were distributed from 0.1-0.95 in the WT 1 dpi group and Sarm1^{-/-} 1 dpi group. There was statistical significance between intact and 1 hpi groups in either WT or Sarm1^{-/-} individually. But in the orientation, there was no statistical significance between WT 1 dpi and Sarm1^{-/-} 1 dpi groups. It indicated that the non-degradable axons do not improve the performance of orientation in Sarm1^{-/-} zebrafish. In addition, the range of cosine of orientation increased to 0.3-1 in WT 3 dpi and Sarm1^{-/-} 3 dpi groups. Comparing to the 1dpi groups, it demonstrates that the performance of rheotaxis is improved after three days recovery from injury in both WT and Sarm1^{-/-}. However, there was no statistical significance between WT 3 dpi and Sarm1^{-/-} 3 dpi (**Figure 4.6.2**). Considering the regenerated axons are compatible to the non-degradable severed ones in the Sarm1^{-/-} 3 dpi, the results suggested that the non-degradable axons in Sarm1^{-/-} do not retard the functional recovery of injured nerves. Taken together, these results show that non-degradable axon does not improve or suppress the performance of orientation in Sarm1^{-/-}. In other words, the maintenance of severed axons

in Sarm1$^{-/-}$ zebrafish does not affect the re-innervation of sensory receptors with regenerative axons, or restoration of sensory function after circuit repair.
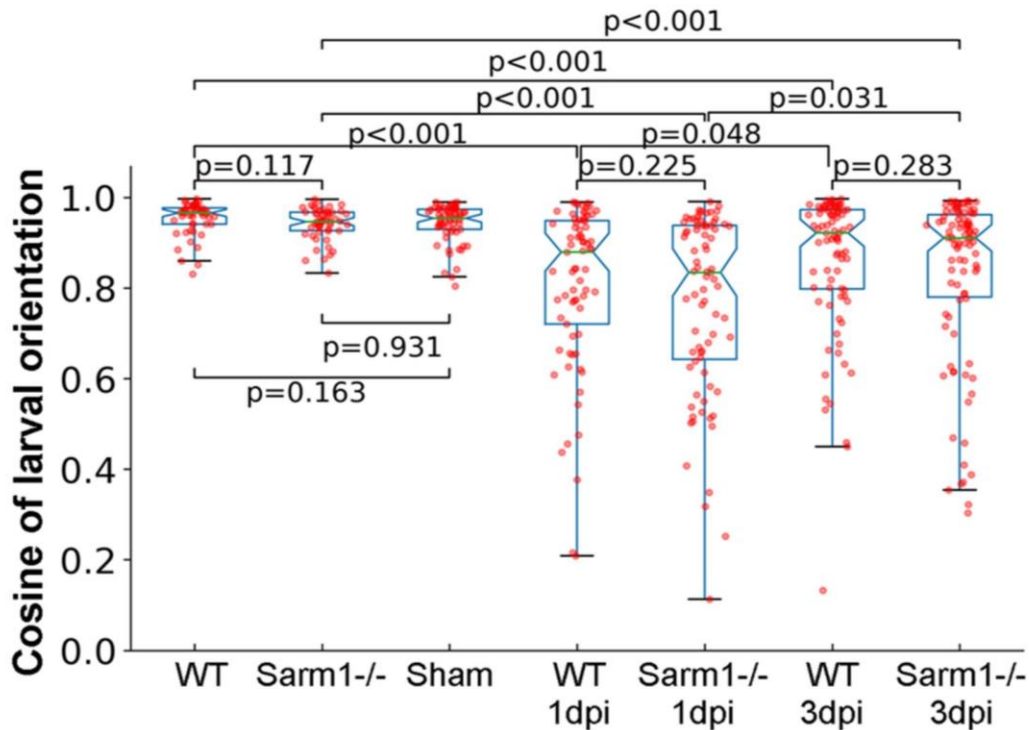

Figure 4.6.2 Equivalent sensorimotor recovery after nerve regeneration in wild type and Sarm1$^{-/-}$ zebrafish. Rheotaxis of 7 dpf larva in the indicated groups. Sham: sham ablation of the lateralis nerves. 1 dpi: 1 day post injury; 3 dpi: 3 days post injury. *p* values were from the Wilcoxon rank sum test. n = 7 for each group, 10 trails for each larva (modified from Tian et al., 2018).

4.7 Schwann cells do not change the phenotypes after axon severing in Sarm1-deficient zebrafish

Schwann cells support, fasciculate and myelinate sensory axons in vertebrates. They also present phagocytic activity to eliminate damaged axons (Lutz and Barres, 2014). To assess the morphology of Schwann cells and the interaction between Schwann cells and axons, I generated the *Tg[SILL:mCherry; gSAGFF202A; UAS:GFP]* line. The confocal images showed that the green fluorescence labelled Schwann cells ensheathed and distributed along the red fluorescence lateralis afferent neurons. There was no obvious difference in WT and Sarm1$^{-/-}$ zebrafish larvae (**Figure 4.7.1A**). Next, I tested the calcium activity of the Schwann cells of 4 dpf larvae upon injury. In the *Tg[Sarm1$^{-/-}$; gSAGFF202A;*

UAS:GCaMP7a] larva, calcium influx was triggered normally during transection, comparing to the WT (**Figure 4.7.1B**). Therefore, these data suggest that Schwann cells develop and fasciculate sensory axons normally in Sarm1-deficient zebrafish.
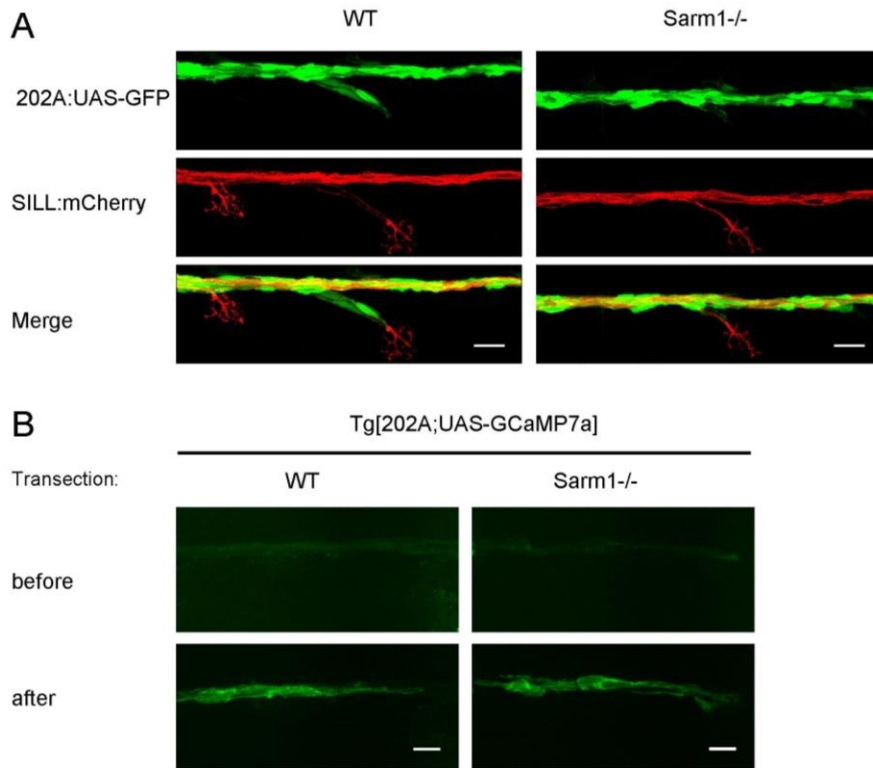
Figure 4.7.1 Loss of Sarm1 does not influence the morphology and calcium influx of Schwann cells in lateral line. A) Confocal images of a double transgenic 5 dpf larva showing Schwann cells marked by expression of GFP (green) under the control of the *Tg[gSAGFF202A]* Gal4 driver, and lateralis afferent neurons marked by expression of mCherry under the control of the SILL enhancer (red). WT (top), Sarm1$^{-/-}$ (bottom). Scale bar 20 μm. B) Confocal images show the calcium signal in Schwann cells before and after transection in WT and Sarm1$^{-/-}$. The GCaMP7a labeled Schwann cells were controlled by the gSAGFF202A-Gal4 driver with UAS-GCaMP7a, Scale bar 20 μm (modified from Tian et al., 2020).

Upon severing, fragmented axons are quickly cleared by the Schwann cells. With the high-resolution intravital microscopy, I observed that the fragmented axons were engulfed and were degraded by Schwann cells in WT (**Figure 4.7.2A**). However, the engulfment and clearance events did not occur in Sarm1$^{-/-}$, because no axonal fragmentation occurred (**Figure 4.7.2B**).

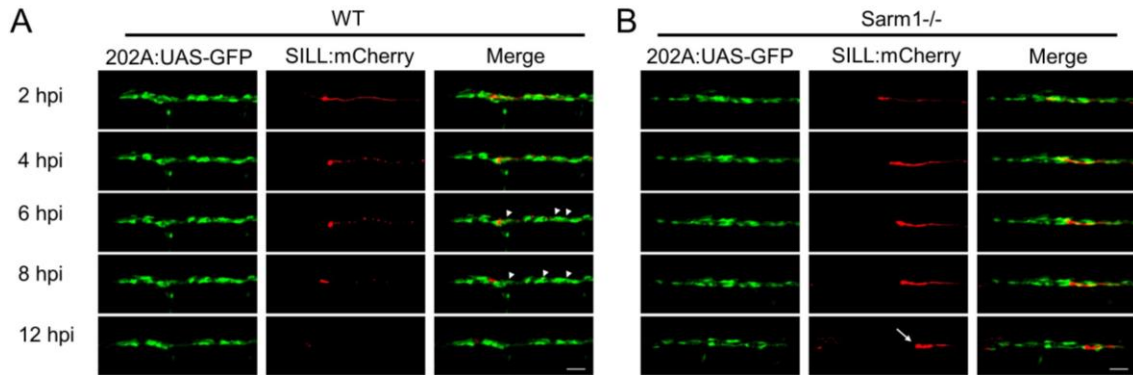**Figure 4.7.2 Schwann cells involve in axon debris clearance.** A, B) Images show the indicated time points after axon transection (hours post injury = hpi) from a videomicroscopic recording of Schwann cells (green) and their interaction with axons (red) in WT and Sarm1$^{-/-}$. White arrowheads indicate Schwann cells engulfing axonal debris in the WT. A white arrow indicates degradation-resistant axon segment in Sarm1$^{-/-}$. Please note that the proximal axon stumps in are not visible in these images because they are outside the focal plane (modified from Tian et al., 2020).

When an injury generates a gap in the glia, wounded-adjacent Schwann cells actively move and extend cellular processes resembling filopodia to reconstitute a continuous glial scaffold rapidly. Although continuous glia is not necessary for the regrowth of proximal axon stump, it prevents regenerating growth cones from straying, in turn facilitating end-organ *de novo* innervation and circuit reconstitution (Rosenberg et al., 2014; Xiao et al., 2015a). Thus, I decided to assess Schwann-cell behavior immediately after axon severing and during axon regeneration by combining *Tg[gSAGFF202A;UAS-GFP; SILL:mCherry]* double transgenic lines with Sarm1$^{-/-}$. As expected, I found that Schwann cells adjacent to the wound quickly extended filopodia to close the gap in the glial scaffold ahead of axonal regeneration in WT animals. The re-growing axons then followed these sub-cellular glial bridges to reconstitute the nerve, suffering mild de-fasciculation restricted to a small area within the injury (**Figure 4.7.3A** and **Figure 4.7.4**). In contrast, injury-adjacent Schwann cells did not migrate or produce filopodia-like projections ahead of axonal regeneration in Sarm1$^{-/-}$. Nonetheless, regenerating axons eventually negotiated the persistent larger gap to grow along the distal glial scaffold. However, the reforming nerves presented more pronounced local de-fasciculation, and the Schwann cells finally filled up the gaps in Sarm1$^{-/-}$ (**Figure 4.7.3B** and **Figure 4.7.5**). This result indicates that the filopodia-bridge

from Schwann cells is not essential for the regrowth of axons in Sarm1$^{-/-}$ zebrafish (Tian et al., 2020).
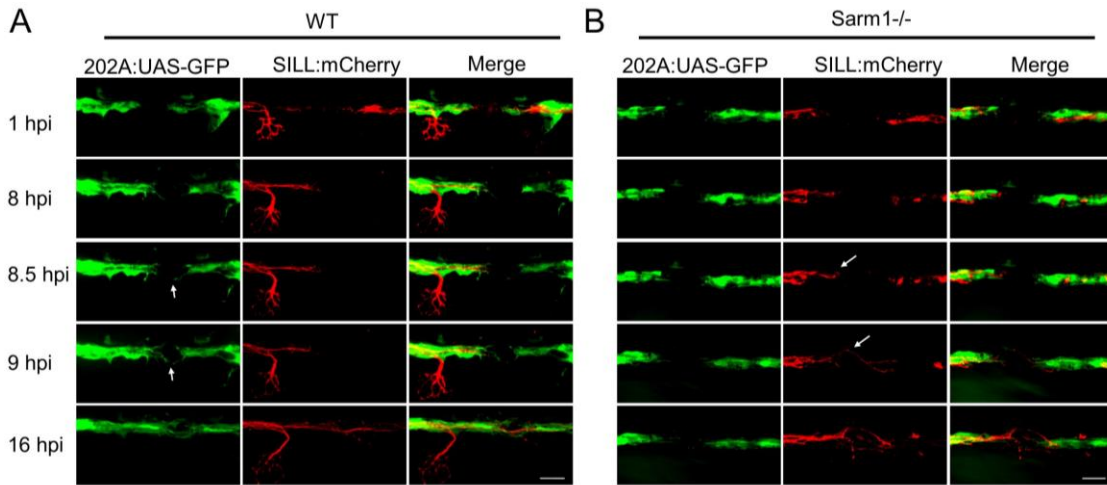
Figure 4.7.3 Filopodia-bridge from Schwann cells is not essential for the regrowth of axons in Sarm1$^{-/-}$ zebrafish. A) Images show the discrete local defasciculation of regenerated sensory fiber (red) and the bridging of the glial gap by Schwann cells (green) in a WT specimen. B) Equivalent experiment, images showing a more pronounced local defasciculation of the regenerated sensory fiber (red) in a Sarm1$^{-/-}$ specimen. Note that the bridging of the glial gap does not occur (modified from Tian et al., 2020).

Figure 4.7.4 Series of images enlarged from Figure 4.7.3A. They show eight time points during the repair of the gap in the Schwann cell scaffold (A-H) and axonal regeneration after transection (A'-H') in a WT animal. Rostral is left and caudal is right. In all panels, the green asterisks show the location of the pioneering growth cone of the regenerating axons. In A-D' the purple arrowheads mark the

filopodia-like extensions from Schwann cells adjacent to the glial gap. At the start of the series, (A, A')
the axonal terminal stump and the Schwann cells proximal to the gap co-localize (near juxtaposition of
the green asterisk and the purple arrowhead. In B, a Schwann cell extends a filopodium across the gap,
whereas the axons (B') do not grow along this extension across the gap. In C, several extensions from
Schwann cells are clearly visible at the top and bottom aspects of the image. The shape of the lower
extension from a Schwann cell did not change, suggesting that they are stabilized, perhaps through
interactions with the substrate. Proximal axons (C') start to grow along these Schwann-cell protrusions.
In D, the extensions from the anterior and posterior Schwann cells have crossed the gap, physically
interact and commence to reconstitute a continuous glial scaffold. The axonal projections (D'), however,
have suffered a retraction towards the proximal stump. E-F show a continuation of Schwann cells
behavior, increasing the contacts and closing the gap, which is obvious by the smaller area of the gap
(distance between proximal and distal Schwann cells). E'-F' show a more robust and persistent
extension of the axonal growth cones, which grow nearly strictly along the Schwann cells extensions.
G-H show the Schwann cells closing the gap. G'-H' show axonal extension across the gap and along
the distal Schwann cells. Although the gap in the glial scaffold is much reduced, nerve fibers show
discrete defasciculation (H') (modified from Tian et al., 2020).
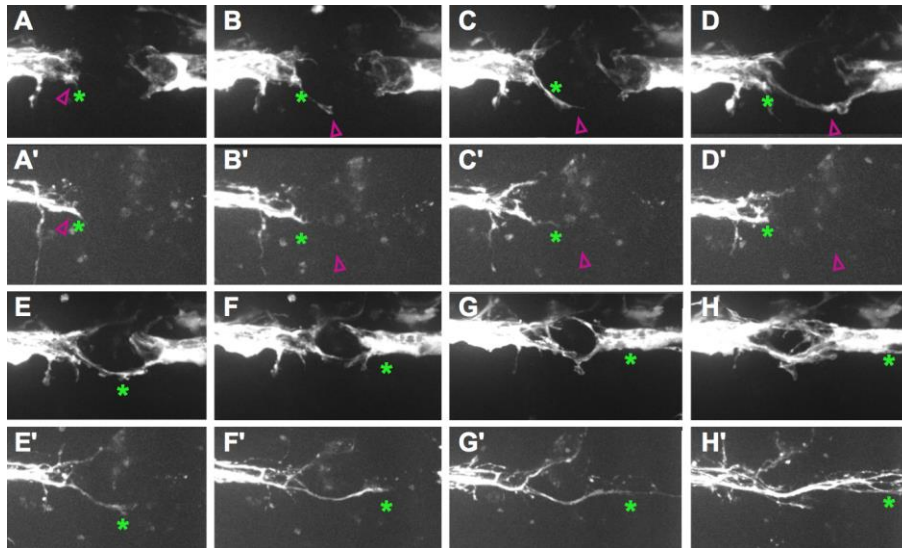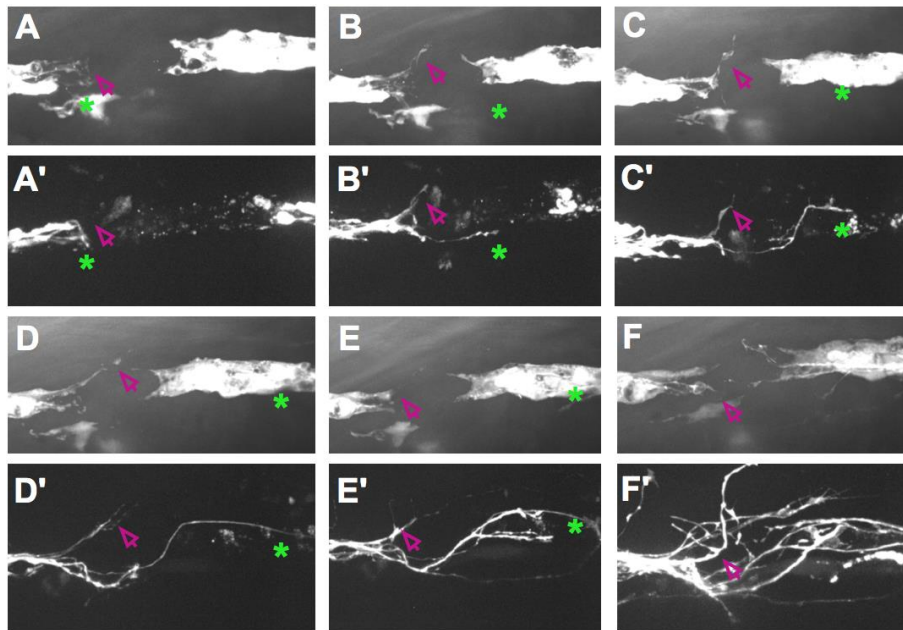

Figure 4.7.5 Series of images enlarged from Figure 4.7.3B. They show six time points during the
repair of the gap in the Schwann cell scaffold (A-F) and axonal regeneration after transection (A'-F') in
a Sarm1$^{-/-}$ specimen. In all panels, the green asterisks show the location of the pioneering growth cone
of the regenerating axons, and the purple arrowheads mark filopodia-like extensions from Schwann
cells. Unlike the wild-type situation, the Schwann cells adjacent to the gap form small filopodia-like
extensions (B-D) that never cross the gap. The proximal stump eventually forms growth cones that cross

the gap at various locations (C') and, upon finding distal Schwann cells, grow along the glial scaffold (D'-F'). Nerve fibers show extensive local defasciculation (F') (modified from Tian et al., 2020).

After injury, the denervated Schwann cells are changing the state from myelinating to a progenitor-like by partial dedifferentiation rapidly. This is confirmed by checking the expression of terminal-phenotype markers, including myelin and myelin related proteins (Sasaki et al., 2018; Soto and Monje, 2017). In addition, the progenitor state Schwann cells is able to proliferate and migrate along the axons, which enhances their regenerative function (Carr and Johnston, 2017). I hypothesized that the distal Schwann cells may not dedifferentiate and retain the terminal phenotype, because the non-degradable axons maintain the Schwann cells in $Sarm1^{-/-}$. This would explain why Sarm1-deficient SCs loss phagocytic and protrusive activities after axon transection. Following this hypothesis, I performed the immunostaining of transected samples with an antibody against Claudin-k, which localizes the junctions between mature Schwann cells and was downregulated in denervated glia (Xiao et al., 2015a). In WT specimens, Claudin-k maintained strong expression along the entire lateralis afferent nerves up to 6 hours post injury (hpi), suggesting that the distal Schwann cells remain mature during distal axon fragmentation. After 10 hpi, the injured axons degenerated and the Schwann cells in the distal part had remarkably less Claudin-k than proximal ones. Finally, the Claudin-k was conspicuously absent from the distal Schwann cells even after axons regeneration had commenced (**Figure 4.7.6B**). By contrast, Claudin-k remained strongly expressed after axon severing in $Sarm1^{-/-}$ larva from 6 hpi to 24 hpi, with no obvious difference between Schwann cells located at both sides of the transected site (**Figure 4.7.6C**). Next, I assessed myelination of axons with the 6D2 monoclonal antibody, which recognizes a carbohydrate epitope in the piscine p0-like myelin glycoproteins IP1 and IP2 (López-Schier and Hudspeth, 2005). In the WT specimens, the immunostaining of 6D2 did not change up to 10 hpi. Compared to Claudin-k, the 6D2 was degraded much slower in the distal part after injury (**Figure 4.7.6D**). It disappeared around 24 hpi in WT. However, the expression of 6D2 was retained in Sarm1-deficient samples after injury (**Figure 4.7.6E**). Taken together, these results reveal that Schwann cells distal to the injury do not de-differentiate in $Sarm1^{-/-}$ specimens (Tian et al., 2020).
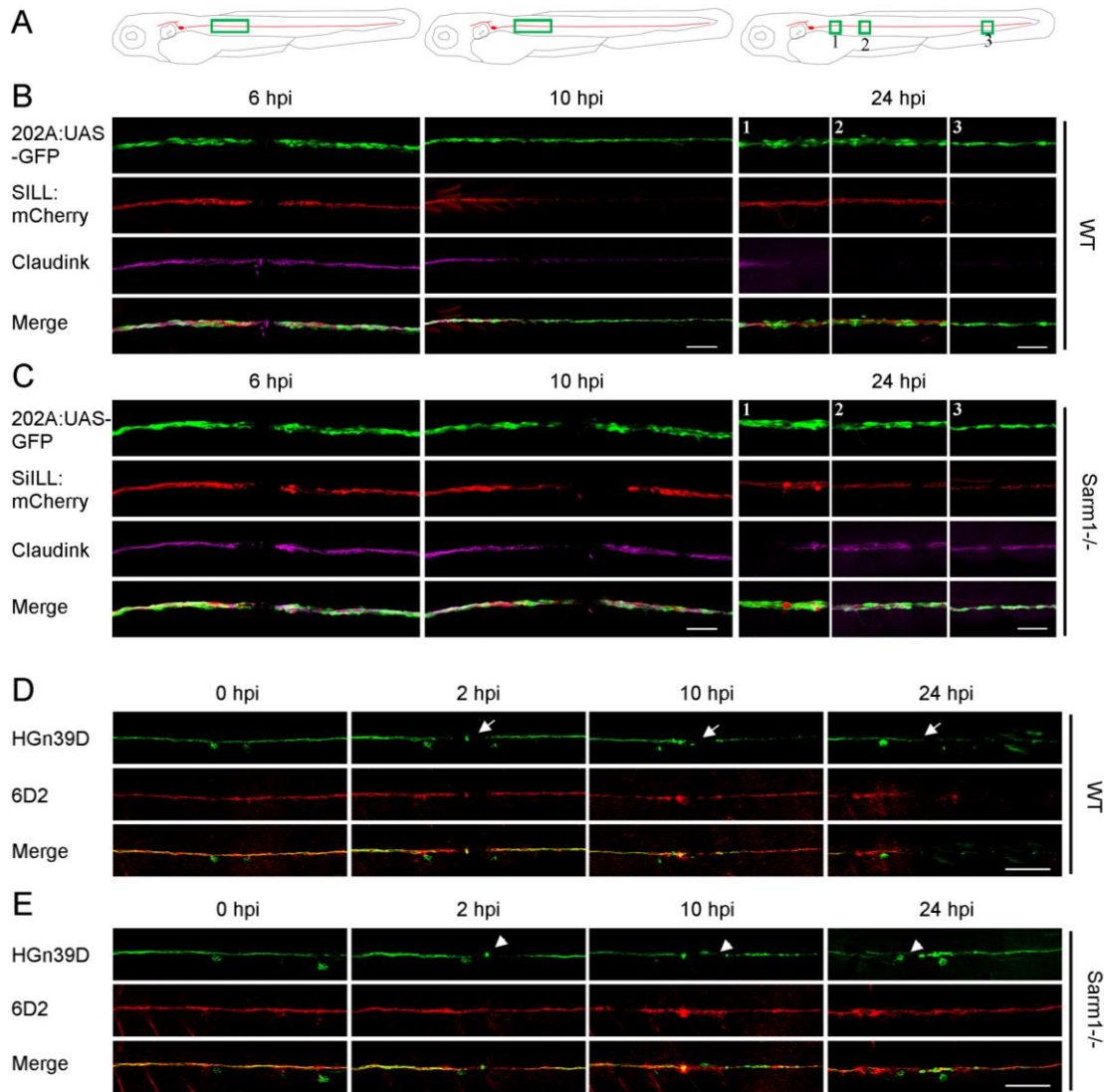
Figure 4.7.6 Non-degradable Sarm1-deficient axons maintain the tight junction and myelin of the distal segments. A-C) Schematic model of the confocal imaging locations on severed axons (A). Confocal images of WT (B) and Sarm1$^{-/-}$ (C) specimens in 6 hpi, 10 hpi and 24 hpi. hpi = hour post injury. The specimens were the *Tg[gSAGFF202A;UAS:EGFP; SILL:mCherry]* lines and were stained with Claudin-k (magenta) antibody. Scale bar 50μm. D-E) Confocal images of WT (D) and Sarm1$^{-/-}$ (E) specimens expressing EGFP in sensory neurons of the lateral line (green) and stained with the monoclonal antibody 6D2. Immunostainings were performed at indicated time points after axon severing (hpi). The arrows point to the cutting sites. Scale bar 50 μm (modified from Tian et al., 2020).

Next, I used live imaging to investigate the dynamics of axons and associated myelin after injury in 4 dpf larvae from WT or Sarm1$^{-/-}$. The myelin was labelled by expressing membrane-targeted EGFP fused to the myelin binding protein. In the WT larvae, the

degradation of myelin happened later than the fragmentation of severed axons. Around 8 hpi, the severed axons were undergoing fragmentation and degradation, but the morphology of myelin was normal. From 12 hpi, most axonal debris had already been cleared. Meanwhile, the myelin was collapsing and fragmenting. Until 16 hpi, the regenerative axons grew normally, while the myelin was still present (**Figure 4.7.7A**). In contrast, the myelin did not change after severing axons in the Sarm1$^{-/-}$ samples. Moreover, the regrowing axons were not affected by the non-degradable axons and myelin (**Figure 4.7.7B**). These results suggest that the degradation of myelin is a consequence of axon fragmentation after injury. Sarm1-deficient neurons keep the distal axons and their associated myelin intact after axotomy, and the clearance of myelin is not necessary for axon regrowth (Tian et al., 2020).
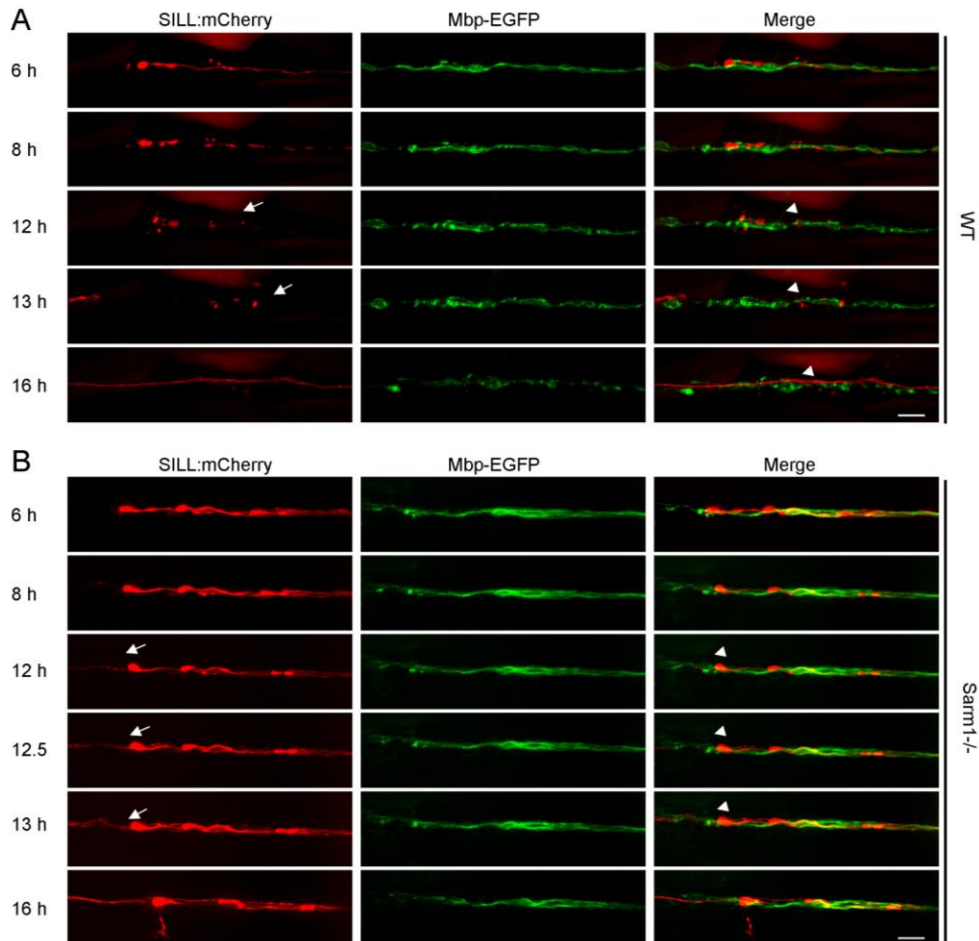

Figure 4.7.7 Clearance of axonal and myelin debris is not essential for axon regeneration. A) Live imaging of the *Tg[Mbp-EGFP; SILL:mCherry]* after severing. The arrows indicated the fragmented

axons and the arrowheads the fragmented myelin. Scale bar 20 μm. B) Live imaging of the Sarm1^{-/-} in *Tg[Mbp-EGFP; SILL:mCherry]* after severing. Arrows indicate regrowing axons, and arrowheads indicate the juxtaposition between the regrowing axons. Scale bar 20 μm (modified from Tian et al., 2020).

4.8 Schwann cells are not essential for the maintenance of Sarm1-deficient axonal segments

To know whether Schwann cells are necessary for the maintenance of severed Sarm1-deficient axons, I generated a double knockout zebrafish line concurrently deficient in Sarm1 and Erbb2, the latter being required for Schwann cells migration along the axons (Lyons et al., 2005). Loss of Erbb2 leads to the lateralis nerve defasciculation in zebrafish (Lyons et al., 2005; Xiao et al., 2015a). In the Erbb2-deficient specimens, the distal portion of severed axons fragmented and were cleared, but with a significant delay of fragmentation time, as compared to WT specimens (**Figure 4.8.1A**). In WT, the average fragmentation time was around 4 hours after axon severed, but it delayed to 12 hours in the Erbb2^{-/-}. By contrast, in Sarm1^{-/-}Erbb2^{-/-}, severed axons did not fragment or degrade, as well as the fish lacking only Sarm1 (**Figure 4.8.1B**). Similar to the Erbb2^{-/-}, the regeneration of axons was not affected in the double knockouts line. At a later time, the axonal debris was cleared in both Erbb2^{-/-} and Sarm1^{-/-}Erbb2^{-/-} specimens, indicating that the clearance of axon debris was not fully dependent on Schwann cells (**Figure 4.8.1A**). Taken together, maintenance of severed axon in Sarm1^{-/-} occurs independently of Schwann cells, and the Schwann cells are partially involved in axon debris clearance (Tian et al., 2020).
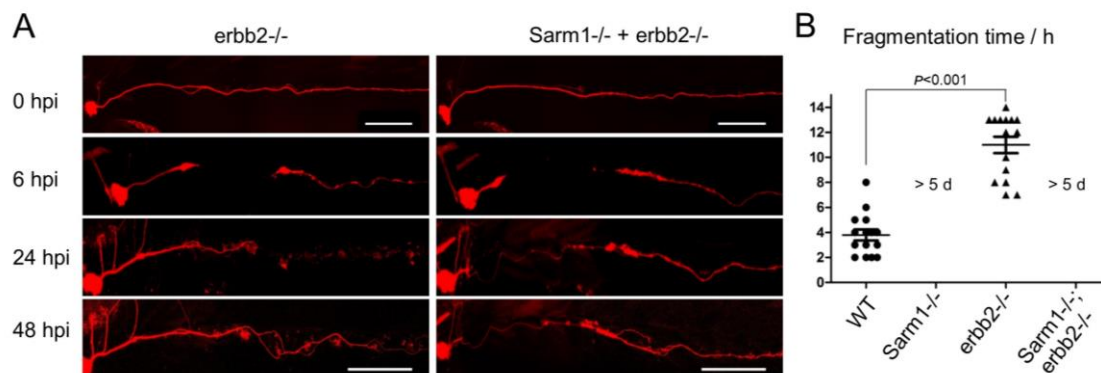
Figure 4.8.1 Schwann cells are not essential for the maintenance of Sarm1-deficient axonal segments. A) Images of mCherry-expressing (red) transected axons in Erbb2$^{-/-}$ and Sarm1$^{-/-}$; Erbb2$^{-/-}$ double knockouts. Scale bar 100 μm. B) Quantification of transected axon fragmentation in Erbb2$^{-/-}$ and Sarm1$^{-/-}$; Erbb2$^{-/-}$. Error bar = SEM, *p* value from one-way ANOVA, n = 15 (each group) (modified from Tian et al., 2020).

Next, I expressed the ratTRPV1-tgRFP and EGFP into the *Tg[Erbb2$^{-/-}$; Sarm1$^{-/-}$]* larvae to label the axons with GFP alone or both GFP and ratTRPV1-tgRFP. The posterior lateral nerve of 4 dpf positive larvae were severed with laser. One hour later, the larvae were incubated with capsaicin for one hour. The images were taken with confocal microscopy 10 hours later. As shown in the representative images, the ratTRPV1-tgRFP and GFP positive axon was degraded in presence of capsaicin (the arrow indicating one), although the axons lacked Schwann cells. In contrast, the axon without ratTRPV1-tgRFP was not degraded (the arrowhead indicating GFP-positive one) (**Figure 4.8.2**). These results suggest that the axoplasmic calcium influx which induces the axon fragmentation was not completely dependent on Schwann cells. Moreover, Schwann cells are not essential for the maintenance of severed Sarm1-deficient axonal segments.
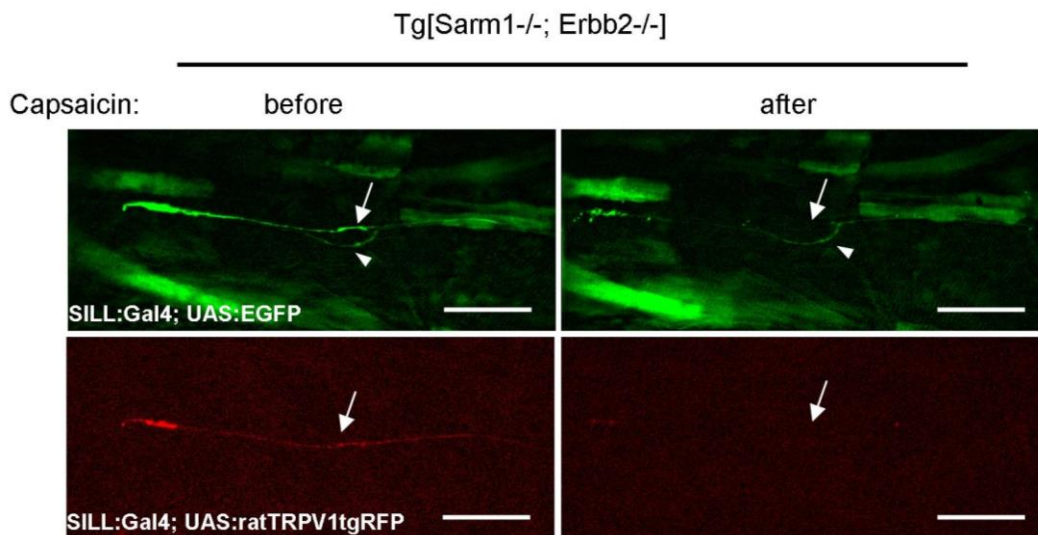
Figure 4.8.2 Schwann cells are dispensable for the clearance of Sarm1-deficient axonal debris. Confocal images of the GFP labeled axons (SILL:Gal4; UAS-EGFP) with or without Trpv1 positive axons (SILL:Gal4; UAS:ratTRPV1-tgRFP) in Erbb2$^{-/-}$ and Sarm1$^{-/-}$ double knockouts before and after capsaicin incubation. Arrowheads indicate the GFP labelled axons. Arrows indicate the GFP and ratTRPV1 double expressed axon. Scale bar 50 μm.

4.9 Loss of Sarm1 slightly delays the remyelination of regenerative axons.

Axons are wrapped by myelin which isolates the axons from the outside environment, enhances the action potential conduction, and maintains the nerve fasciculation (Raphael and Talbot, 2011). To assess the myelination of axons, I generated the *Tg[HGn39D; mbp-tgRFP]* lines in a WT or Sarm1^{-/-} background. I observed that the myelin ensheathed axons of posterior sensory neurons of WT and Sarm1-deficient zebrafish larvae. However, the morphology and density of the myelin did not show any obvious difference between WT and Sarm1^{-/-} (**Figure 4.9.1A-B**). These images suggest that Sarm1 deficiency does not influence the myelination of axons in the development of posterior lateral line nerves.
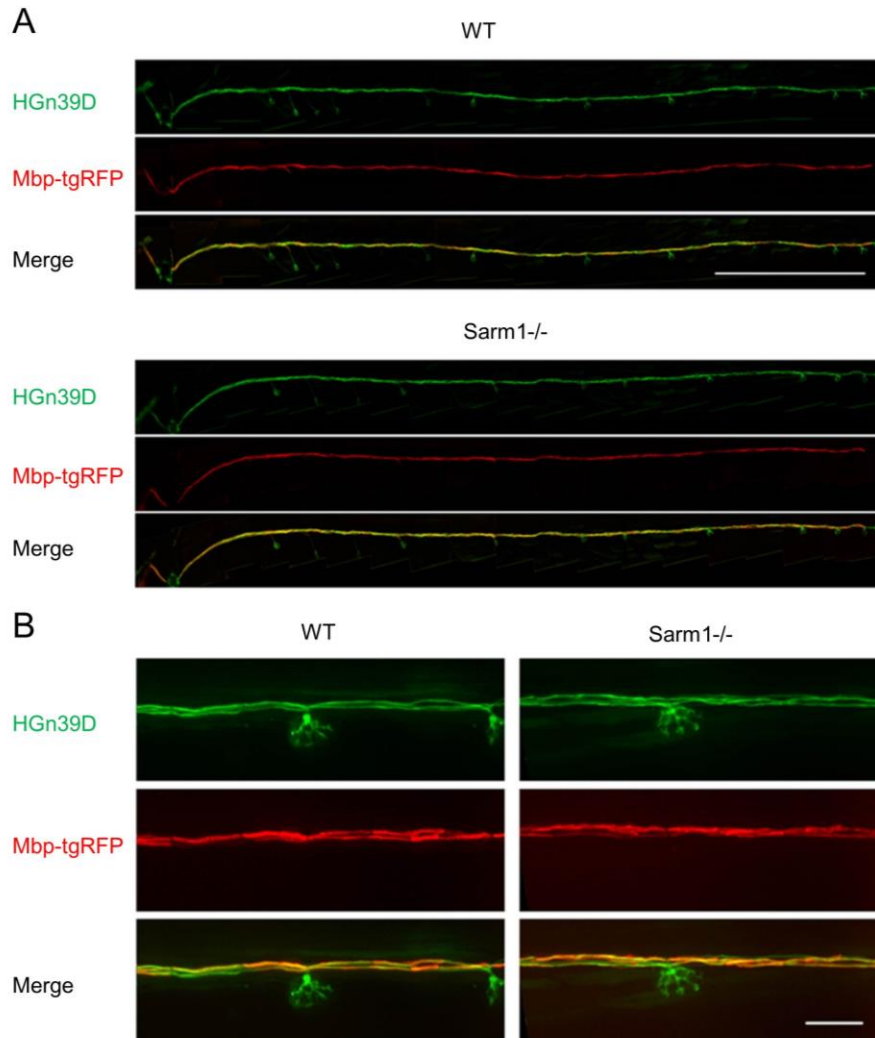
Figure 4.9.1 Overview of the myelination in wild type and Sarm1^{-/-} zebrafish. A) Confocal images of whole view of axons and myelin in WT (top) and Sarm1^{-/-} (down). The samples were the

Tg[HGn39D; mbp-tgRFP] lines. Scale bar 400 μm. B) High magnification images of the axons and myelin in WT and Sarm1$^{-/-}$. Axons were green (HGn39D) and myelin (Mbp-tgRFP) was red. Scale bar 50 μm.

The peripheral neurons can recover functionally from injury, in which the regenerative axons are myelinated by Schwann cells (Ceci et al., 2014). I continued the live imaging to track the remyelination capacity of Schwann cells after severing axons in WT and Sarm1$^{-/-}$ zebrafish larvae. The dynamic of new myelin formation was displayed with a montage of time-lapse images. I found that the myelination was starting earlier than 48 hpi and the myelin was much thicker in the WT than in the Sarm1$^{-/-}$. In addition, the myelination of regenerated axons was completed quickly in the WT animals. By contrast, in the Sarm1$^{-/-}$ ones, the myelination of regenerated axons was a bit slower, indicating that the myelination capacity of the Schwann cells was not disrupted in the Sarm1$^{-/-}$ (**Figure 4.9.2A-B**). These results suggest that loss of Sarm1 only marginally affects the myelination of regenerated axons.
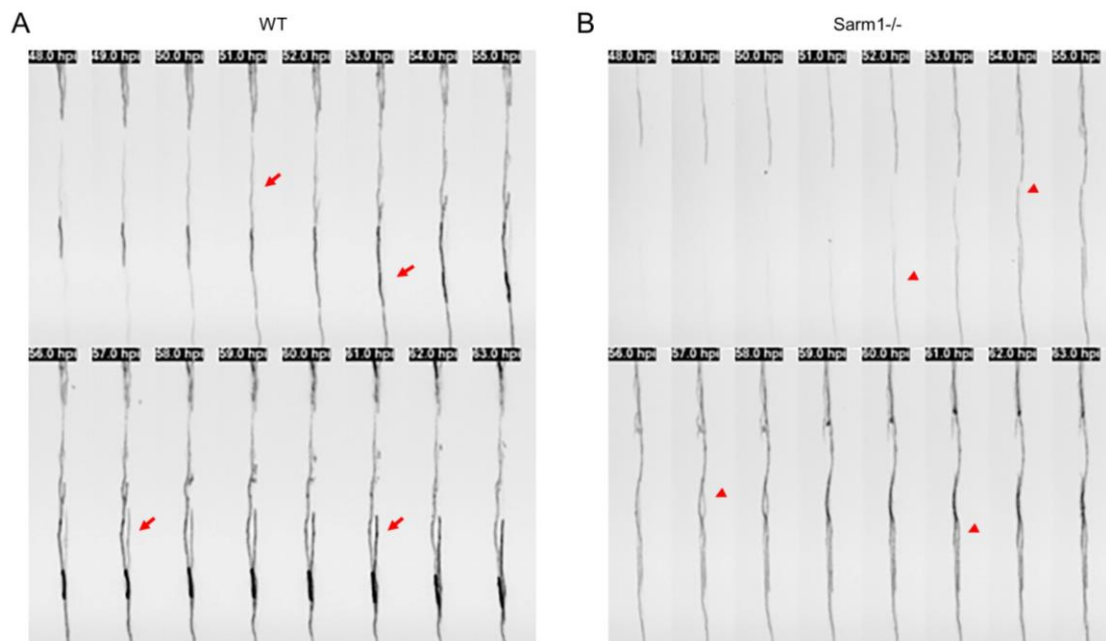
Figure 4.9.2 Remyelination is slightly slower in Sarm1$^{-/-}$ zebrafish. A) Montage images showing a time lapse imaging of *Tg[mbp:tgRFP]* after axotomy. The red arrows indicate the process of remyelination in WT. B) Montage images displaying the time lapse imaging of the Sarm1$^{-/-}$ in *Tg[mbp:tgRFP]* after axotomy. The red arrowheads indicate the progress of remyelination in Sarm1$^{-/-}$.

4.10 The recruitment of macrophages is not impaired in Sarm1-deficient zebrafish

Macrophages are recruited into the injured axons for clearing the axon debris (Bendszus and Stoll, 2003). Sarm1 has an essential role in CCL5 induction in macrophages (Gürtler et al., 2014). I wondered whether macrophages lose the capacity to move into the injured axons and eradicate the axon debris for regeneration in Sarm1$^{-/-}$ zebrafish larvae. In order to observe the recruitment of macrophages, I generated the transgenic line, *Tg[mfap4: EGFP-CAAX]*, which allows live, long-term analysis of macrophage behavior (Walton et al., 2015). The time-lapse images started from 30 mins after severing the axons of posterior sensory nerves. The panels scope the images from 3 hours post injury to 14 hours post injury. In the WT larva, the macrophages were recruited to the distal segments of axons and cleared the fragmented axons. In the stage of axonal regeneration, the macrophages still stayed in surrounding of the regenerating axons. In the Sarm1$^{-/-}$, the macrophages were recruited to and moved along with the transected axons. The movement of the macrophages suggested that they were screening and surveilled the intact of the axons. Even in the Erbb2$^{-/-}$, which lack of Schwann cells, the macrophages moved to the injury axons for cleaning the debris (**Figure 4.10A**). Next, I found that the onset of recruitment and number of macrophages at the wound did not differ between WT and Sarm1 or Erbb2 knockout (**Figure 4.10B**). The retention time of macrophages at the proximal side of the wound was unaltered in Sarm1$^{-/-}$ or Erbb2$^{-/-}$, although on average slightly lengthened in the absence of Schwann cells (**Figure 4.10C**). However, I found a significant increase in the size of the engulfed debris by macrophages in Erbb2$^{-/-}$ animals (**Figure 4.10D**). When I fragmented axons with ratTRPV1/Capsaicin in WT or Sarm1$^{-/-}$, I found macrophages were still recruited to the axon debris (**Figure 4.10E**). These results reveal that loss of Sarm1 does not affect focal damage resolution by macrophages, which are recruited to the wound independently of Schwann cells. We did notice discrete and highly mobile axon fragments that were not associated to EGFP(+) cells in WT and Erbb2$^{-/-}$ zebrafish but not in Sarm1-deficient fish. This observation suggests that loss of Sarm1 does not affect the recruitment and the phagocytic activity of macrophages (Tian et al., 2020).
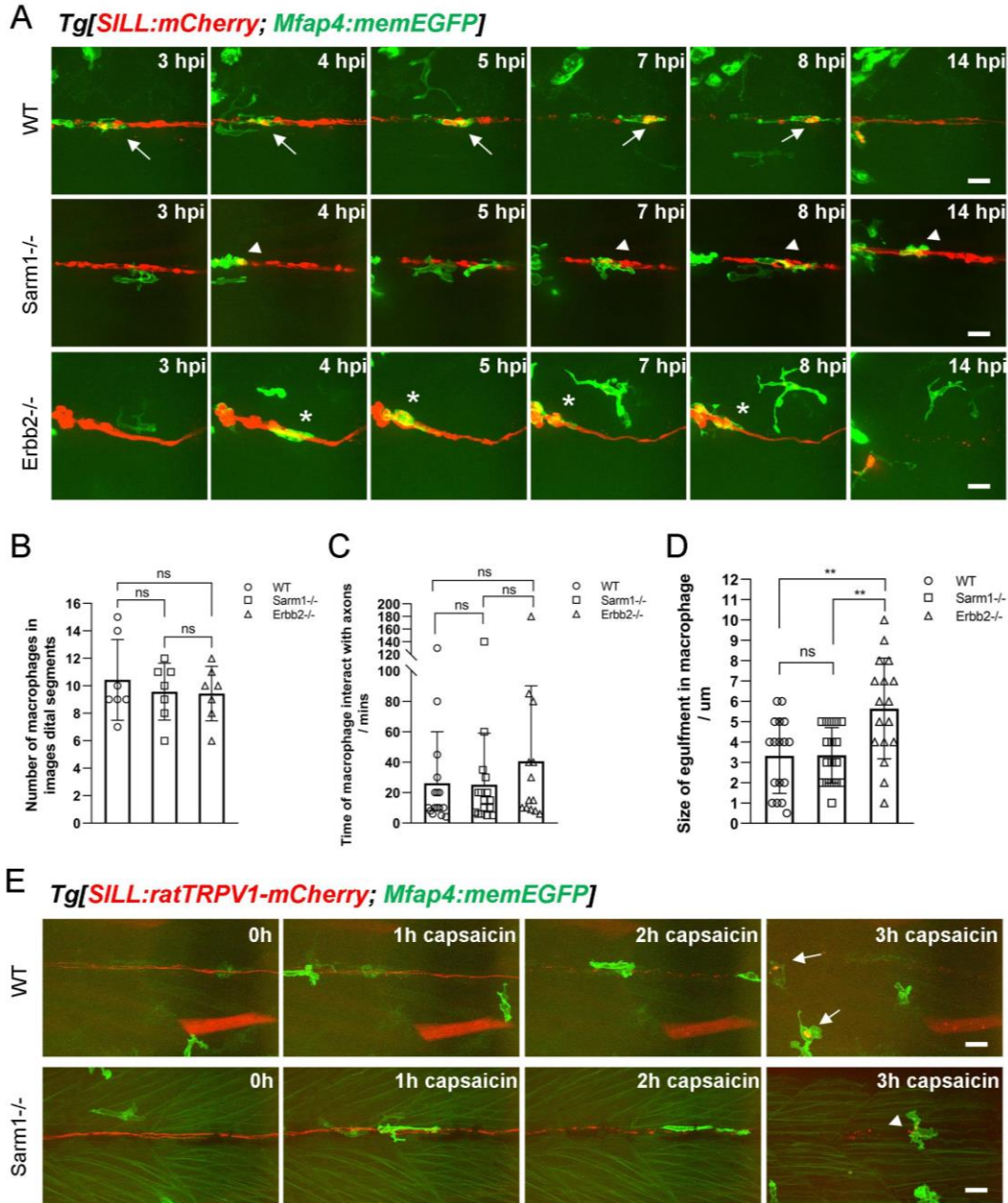
Figure 4.10 Loss of Sarm1 does not impair the recruitment of macrophages to injury axons. A) Images showing the time lapse imaging of *Tg[SILL:mCherry; mfap4:EGFP-CAAX]* after severing. The arrows indicate macrophages in the severed WT axons. The arrowheads indicate macrophages in the severed Sarm1-deficient axons. The asterisks indicate macrophages surround and engulf the injury axons in Erbb2$^{-/-}$. B) Quantification of the number of macrophages recruited to the injury site and adjacent axon segments. C) Quantification of the time macrophages interact with axon segments. D) Quantification of the size of debris within macrophages. one-way ANOVA was conducted firstly, then the T-test was performed between two individual group. E) Time lapse images showing macrophages

were recruited into the fragment axons which were induced by ratTRPV1/Capsaicin (modified from Tian et al., 2020).

4.11 Loss of Sarm1 protects Schwann cells against chemotoxicity

Chemotherapeutic agents invariably cause peripheral neuropathy in clinical trials, leading to permanent neuronal dysfunction (Cavaletti et al., 2011; Fukuda et al., 2017). Previous studies have revealed that the denervated Schwann cells become susceptible to chemotoxicity (Diezi et al., 2013). Therefore, I hypothesized that the protracted maintenance of severed axons in Sarm1$^{-/-}$ zebrafish might counteract glial vulnerability to chemotoxicity. To test this possibility, I treated WT and Sarm1-deficient zebrafish with several chemical compounds that are under clinical trials or that are currently used as first-line treatment for common cancers in humans. First, I used 10-Hydroxycamptothecin (10-HCT), which is extremely toxic to denervated glia in zebrafish (Bremer et al., 2017), and counted Schwann cells using the fluorescence transgenic marker *Tg[gSAGFF202A; UAS:EGFP]*. This marker is ideal for the experiment because the intensity of green fluorescence does not change in denervated Schwann cells and, therefore, it is independent of the maturity of the glia. Specifically, the *Tg[gSAGFF202A; UAS:EGFP; SILL:mCherry]* and *Tg[gSAGFF202A; UAS:EGFP; SILL:mCherry; Sarm1$^{-/-}$]* samples were collected at 4 dpf. These samples were separated into five groups, control, 48 hpi, 10-HCT (48 h), 24 h 10-HCT/hpi and 48 h 10-HCT/hpi. The control and 10-HCT groups were the intact samples without axon transection and were exposed to DMSO (1% V/V) or 10-HCT individually. The groups with hpi (hour-post injury) were the transected samples in which all the axons of the posterior lateral-line were severed with laser on one side of the fish. The images displayed the axons (red) and Schwann cells (green) in the indicated groups (**Figure 4.11.1A**). With the quantification of the number of Schwann cells, I confirmed that the 10-HCT does not affect the Schwann cells associated to viable axons, in both WT and Sarm1$^{-/-}$. However, there was a significant reduction of the number of Schwann cells in 10-HCT treated WT zebrafish with axon transection at 24 hpi. With long-time treatment, the decrease in the number of Schwann cells was more pronounced. By contrast, the number of distal Schwann cells was only marginally affected in axon

transected Sarm1$^{-/-}$ zebrafish at 24 hpi with 10-HCT treatment specimens, and nearly identical to untreated zebrafish (**Figure 4.11.1B**).

Platinum-based, taxanes and some alkaloids are effective chemotherapeutic agents used as standards-of-care for various malignancies, despite their severe neuropathic effects that include glial destruction (Imai et al., 2017). I selected some of these agents including oxaliplatin, cisplatin, paclitaxel, docetaxel and vincristine, to test their effect on Schwann cells. The 4 dpf *Tg[gSAGFF202A; UAS:EGFP; SILL:mCherry]* or *Tg[gSAGFF202A; UAS:EGFP; SILL:mCherry; Sarm1$^{-/-}$]* larvae were divided into the following groups, WT, WT sever, Sarm1$^{-/-}$ and Sarm1$^{-/-}$ sever. The sever-related groups were the one-side posterior lateral-line transected animals. All the groups were treated with the indicated agent respectively. As showed in the graphs, these drugs do not affect the number of Schwann cells in intact WT or Sarm1$^{-/-}$; however, they all invariably killed the Schwann cells of the distal segments in the axon transected WT zebrafish. The number of Schwann cells from the axon transected WT zebrafish was reduced to almost half of the number of axon intact WT ones. In contrast, the number of Schwann cells was not affected in the Sarm1-deficient related groups (**Figure 4.11.1C-D**). Collectively, I found that upon nerve transection, all these drugs invariably killed injury-distal Schwann cells in wild-type specimens but not in Sarm1$^{-/-}$ zebrafish (Tian et al., 2020).
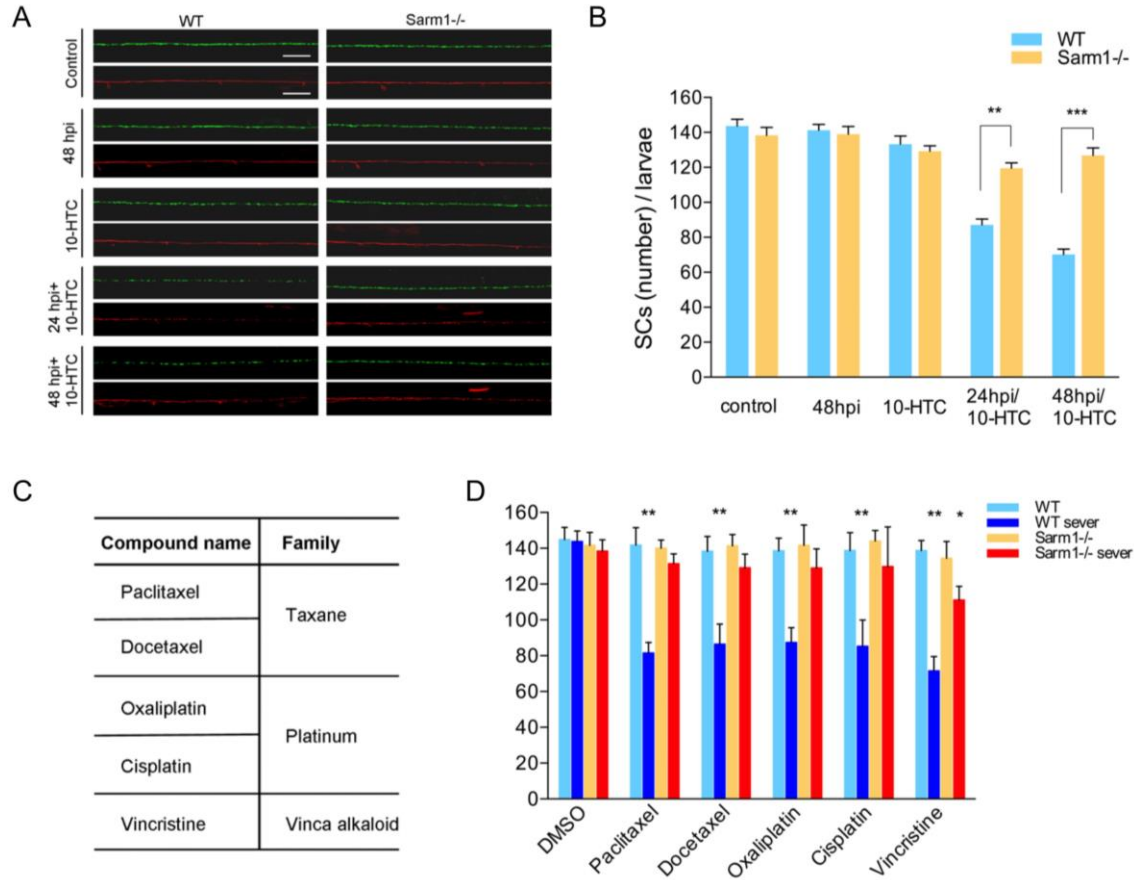
Figure 4.11.1 Loss of Sarm1 protects Schwann cells against chemotoxicity. A) Confocal images showing Schwann cells (green) and lateralis sensory axons (red) in a control specimen (in which axons were not transected), in a specimen 48 hours after axon transection, and in specimens treated with 10-HCT (10-Hydroxycamptothecin). Left column is WT and right column shows Sarm1^{-/-}. In all cases, the final concentration of 10-HCT was 40 μM. Scale bar 100 μm. B) Quantification of the Schwann cells from A). Data are shown as mean ± SEM. ** means $p < 0.01$, two-way ANOVA, $n = 8$ (each group), followed by T-test for two individual group. C) Table for the chemicals used in the experiment. D) Quantification of Schwann cells of WT, WT severed, Sarm1^{-/-} and Sarm1^{-/-} severed with the treatment of the indicated chemical compounds for 48 hours. Concentrations: Paclitaxel 40 μM, Docetaxel 0.1 μM, Oxaliplatin 500 μM, Cisplatin 50 μM, Vincristine 50 μM. Data are shown as mean ± SEM. * means $p < 0.05$; ** means $p < 0.01$, three-way ANOVA, $n = 8$ (each group), followed by T-test for two individual group (modified from Tian et al., 2020).

In Sarm1^{-/-} zebrafish, severed axons remained and did not degrade. These non-degradable axons could support the Schwann cell against drug exposure. To answer this hypothesis, I generated the transgenic line, *Tg[SILL:ratTRPV1-tgRFP; gSAGFF202A; UAS:EGFP;*

sarm1$^{-/-}$], which enables me to degrade the severed Sarm1-deficient axons with capsaicin. In the WT related groups, the number of Schwann cells was significantly decreased in the axon transected groups in presence of 10-HCT or Vincristine, as comparing to the axon intact groups. By contrast, in the Sarm1-deficient related groups, the number of Schwann cell was no statistical difference between the control and the axon severed groups in presence of 10-HCT or Vincristine. These results are consistent to the previous conclusion. As expected, the numbers of Schwann cells were decreased to around 110 in axon ablated Sarm1-deficient larvae in presence of 10-HCT or Vincristine, in which Sarm1-deficient axons were forced to fragment by ratTRPV1/capsaicin. This number is significantly less than the Sarm1-deficient axons severed groups with the treatment of 10-HCT or Vincristine, although it was slightly more than the WT severed groups upon 10-HCT or Vincristine treatment (**Figure 4.11.2**). Taken together, these data indicate that ablation of the axons in Sarm1 deficient neurons could attenuate the protection roles of non-degradable axons in Schwann cells against chemotoxicity. Importantly, because none of these drugs affect Schwann cells associated with intact axons, I conclude that non-degradable axons protect Schwann cells from chemical stress (Tian et al., 2020).
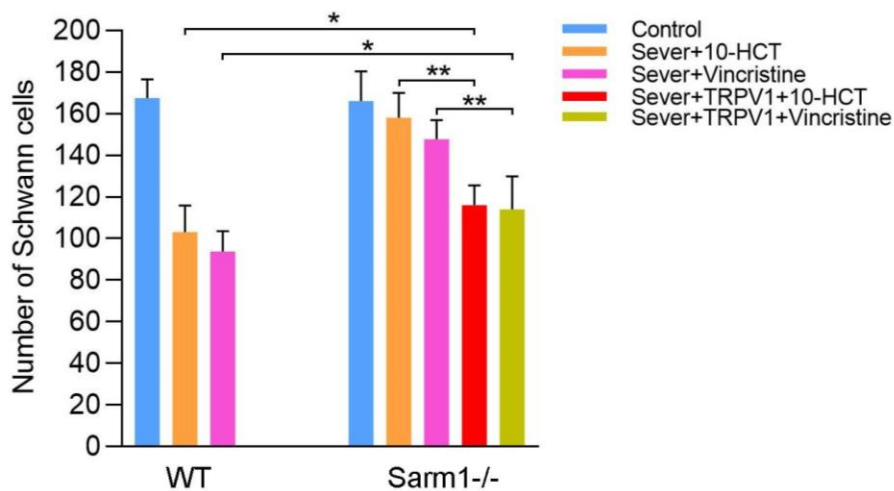
Figure 4.11.2 Ablation of Sarm1-deficient axon attenuates the survival of Schwann cells against drugs in Sarm1$^{-/-}$ zebrafish. Quantification of Schwann cells of WT, WT severed+10-HCT, WT severed+Vincristine groups, and Sarm1$^{-/-}$, Sarm1$^{-/-}$ severed+10-HCT, Sarm1$^{-/-}$ severed+Vincristine, Sarm1$^{-/-}$ severed+TRPV1+10-HCT, Sarm1$^{-/-}$ severed+TRPV1+Vincristine. Data are shown as mean ± SEM. * means $p < 0.05$; ** means $p < 0.01$, two-way ANOVA, n = 8 (each group) followed by T-test for two individual group (modified from Tian et al., 2020).

5. Discussion

Sensory neurons connect sensory receptors, muscles and skin to the central nervous system enabling animals to perform the essential activities in daily life (Abraira and Ginty, 2013). Chemical stress, chronic metabolic disease, or physical damage from head concussions, motor-vehicle and sporting accidents cause neural injury, leading to axon degeneration in peripheral and autonomic neuropathies in humans (McKee and Daneshvar, 2015). Nerve injury or glial cells loss has a significant negative impact on the quality of life of the affected individuals. Understanding the mechanism of axon degeneration and the function of its associated glial cells is essential for screening new therapeutic methods to protect neuropathy in clinical trials.

Zebrafish is an ideal vertebrate model for screening the therapeutic agents. In my thesis, I address the effect of absence of Sarm1 on axon degeneration and Schwann cells systematically and reveal the possibility to block axon degeneration with loss of Sarm1 as a target for developing therapeutic applications. Specifically, I have generated Sarm1$^{-/-}$ zebrafish, which impede the degeneration of severed axons in the peripheral and central nervous systems. The inhibition of axon degeneration was independent of the Schwann cells that surround and ensheath the axons in Sarm1$^{-/-}$ zebrafish. Moreover, prevention of axon fragmentation was mediated by attenuating the calcium influx in the axoplasm but not in mitochondria or the endoplasmic reticulum. Synthetic elevation of the axoplasmic calcium could fragment the Sarm1-deficient axons, suggesting that the calcium influx is the downstream event in Sarm1 mediated axon degeneration. I also revealed that loss of Sarm1 does not affect viability, touch-evoked response, and rheotaxis of zebrafish. The electrophysiology tests showed that the physiological activities of sensory neurons were normal in the Sarm1$^{-/-}$ zebrafish. Furthermore, non-degradable axons maintain the structure of myelin and Schwann cells, which do not repel the regrowth axons in the sensory nervous system. The morphology and the myelination capacity of Schwann cells were normal in the Sarm1-deficient zebrafish. Intriguingly, I found that loss of Sarm1 enhances the resistance of Schwann cells to chemotoxicity, which is dependent on the non-degradable axons. Taken together, targeting the Sarm1 is an ideal strategy for developing therapeutic applications.

Sarm1 is essential for the degeneration of severed sensory neurons in zebrafish

My work reveals that the pro-degenerative protein Sarm1 is functionally conserved from invertebrate to vertebrate (Osterloh et al., 2012). Considering that zebrafish is an optimal model for high-resolution live imaging (Friedrich et al., 2010), Sarm1-deficient zebrafish is a welcome addition for future studies of Sarm1 function *in vivo*. During my work, I generated a Sarm1 knockout zebrafish and performed systematic tests with sensory neurons that are ideal for imaging the dynamics of axon degeneration and regeneration (Villegas et al., 2012). In the Sarm1$^{-/-}$ zebrafish larvae, the distal segments of the severed axons did not degrade demonstrating that Sarm1 is essential for Wallerian axon degeneration.

Because Sarm1 is well conserved across species, I wondered about the benefit of fast axonal degradation to the organism, in particular because some invertebrates that include crayfish, roundworm and leech maintain injured axons with no signs of degeneration (Frank et al., 1975). Strikingly, the lack of axon degeneration may have been selected because severed axon segments in *C. elegans* reseal to reconstitute the neuronal circuit rapidly. This appears to be a very effective strategy to recover neural function with high fidelity (Neumann et al., 2015). Yet, axon resealing has not been observed in other species, begging the question of why vertebrates do not use a similar mechanism after nerve injury. One possibility is that the degradation of severed axons is too fast to enable resealing (Gumy et al., 2010). Alternatively, resealing events may have remained hidden owing to the technical difficulties associated to imaging axonal behavior in living vertebrates. Taking advantage of zebrafish lacking Sarm1 and its amenability for high-resolution intravital imaging, I tested whether the protracted maintenance of severed axons allows axon-segments resealing. To this end, I developed an approach that uses the photoactivatable fluorescent protein Kaede to mark individual sensory neurons and unambiguously distinguish proximal and distal axon segments after transection. After imaging more than 20 samples, I never observed fusion events between axonal segments. Instead, regenerating axons grew past the non-degradable distal segments to reinnervate peripheral synaptic targets. The regenerative ability of sensory axons was not affected in Sarm1$^{-/-}$ zebrafish.

Loss of Sarm1 attenuates the axoplasmic calcium influx but not mitochondrial or ER calcium uptake

During Wallerian axon degeneration, the cytoskeleton loses its integrity. Ca^{2+} influx during axon fragmentation activates Calpain to cleave the microtubule-associated components and axonal neurofilament (Johnson et al., 1991). Previous studies have shown that knockdown Sarm1 in cultured neurons attenuate calcium influx (Summers et al., 2014) (Loreto et al., 2015). To understand the role of Ca^{2+} in Sarm1-mediated axon fragmentation, I expressed a genetically-encoded fluorescent calcium indicator in sensory neurons of normal and Sarm1-deficient embryos to monitor axoplasmic calcium before and after severing. My results indicate that calcium influx is blocked in Sarm1-deficient axons transected with a laser beam. By contrast, a strong calcium influx preceding axonal fragmentation occurs in the wild-type specimens. Following this finding, I enforced calcium influx in Sarm1-deficient axons using a chemogenetic approach (Chen et al., 2016), which readily induced the degradation of Sarm1-deficient axons.

Increasing the threshold of mitochondrial Ca^{2+} release can limit white matter loss in traumatic brain injury and temporarily delay axon degeneration for up to 4 hours after axotomy (Barrientos et al., 2011; Büki et al., 1999). In addition, calcium release from axonal endoplasmic reticulum (ER) contributes to axonal degeneration in *ex vivo* and *in vitro* mouse and rat model systems (Villegas et al., 2014). This raises the question of what are the activities of mitochondrial and ER calcium in Sarm1-deficient axons after severing. My results show that the calcium influx in mitochondria and ER are enhanced after axon transection in wild type and Sarm1$^{-/-}$ zebrafish, suggesting that loss of Sarm1 inhibits axon degeneration by attenuating the axoplasmic calcium influx but not calcium uptake by mitochondria or the ER.

Transected sensory neurons recover functionally in Sarm1$^{-/-}$ zebrafish

Functional recovery from injury is important for the nervous system, which includes re-innervation of sensory receptors by regenerating axons and restoration of sensory function after circuit repair (Graciarena et al., 2014). In my thesis, I use behavioral performance of zebrafish to evaluate the function of sensory neurons (Chiu and Prober, 2013; Sztal et al.,

2016). Specifically, I conducted the experiments of touch-evoked response and rheotaxis with wild type and Sarm1-deficient larvae. The results show that the acceleration and swimming distance of touch-evoked response and the performance of rheotaxis were not significantly different between wild type and Sarm1$^{-/-}$ zebrafish. In addition, the electrophysiological results showed that spontaneous and evoked neuronal activities of afferent neurons are normal in Sarm1$^{-/-}$ samples, compared to the wild type siblings. These results indicate that loss of Sarm1 does not impair the electrophysiology activities of sensory neurons and the behavioral performance of animals.

The rheotaxis was eliminated in the unilateral lateral line transected larvae (Oteiza et al., 2017). Thus, I assessed the impact of loss of Wallerian axon degeneration on sensorimotor recovery. The rheotaxis tests were conducted on the one-side lateral-line transected animals (one day and three days after transection). My data show that the performance of rheotaxis was severely disrupted in wild type and Sarm1-deficient larvae after severing the lateral line axons, compared to the non-transected ones. However, there was no statistical significance between the axon transected wild type and the axon transected Sarm1 deficient animals. Furthermore, the quantification showed that the performance of rheotaxis rom three-days recovery groups (wild type and Sarm1 deficient) were better than the one-day transected ones, but it did not recover to the level of intact animals. However, the performance of rheotaxis after three-days recovery was not statistically different in wild type compared to Sarm1 deficient animals. Taken together, my work demonstrates that maintenance of non-degradable axonal fragments has no detrimental effect on the repair of sensory circuit in zebrafish. The sensorimotor recovery is not contingent upon the speed of clearing severed axons, revealing that the axonal destructive and nerve reconstructive processes occur in parallel.

Sarm1 deficiency delays the remyelination of regenerative axons after injury

Glial Schwann cells wrap the axons and support myelin to maintain the axons fasciculation and insulation with the outside environment. If Schwann cells migration is impeded, posterior lateral-line sensory axons cannot grow normally (Lyons et al., 2005). Upon nerve injury, Schwann cells help regrowing axons negotiate the injury gap (Glenn and Talbot,

2013). In addition, Schwann cells also dictate the onset and timing of axon fragmentation after injury (Wong et al., 2017).

My data show that the Schwann cells adjacent to nerve injury in Sarm1-deficient zebrafish behave dramatically differently than those of wild-type specimens. Specifically, Schwann cells in Sarm1$^{-/-}$ zebrafish do not migrate or extend projections to bridge the gap in the glial scaffold, indicating that these cells do sense missing intercellular contacts or glial discontinuity but they do not migrate to the injury site quickly. In wild-type specimens, however, I observed that filopodia-like structures emerged from Schwann cells at both sides of the injury in wild-type animals, suggesting that repair-inducing signals are likely diffusible, affecting glial cells independently of their association with axons. It remains to be determined whether the source of such signals is the degrading axons, the denervated Schwann cells, or other cells that are recruited to the wound.

Furthermore, my data reveal that loss of Sarm1 does not attenuate the calcium influx in Schwann cell upon stimulation. The GCaMP7a labeled Schwann cells had a dramatic calcium influx upon laser ablation in both wild type and Sarm1$^{-/-}$ zebrafish larvae. In addition, the immunostaining and live imaging results show that the myelin and the structure between axons and Schwann cells are maintained in the distal part of severed neurons in Sarm1-deficient specimens, suggesting that non-degradable axons may facilitate Schwann cells to maintain the myelin and the interactive structure of axons and SCs after nerve injury. Moreover, my findings show that the process of remyelination is slightly delayed in Sarm1-deficient zebrafish. Next, my data demonstrate that severed axons do not fragment in the Erbb2 and Sarm1 double knockouts that are lack of Schwann cells in the lateral-line, indicating that the non-degradable axons in Sarm1$^{-/-}$ zebrafish were independent of Schwann cells. Taken together, these results reveal that severed Sarm1-dificient sensory axons are maintained independently of Schwann cells, and that the non-degradable axons do not repel the remyelination of the regenerative axons.

Macrophages are recruited to the injured axons in Sarm1-deficient zebrafish

Macrophages are involved in clearing the debris of axon and myelin (Bendszus and Stoll, 2003). The recent published work indicated that Sarm1 functions in the neuronal immune

response through the JNK-c-Jun signaling pathway. Inhibition of one component of this signaling pathway could effectively abolish the recruitment of immune cells to injury afflicted neural tissues (Wang et al., 2018). Yet, there is no direct evidence for possible defects of the recruitment of immune cells *in vivo* in Sarm1-deficient animals. With the advantage of transparent zebrafish larva, I imaged the movement of macrophages in response to axon injury with high-resolution microscopy. My data show that macrophages moved to the injury axons to engulf and to clean the axon debris in wild type zebrafish. Strikingly, in Sarm1$^{-/-}$ zebrafish, the macrophages were recruited to the distal part of the axons from the far- side to the transected site. They were moving along the axons and stayed with the axons, suggesting that these macrophages acted as the surveillances in the transected Sarm1-deficient axons. When macrophages were moving along the non-degradable axons in Sarm1$^{-/-}$ zebrafish, they preferred to stay and surround the bulbs which were detaching from the entire axons. In sum, loss of Sarm1 does not impair the recruitment of macrophages in the zebrafish after nerve injury. Instead, the macrophages act as the surveillance in the Sarm1$^{-/-}$ zebrafish larvae. Furthermore, the phagocytic activity of macrophages was not impaired in Sarm1$^{-/-}$ zebrafish. My data supply the direct *in vivo* live imaging of the macrophages in response to axon fragmentation in Sarm1 deficient animals.

Non-degradable axons maintain and protect the Schwann cells against chemotoxicity in Sarm1$^{-/-}$ zebrafish

Many chemotherapeutic agents invariably cause peripheral neuropathy, leading to permanent neuronal dysfunction in clinical trials (Starobova and Vetter, 2017). Previous studies have revealed that Schwann cells become strongly susceptible to chemotoxicity under denervation (Diezi et al., 2013). In zebrafish, axons and Schwann cells could be easily imaged with high-resolution microscope because of the transparence of fish and superficial localization of lateral-line nerves (Xiao et al., 2015a). It enabled me to test the effect of chemicals on axonal degeneration, regeneration, and Schwann cells survival in live animals. 10-HCT has been shown to reduce integrity of denervated Schwann cell (Bremer et al., 2017), and platinum based agents, taxanes and some alkaloids are effective chemotherapeutic agents used as standards-of-care for various human malignancies, despite their severe neuropathic effects that include glial destruction (Imai et al., 2017). In

my thesis, I found the number of Schwann cells decreased dramatically with the treatment of 10-HCT and chemotherapy agents, such as Paclitaxel, Docetaxel, Oxaliplatin, Cisplatin, and Vincristine, in axonal transection wild type animals; however, the same doses of agents did not influence the number of Schwann cells in the axon intact wild type animals. The results suggest that nerve injury enhances the sensitivity of Schwann cells to chemotherapy agents. In contrast, the number of Schwann cells was maintained in the presence of chemicals in the Sarm1 deficient animals, even when the axons were transected. The non-degradable axons which sustain the structure between axons and Schwann cells and the myelination of transected axons could result in the protective effect. Then, I used the chemogenetic approach to fragment Sarm1-deficient axons before chemicals incubation. The results show that the number of Schwann cells is reduced in presence of chemicals when the Sarm1-deficient axons are forced to fragment.

Loss of Sarm1 improves functional recovery after vincristine-mediated neurotoxicity, and traumatic brain injury in mice (Geisler et al., 2016; Henninger et al., 2016). However, the therapeutic potential of blocking axon degeneration by inhibiting Sarm1 systemically remains uncertain. My data demonstrated that chronic and systemic loss of Sarm1 is compatible with zebrafish viability and sensorineural function. Interestingly, data from the Genetic Testing Registry illustrate that Sarm1 variants in humans have only been associated to congenital defect of folate absorption (Landrum et al., 2013). Dietary reduction of folates can prevent the appearance of symptoms of folate absorption defect. Therefore, in zebrafish, mouse and humans, Sarm1 appears to be a non-essential protein whose deficit is associated to mild conditions. As a discrete hierarchical factor in axon degeneration, Sarm1 is an ideal target for pharmacological interventions.

Conclusion

I firstly generated Sarm1 deficient zebrafish by CRISPR-mediated genome engineering tool. With this knock-out zebrafish, I provide a comprehensive understanding the function of Sarm1 from the sub-cellular to the organismal level. To validate these studies, I used genetic manipulations of sensory neurons and several transgenic fluorescent sensors in neurons and Schwann cells to characterize the consequences of Sarm1 loss.

In brief, I reveal that loss of Sarm1 is well tolerated by zebrafish. Sarm1-deficient zebrafish are viable, and perform touch-evoked response and rheotaxis normally. Axon degeneration is blocked in the Sarm1-deficient zebrafish, but Sarm1-deficient regenerative axons fasciculate and regain synaptic connectivity, suggesting that absence of competition between non-degradable axon fragments and re-growing fibers, and that neuronal-circuit repair is not contingent upon rapid clearance of damaged axons. The striking resealing of severed axons observed in *C. elegans* is not a general feature of the nervous system, even when severed axons are non-degradable.

In addition, I show with unprecedented spatial and temporal detail by intravital microscopy the response of Schwann cells to neuronal damage and axonal regeneration in normal condition and when Wallerian axon degeneration is disrupted. The results deepen our understanding of the cellular environment that enables Schwann cell reprogramming upon nerve damage. Furthermore, the protracted maintenance of transected axons dramatically improves Schwann-cell tolerance to chemotoxicity after nerve injury. Meanwhile, loss of Sarm1 does not affect the recruitment of macrophages to the injured axons.

Importantly, these data strongly support the idea that direct interventions to inhibit axon degradation systemically are promising strategies to reduce chronic consequences of nerve injury. Because TIR domain dimerization is necessary and sufficient to degrade NAD+, it renders Sarm1 amenable to inhibition by small molecules, as it has been demonstrated for the TIR domain of TLR2. Thus, the findings in this work encourage the development of Sarm1 inhibitors for therapeutic applications.

6. References

Abdesselem, H., Shypitsyna, A., Solis, G.P., Bodrikov, V., and Stuermer, C.A. (2009). No Nogo66-and NgR-mediated inhibition of regenerating axons in the zebrafish optic nerve. Journal of Neuroscience *29*, 15489-15498.

Abe, N., Borson, S.H., Gambello, M.J., Wang, F., and Cavalli, V. (2010). Mammalian target of rapamycin (mTOR) activation increases axonal growth capacity of injured peripheral nerves. Journal of Biological Chemistry *285*, 28034-28043.

Abraira, V.E., and Ginty, D.D. (2013). The sensory neurons of touch. Neuron *79*, 618-639.

Addington, J., and Freimer, M. (2016). Chemotherapy-induced peripheral neuropathy: an update on the current understanding. F1000Research *5*.

Akanyeti, O., Thornycroft, P.J., Lauder, G.V., Yanagitsuru, Y.R., Peterson, A.N., and Liao, J.C. (2016). Fish optimize sensing and respiration during undulatory swimming. Nature communications *7*, 11044.

Alunni, A., and Bally-Cuif, L. (2016). A comparative view of regenerative neurogenesis in vertebrates. Development *143*, 741-753.

Andermann, P., Ungos, J., and Raible, D.W. (2002). Neurogenin1 defines zebrafish cranial sensory ganglia precursors. Developmental biology *251*, 45-58.

Ando, R., Hama, H., Yamamoto-Hino, M., Mizuno, H., and Miyawaki, A. (2002). An optical marker based on the UV-induced green-to-red photoconversion of a fluorescent protein. Proceedings of the National Academy of Sciences *99*, 12651-12656.

Angers, A., and Drapeau, P. (2014). Itch is required for lateral line development in zebrafish. PloS one *9*, e111799.

Anichtchik, O., Diekmann, H., Fleming, A., Roach, A., Goldsmith, P., and Rubinsztein, D.C. (2008). Loss of PINK1 function affects development and results in neurodegeneration in zebrafish. Journal of Neuroscience *28*, 8199-8207.

Argyriou, A.A., Polychronopoulos, P., Iconomou, G., Chroni, E., and Kalofonos, H.P. (2008). A review on oxaliplatin-induced peripheral nerve damage. Cancer treatment reviews *34*, 368-377.

Armstrong, G.A., and Drapeau, P. (2013). Loss and gain of FUS function impair neuromuscular synaptic transmission in a genetic model of ALS. Human molecular genetics *22*, 4282-4292.

Asgharsharghi, A. (2019). Spatiotemporal stucture of rheotactic behavior in larval zebrafish. In School of Life Sciences (Technical University of Munich).

Auer, F., Vagionitis, S., and Czopka, T. (2018). Evidence for myelin sheath remodeling in the CNS revealed by in vivo imaging. Current Biology *28*, 549-559. e543.

Balaji, S.P., Chand, C.V., Justin, A., and Ramanathan, M. (2015). Telmisartan mediates anti-inflammatory and not cognitive function through PPAR-γ agonism via SARM and MyD88 signaling. Pharmacology Biochemistry and Behavior *137*, 60-68.

Baraban, S.C., Dinday, M.T., and Hortopan, G.A. (2013). Drug screening in Scn1a zebrafish mutant identifies clemizole as a potential Dravet syndrome treatment. Nature communications *4*, 2410.

Baral, P., and Utaisincharoen, P. (2013). Sterile-α-and armadillo motif-containing protein inhibits the TRIF-dependent downregulation of signal regulatory protein α to interfere with intracellular bacterial elimination in Burkholderia pseudomallei-infected mouse macrophages. Infection and immunity *81*, 3463-3471.

Barrientos, S.A., Martinez, N.W., Yoo, S., Jara, J.S., Zamorano, S., Hetz, C., Twiss, J.L., and Alvarez, J. (2011). Axonal degeneration is mediated by the mitochondrial permeability transition pore. Journal of Neuroscience *31*, 966-978.

Becker, C.G., and Becker, T. (2002). Repellent guidance of regenerating optic axons by chondroitin sulfate glycosaminoglycans in zebrafish. Journal of Neuroscience *22*, 842-853.

Becker, T., and Becker, C.G. (2014). Axonal regeneration in zebrafish. Current Opinion in Neurobiology *27*, 186-191.

Belin, S., Nawabi, H., Wang, C., Tang, S., Latremoliere, A., Warren, P., Schorle, H., Uncu, C., Woolf, C.J., and He, Z. (2015). Injury-induced decline of intrinsic regenerative ability revealed by quantitative proteomics. Neuron *86*, 1000-1014.

Bendszus, M., and Stoll, G. (2003). Caught in the act: in vivo mapping of macrophage infiltration in nerve injury by magnetic resonance imaging. Journal of Neuroscience *23*, 10892-10896.

Bernhardson, B.-M., Tishelman, C., and Rutqvist, L.E. (2007). Chemosensory changes experienced by patients undergoing cancer chemotherapy: a qualitative interview study. Journal of pain and symptom management *34*, 403-412.

Bernhardt, R., Tongiorgi, E., Anzini, P., and Schachner, M. (1996). Increased expression of specific recognition molecules by retinal ganglion cells and by optic pathway glia accompanies the successful regeneration of retinal axons in adult zebrafish. Journal of Comparative Neurology *376*, 253-264.

Berry, M., Ahmed, Z., Morgan-Warren, P., Fulton, D., and Logan, A. (2016). Prospects for mTOR-mediated functional repair after central nervous system trauma. Neurobiology of disease *85*, 99-110.

Bin, J.M., and Lyons, D.A. (2016). Imaging myelination In Vivo Using transparent animal models. Brain Plasticity *2*, 3-29.

Boehmerle, W., Huehnchen, P., Peruzzaro, S., Balkaya, M., and Endres, M. (2014). Electrophysiological, behavioral and histological characterization of paclitaxel, cisplatin, vincristine and bortezomib-induced neuropathy in C57Bl/6 mice. Scientific reports *4*, 6370.

Boerboom, A., Dion, V., Chariot, A., and Franzen, R. (2017). Molecular mechanisms involved in Schwann cell plasticity. Frontiers in molecular neuroscience *10*, 38.

Boyette-Davis, J., and Dougherty, P. (2011). Protection against oxaliplatin-induced mechanical hyperalgesia and intraepidermal nerve fiber loss by minocycline. Experimental neurology *229*, 353-357.

Bradke, F., Fawcett, J.W., and Spira, M.E. (2012). Assembly of a new growth cone after axotomy: the precursor to axon regeneration. Nature Reviews Neuroscience *13*, 183.

Bremer, J., Skinner, J., and Granato, M. (2017). A small molecule screen identifies in vivo modulators of peripheral nerve regeneration in zebrafish. PloS one *12*, e0178854.

Bretaud, S., Allen, C., Ingham, P.W., and Bandmann, O. (2007). p53 ‑ dependent neuronal cell death in a DJ ‑ 1 ‑ deficient zebrafish model of Parkinson's disease. Journal of neurochemistry *100*, 1626-1635.

Brochier, C., Jones, J.I., Willis, D.E., and Langley, B. (2015). Poly (ADP-ribose) polymerase 1 is a novel target to promote axonal regeneration. Proceedings of the National Academy of Sciences *112*, 15220-15225.

Brösamle, C., and Halpern, M.E. (2002). Characterization of myelination in the developing zebrafish. Glia *39*, 47-57.

Brushart, T., Aspalter, M., Griffin, J., Redett, R., Hameed, H., Zhou, C., Wright, M., Vyas, A., and Höke, A. (2013). Schwann cell phenotype is regulated by axon modality and central–peripheral location, and persists in vitro. Experimental neurology *247*, 272-281.

Buggs, R.J., Renny ‑ Byfield, S., Chester, M., Jordon ‑ Thaden, I.E., Viccini, L.F., Chamala, S., Leitch, A.R., Schnable, P.S., Barbazuk, W.B., and Soltis, P.S. (2012). Next ‑ generation sequencing and genome evolution in allopolyploids. American Journal of Botany *99*, 372-382.

Büki, A., Siman, R., Trojanowski, J.Q., and Povlishock, J.T. (1999). The role of calpain-mediated spectrin proteolysis in traumatically induced axonal injury. Journal of neuropathology and experimental neurology *58*, 365-375.

Burgess, H.A., and Granato, M. (2007). Sensorimotor gating in larval zebrafish. Journal of Neuroscience *27*, 4984-4994.

Carozzi, V., Canta, A., and Chiorazzi, A. (2015). Chemotherapy-induced peripheral neuropathy: what do we know about mechanisms? Neuroscience letters *596*, 90-107.

Carr, M.J., and Johnston, A.P. (2017). Schwann cells as drivers of tissue repair and regeneration. Current opinion in neurobiology *47*, 52-57.

Carty, M., and Bowie, A.G. (2019). SARM: From immune regulator to cell executioner. Biochemical pharmacology *161*, 52-62.

Carty, M., Goodbody, R., Schröder, M., Stack, J., Moynagh, P.N., and Bowie, A.G. (2006). The human adaptor SARM negatively regulates adaptor protein TRIF–dependent Toll-like receptor signaling. Nature immunology *7*, 1074.

Cavaletti, G., Alberti, P., and Marmiroli, P. (2011). Chemotherapy-induced peripheral neurotoxicity in the era of pharmacogenomics. The lancet oncology *12*, 1151-1161.

Cavaletti, G., Gilardini, A., Canta, A., Rigamonti, L., Rodriguez-Menendez, V., Ceresa, C., Marmiroli, P., Bossi, M., Oggioni, N., and D'Incalci, M. (2007). Bortezomib-induced peripheral neurotoxicity: a neurophysiological and pathological study in the rat. Experimental neurology *204*, 317-325.

Cavaletti, G., Tredici, G., Petruccioli, M., Donde, E., Tredici, P., Marmiroli, P., Minoia, C., Ronchi, A., Bayssas, M., and Etienne, G.G. (2001). Effects of different schedules of

oxaliplatin treatment on the peripheral nervous system of the rat. European journal of cancer *37*, 2457-2463.

Ceci, M.L., Mardones-Krsulovic, C., Sánchez, M., Valdivia, L.E., and Allende, M.L. (2014). Axon-Schwann cell interactions during peripheral nerve regeneration in zebrafish larvae. Neural development *9*, 22.

Cersosimo, R.J. (2005). Oxaliplatin-associated neuropathy: a review. Annals of Pharmacotherapy *39*, 128-135.

Chang, N., Sun, C., Gao, L., Zhu, D., Xu, X., Zhu, X., Xiong, J.-W., and Xi, J.J. (2013). Genome editing with RNA-guided Cas9 nuclease in zebrafish embryos. Cell research *23*, 465.

Chawla, S., Vanhoutte, P., Arnold, F.J., Huang, C.L.H., and Bading, H. (2003). Neuronal activity‐dependent nucleocytoplasmic shuttling of HDAC4 and HDAC5. Journal of neurochemistry *85*, 151-159.

Chen, C.-Y., Lin, C.-W., Chang, C.-Y., Jiang, S.-T., and Hsueh, Y.-P. (2011). Sarm1, a negative regulator of innate immunity, interacts with syndecan-2 and regulates neuronal morphology. The Journal of cell biology *193*, 769-784.

Chen, S., Chiu, C.N., McArthur, K.L., Fetcho, J.R., and Prober, D.A. (2016). TRP channel mediated neuronal activation and ablation in freely behaving zebrafish. nature methods *13*, 147.

Chitnis, A.B., Dalle Nogare, D., and Matsuda, M. (2012). Building the posterior lateral line system in zebrafish. Developmental neurobiology *72*, 234-255.

Chiu, C.N., and Prober, D.A. (2013). Regulation of zebrafish sleep and arousal states: current and prospective approaches. Frontiers in neural circuits *7*, 58.

Cho, Y., Shin, J.E., Ewan, E.E., Oh, Y.M., Pita-Thomas, W., and Cavalli, V. (2015). Activating injury-responsive genes with hypoxia enhances axon regeneration through neuronal HIF-1α. Neuron *88*, 720-734.

Chuang, C.-F., and Bargmann, C.I. (2005). A Toll-interleukin 1 repeat protein at the synapse specifies asymmetric odorant receptor expression via ASK1 MAPKKK signaling. Genes & development *19*, 270-281.

Ciura, S., Lattante, S., Le Ber, I., Latouche, M., Tostivint, H., Brice, A., and Kabashi, E. (2013). Loss of function of C9orf72 causes motor deficits in a zebrafish model of amyotrophic lateral sclerosis. Annals of neurology *74*, 180-187.

Clements, M.P., Byrne, E., Guerrero, L.F.C., Cattin, A.-L., Zakka, L., Ashraf, A., Burden, J.J., Khadayate, S., Lloyd, A.C., and Marguerat, S. (2017). The wound microenvironment reprograms Schwann cells to invasive mesenchymal-like cells to drive peripheral nerve regeneration. Neuron *96*, 98-114. e117.

Conforti, L., Janeckova, L., Wagner, D., Mazzola, F., Cialabrini, L., Di Stefano, M., Orsomando, G., Magni, G., Bendotti, C., and Smyth, N. (2011). Reducing expression of NAD+ synthesizing enzyme NMNAT1 does not affect the rate of Wallerian degeneration. The FEBS journal *278*, 2666-2679.

Cong, L., Ran, F.A., Cox, D., Lin, S., Barretto, R., Habib, N., Hsu, P.D., Wu, X., Jiang, W., and Marraffini, L.A. (2013). Multiplex genome engineering using CRISPR/Cas systems. Science *339*, 819-823.

Coombs, S., and Conley, R.A. (1997). Dipole source localization by the mottled sculpin II. The role of lateral line excitation patterns. Journal of Comparative Physiology A *180*, 401-415.

Couillault, C., Pujol, N., Reboul, J., Sabatier, L., Guichou, J.-F., Kohara, Y., and Ewbank, J.J. (2004). TLR-independent control of innate immunity in Caenorhabditis elegans by the TIR domain adaptor protein TIR-1, an ortholog of human SARM. Nature immunology *5*, 488.

Coutsouvelis, J., and Corallo, C.E. (2004). Thalidomide‐induced bradycardia and its management. Medical journal of Australia *180*, 366-367.

Curran, M.P., and McKeage, K. (2009). Bortezomib. Drugs *69*, 859-888.

Czopka, T., and Lyons, D.A. (2013). Individual oligodendrocytes have only a few hours in which to generate new myelin sheaths in vivo. Developmental cell *25*, 599-609.

Dambly-Chaudière, C., Cubedo, N., and Ghysen, A. (2007). Control of cell migration in the development of the posterior lateral line: antagonistic interactions between the chemokine receptors CXCR4 and CXCR7/RDC1. BMC developmental biology *7*, 23.

Dasari, S., and Tchounwou, P.B. (2014). Cisplatin in cancer therapy: molecular mechanisms of action. European journal of pharmacology *740*, 364-378.

David, N.B., Sapède, D., Saint-Etienne, L., Thisse, C., Thisse, B., Dambly-Chaudière, C., Rosa, F.M., and Ghysen, A. (2002). Molecular basis of cell migration in the fish lateral line: role of the chemokine receptor CXCR4 and of its ligand, SDF1. Proceedings of the National Academy of Sciences *99*, 16297-16302.

De Rienzo, G., Bishop, J.A., Mao, Y., Pan, L., Ma, T.P., Moens, C.B., Tsai, L.-H., and Sive, H. (2011). Disc1 regulates both β-catenin-mediated and noncanonical Wnt signaling during vertebrate embryogenesis. The FASEB Journal *25*, 4184-4197.

Deckwerth, T.L., and Johnson Jr, E.M. (1994). Neurites can remain viable after destruction of the neuronal soma by programmed cell death (apoptosis). Developmental biology *165*, 63-72.

Dehnhardt, G., Mauck, B., Hanke, W., and Bleckmann, H. (2001). Hydrodynamic trail-following in harbor seals (Phoca vitulina). Science *293*, 102-104.

Di Giovanni, S., Knights, C.D., Rao, M., Yakovlev, A., Beers, J., Catania, J., Avantaggiati, M.L., and Faden, A.I. (2006). The tumor suppressor protein p53 is required for neurite outgrowth and axon regeneration. The EMBO journal *25*, 4084-4096.

Di Stefano, M., Loreto, A., Orsomando, G., Mori, V., Zamporlini, F., Hulse, R.P., Webster, J., Donaldson, L.F., Gering, M., and Raffaelli, N. (2017). NMN deamidase delays Wallerian degeneration and rescues axonal defects caused by NMNAT2 deficiency in vivo. Current Biology *27*, 784-794.

Di Stefano, M., Nascimento-Ferreira, I., Orsomando, G., Mori, V., Gilley, J., Brown, R., Janeckova, L., Vargas, M., Worrell, L., and Loreto, A. (2015). A rise in NAD precursor

nicotinamide mononucleotide (NMN) after injury promotes axon degeneration. Cell death and differentiation *22*, 731.

Dias, T.B., Yang, Y.-J., Ogai, K., Becker, T., and Becker, C.G. (2012). Notch signaling controls generation of motor neurons in the lesioned spinal cord of adult zebrafish. Journal of Neuroscience *32*, 3245-3252.

Diezi, M., Buclin, T., and Kuntzer, T. (2013). Toxic and drug-induced peripheral neuropathies: updates on causes, mechanisms and management. Current opinion in neurology *26*, 481-488.

Dimopoulos, M., Spencer, A., Attal, M., Prince, H.M., Harousseau, J.-L., Dmoszynska, A., Miguel, J.S., Hellmann, A., Facon, T., and Foà, R. (2007). Lenalidomide plus dexamethasone for relapsed or refractory multiple myeloma. New England Journal of Medicine *357*, 2123-2132.

Doyon, Y., McCammon, J.M., Miller, J.C., Faraji, F., Ngo, C., Katibah, G.E., Amora, R., Hocking, T.D., Zhang, L., and Rebar, E.J. (2008). Heritable targeted gene disruption in zebrafish using designed zinc-finger nucleases. Nature biotechnology *26*, 702.

Drerup, C.M., and Nechiporuk, A.V. (2016). In vivo analysis of axonal transport in zebrafish. In Methods in cell biology (Elsevier), pp. 311-329.

Eggers, R., Tannemaat, M., Ehlert, E., and Verhaagen, J. (2010). A spatio-temporal analysis of motoneuron survival, axonal regeneration and neurotrophic factor expression after lumbar ventral root avulsion and implantation. Experimental neurology *223*, 207-220.

Essuman, K., Summers, D.W., Sasaki, Y., Mao, X., DiAntonio, A., and Milbrandt, J. (2017). The SARM1 toll/interleukin-1 receptor domain possesses intrinsic NAD+ cleavage activity that promotes pathological axonal degeneration. Neuron *93*, 1334-1343. e1335.

Esterberg, R., Hailey, D.W., Rubel, E.W., and Raible, D.W. (2014). ER–mitochondrial calcium flow underlies vulnerability of mechanosensory hair cells to damage. Journal of Neuroscience *34*, 9703-9719.

Esterberg, R., Linbo, T., Pickett, S.B., Wu, P., Ou, H.C., Rubel, E.W., and Raible, D.W. (2016). Mitochondrial calcium uptake underlies ROS generation during aminoglycoside-induced hair cell death. The Journal of clinical investigation *126*, 3556-3566.

Faroni, A., Smith, R., Procacci, P., Castelnovo, L., Puccianti, E., Reid, A., Magnaghi, V., and Verkhratsky, A. (2014). Purinergic signaling mediated by P2X7 receptors controls myelination in sciatic nerves. Journal of neuroscience research *92*, 1259-1269.

Faucherre, A., Pujol-Martí, J., Kawakami, K., and López-Schier, H. (2009). Afferent neurons of the zebrafish lateral line are strict selectors of hair-cell orientation. PloS one *4*, e4477.

Feltri, M.L., Poitelon, Y., and Previtali, S.C. (2016). How Schwann cells sort axons: new concepts. The Neuroscientist *22*, 252-265.

Fontana, X., Hristova, M., Da Costa, C., Patodia, S., Thei, L., Makwana, M., Spencer-Dene, B., Latouche, M., Mirsky, R., and Jessen, K.R. (2012). c-Jun in Schwann cells promotes axonal regeneration and motoneuron survival via paracrine signaling. J Cell Biol *198*, 127-141.

Frank, E., Jansen, J.K., and Rinvik, E. (1975). A multisomatic axon in the central nervous system of the leech. Journal of Comparative Neurology *159*, 1-13.

Friedrich, R., Genoud, C., and Wanner, A.A. (2013). Analyzing the structure and function of neuronal circuits in zebrafish. Frontiers in neural circuits *7*, 71.

Friedrich, R.W., Jacobson, G.A., and Zhu, P. (2010). Circuit neuroscience in zebrafish. Current Biology *20*, R371-R381.

Fromer, M., Roussos, P., Sieberts, S.K., Johnson, J.S., Kavanagh, D.H., Perumal, T.M., Ruderfer, D.M., Oh, E.C., Topol, A., and Shah, H.R. (2016). Gene expression elucidates functional impact of polygenic risk for schizophrenia. Nature neuroscience *19*, 1442.

Fukuda, Y., Li, Y., and Segal, R.A. (2017). A mechanistic understanding of axon degeneration in chemotherapy-induced peripheral neuropathy. Frontiers in neuroscience *11*, 481.

Gaj, T., Gersbach, C.A., and Barbas III, C.F. (2013). ZFN, TALEN, and CRISPR/Cas-based methods for genome engineering. Trends in biotechnology *31*, 397-405.

Gamage, K.K., Cheng, I., Park, R.E., Karim, M.S., Edamura, K., Hughes, C., Spano, A.J., Erisir, A., and Deppmann, C.D. (2017). Death receptor 6 promotes wallerian degeneration in peripheral axons. Current Biology *27*, 890-896.

Gan, P.P., McCarroll, J.A., Po'uha, S.T., Kamath, K., Jordan, M.A., and Kavallaris, M. (2010). Microtubule dynamics, mitotic arrest, and apoptosis: Drug-induced differential effects of βIII-tubulin. Molecular cancer therapeutics *9*, 1339-1348.

Gau, P., Poon, J., Ufret-Vincenty, C., Snelson, C.D., Gordon, S.E., Raible, D.W., and Dhaka, A. (2013). The zebrafish ortholog of TRPV1 is required for heat-induced locomotion. Journal of Neuroscience *33*, 5249-5260.

Geisler, S., Doan, R.A., Strickland, A., Huang, X., Milbrandt, J., and DiAntonio, A. (2016). Prevention of vincristine-induced peripheral neuropathy by genetic deletion of SARM1 in mice. Brain *139*, 3092-3108.

Gerdts, J., Brace, E., Sasaki, Y., DiAntonio, A., and Milbrandt, J. (2015). SARM1 activation triggers axon degeneration locally via NAD+ destruction. Science *348*, 453-457.

Gerdts, J., Summers, D.W., Milbrandt, J., and DiAntonio, A. (2016). Axon self-destruction: new links among SARM1, MAPKs, and NAD+ metabolism. Neuron *89*, 449-460.

Gerdts, J., Summers, D.W., Sasaki, Y., DiAntonio, A., and Milbrandt, J. (2013). Sarm1-mediated axon degeneration requires both SAM and TIR interactions. Journal of Neuroscience *33*, 13569-13580.

Ghysen, A., and Dambly-Chaudière, C. (2007). The lateral line microcosmos. Genes & development *21*, 2118-2130.

Gilley, J., and Coleman, M.P. (2010). Endogenous Nmnat2 is an essential survival factor for maintenance of healthy axons. PLoS biology *8*, e1000300.

Gilley, J., Orsomando, G., Nascimento-Ferreira, I., and Coleman, M.P. (2015). Absence of SARM1 rescues development and survival of NMNAT2-deficient axons. Cell reports *10*, 1974-1981.

Gilmour, D., Knaut, H., Maischein, H.-M., and Nüsslein-Volhard, C. (2004). Towing of sensory axons by their migrating target cells in vivo. Nature neuroscience *7*, 491.

Glenn, T.D., and Talbot, W.S. (2013). Signals regulating myelination in peripheral nerves and the Schwann cell response to injury. Current opinion in neurobiology *23*, 1041-1048.

Gompel, N., Dambly-Chaudière, C., and Ghysen, A. (2001). Neuronal differences prefigure somatotopy in the zebrafish lateral line. Development *128*, 387-393.

Graciarena, M., Dambly-Chaudière, C., and Ghysen, A. (2014). Dynamics of axonal regeneration in adult and aging zebrafish reveal the promoting effect of a first lesion. Proceedings of the National Academy of Sciences *111*, 1610-1615.

Grant, K.A., Raible, D.W., and Piotrowski, T. (2005). Regulation of latent sensory hair cell precursors by glia in the zebrafish lateral line. Neuron *45*, 69-80.

Grolleau, F., Gamelin, L., Boisdron-Celle, M., Lapied, B., Pelhate, M., and Gamelin, E. (2001). A possible explanation for a neurotoxic effect of the anticancer agent oxaliplatin on neuronal voltage-gated sodium channels. Journal of Neurophysiology *85*, 2293-2297.

Grone, B.P., Marchese, M., Hamling, K.R., Kumar, M.G., Krasniak, C.S., Sicca, F., Santorelli, F.M., Patel, M., and Baraban, S.C. (2016). Epilepsy, behavioral abnormalities, and physiological comorbidities in syntaxin-binding protein 1 (STXBP1) mutant zebrafish. PLoS One *11*, e0151148.

Gumy, L. F., Tan, C. L. & Fawcett, J. W. (2010). The role of local protein synthesis and degradation in axon regeneration. Exp. Neurol. 223, 28–37.

Guo, S., Wilson, S.W., Cooke, S., Chitnis, A.B., Driever, W., and Rosenthal, A. (1999). Mutations in the zebrafish unmask shared regulatory pathways controlling the development of catecholaminergic neurons. Developmental biology *208*, 473-487.

Gürtler, C., Carty, M., Kearney, J., Schattgen, S.A., Ding, A., Fitzgerald, K.A., and Bowie, A.G. (2014). SARM regulates CCL5 production in macrophages by promoting the recruitment of transcription factors and RNA polymerase II to the Ccl5 promoter. The Journal of Immunology *192*, 4821-4832.

Gusev, A., Mancuso, N., Won, H., Kousi, M., Finucane, H.K., Reshef, Y., Song, L., Safi, A., McCarroll, S., and Neale, B.M. (2018). Transcriptome-wide association study of schizophrenia and chromatin activity yields mechanistic disease insights. Nature genetics *50*, 538.

Haehnel-Taguchi, M., Akanyeti, O., and Liao, J.C. (2014). Afferent and motoneuron activity in response to single neuromast stimulation in the posterior lateral line of larval zebrafish. Journal of neurophysiology *112*, 1329-1339.

Haehnel-Taguchi, M., Akanyeti, O., and Liao, J.C. (2018). Behavior, Electrophysiology, and Robotics Experiments to Study Lateral Line Sensing in Fishes. Integrative and comparative biology *58*, 874-883.

Haenisch, C., Diekmann, H., Klinger, M., Gennarini, G., Kuwada, J.Y., and Stuermer, C.A. (2005). The neuronal growth and regeneration associated Cntn1 (F3/F11/Contactin) gene is duplicated in fish: expression during development and retinal axon regeneration. Molecular and Cellular Neuroscience *28*, 361-374.

Hao, Y., Frey, E., Yoon, C., Wong, H., Nestorovski, D., Holzman, L.B., Giger, R.J., DiAntonio, A., and Collins, C. (2016). An evolutionarily conserved mechanism for cAMP elicited axonal regeneration involves direct activation of the dual leucine zipper kinase DLK. Elife *5*, e14048.

He, Y., Lu, X., Qian, F., Liu, D., Chai, R., and Li, H. (2017). Insm1a is required for zebrafish posterior lateral line development. Frontiers in molecular neuroscience *10*, 241.

Henninger, N., Bouley, J., Sikoglu, E.M., An, J., Moore, C.M., King, J.A., Bowser, R., Freeman, M.R., and Brown Jr, R.H. (2016). Attenuated traumatic axonal injury and improved functional outcome after traumatic brain injury in mice lacking Sarm1. Brain *139*, 1094-1105.

Hernandez, G., Thornton, C., Stotland, A., Lui, D., Sin, J., Ramil, J., Magee, N., Andres, A., Quarato, G., and Carreira, R.S. (2013). MitoTimer: a novel tool for monitoring mitochondrial turnover. Autophagy *9*, 1852-1861.

Hewamadduma, C.A., Grierson, A.J., Ma, T.P., Pan, L., Moens, C.B., Ingham, P.W., Ramesh, T., and Shaw, P.J. (2013). Tardbpl splicing rescues motor neuron and axonal development in a mutant tardbp zebrafish. Human molecular genetics *22*, 2376-2386.

Higashijima, S.I., Mandel, G., and Fetcho, J.R. (2004). Distribution of prospective glutamatergic, glycinergic, and GABAergic neurons in embryonic and larval zebrafish. Journal of Comparative Neurology *480*, 1-18.

Hoffman, E.J., Turner, K.J., Fernandez, J.M., Cifuentes, D., Ghosh, M., Ijaz, S., Jain, R.A., Kubo, F., Bill, B.R., and Baier, H. (2016). Estrogens suppress a behavioral phenotype in zebrafish mutants of the autism risk gene, CNTNAP2. Neuron *89*, 725-733.

Holloway, M.P., DeNardo, B.D., Phornphutkul, C., Nguyen, K., Davis, C., Jackson, C., Richendrfer, H., Creton, R., and Altura, R.A. (2016). An asymptomatic mutation complicating severe chemotherapy-induced peripheral neuropathy (CIPN): a case for personalised medicine and a zebrafish model of CIPN. NPJ genomic medicine *1*, 16016.

Howe, K., Clark, M.D., Torroja, C.F., Torrance, J., Berthelot, C., Muffato, M., Collins, J.E., Humphray, S., McLaren, K., and Matthews, L. (2013). The zebrafish reference genome sequence and its relationship to the human genome. Nature *496*, 498.

Hsu, C.-H., Wen, Z.-H., Lin, C.-S., and Chakraborty, C. (2007). The zebrafish model: use in studying cellular mechanisms for a spectrum of clinical disease entities. Current neurovascular research *4*, 111-120.

Hwang, W.Y., Fu, Y., Reyon, D., Maeder, M.L., Tsai, S.Q., Sander, J.D., Peterson, R.T., Yeh, J.J., and Joung, J.K. (2013). Efficient genome editing in zebrafish using a CRISPR-Cas system. Nature biotechnology *31*, 227.

Ide, C. (1996). Peripheral nerve regeneration. Neuroscience research *25*, 101-121.

Imai, S., Koyanagi, M., Azimi, Z., Nakazato, Y., Matsumoto, M., Ogihara, T., Yonezawa, A., Omura, T., Nakagawa, S., and Wakatsuki, S. (2017). Taxanes and platinum derivatives impair Schwann cells via distinct mechanisms. Scientific reports *7*, 5947.

Jessen, K., Mirsky, R., and Lloyd, A. (2015). Schwann cells: development and role in nerve repair. Cold Spring Harb Perspect Biol 7: a020487.

Jessen, K.R., and Mirsky, R. (2005). The origin and development of glial cells in peripheral nerves. Nature Reviews Neuroscience *6*, 671.

Johnson, G.V., Greenwood, J.A., Costello, A.C., and Troncoso, J.C. (1991). The regulatory role of calmodulin in the proteolysis of individual neurofilament proteins by calpain. Neurochemical research *16*, 869-873.

Johnstone, T.C., Park, G.Y., and Lippard, S.J. (2014). Understanding and improving platinum anticancer drugs–phenanthriplatin. Anticancer research *34*, 471-476.

Jordan, M.A., and Wilson, L. (2004). Microtubules as a target for anticancer drugs. Nature Reviews Cancer *4*, 253.

Jortner, B.S. (2000). Mechanisms of toxic injury in the peripheral nervous system: neuropathologic considerations. Toxicologic pathology *28*, 54-69.

Jung Kim, M., Ho Kang, K., Kim, C.-H., and Choi, S.-Y. (2008). Real-time imaging of mitochondria in transgenic zebrafish expressing mitochondrially targeted GFP. Biotechniques *45*, 331-334.

Kaslin, J., Nystedt, J.M., Östergård, M., Peitsaro, N., and Panula, P. (2004). The orexin/hypocretin system in zebrafish is connected to the aminergic and cholinergic systems. Journal of Neuroscience *24*, 2678-2689.

Kautio, A.-L., Haanpää, M., Kautiainen, H., Kalso, E., and Saarto, T. (2011). Burden of chemotherapy-induced neuropathy—a cross-sectional study. Supportive Care in Cancer *19*, 1991-1996.

Kawai, H., Arata, N., and Nakayasu, H. (2001). Three‐dimensional distribution of astrocytes in zebrafish spinal cord. Glia *36*, 406-413.

Kawakami, K. (2007). Tol2: a versatile gene transfer vector in vertebrates. Genome biology *8*, S7.

Kim, Y., Zhou, P., Qian, L., Chuang, J.-Z., Lee, J., Li, C., Iadecola, C., Nathan, C., and Ding, A. (2007). MyD88-5 links mitochondria, microtubules, and JNK3 in neurons and regulates neuronal survival. Journal of Experimental Medicine *204*, 2063-2074.

Kimmel, C.B. (1993). Patterning the brain of the zebrafish embryo. Annual review of neuroscience *16*, 707-732.

Knöferle, J., Koch, J.C., Ostendorf, T., Michel, U., Planchamp, V., Vutova, P., Tönges, L., Stadelmann, C., Brück, W., and Bähr, M. (2010). Mechanisms of acute axonal degeneration in the optic nerve in vivo. Proceedings of the National Academy of Sciences *107*, 6064-6069.

Koeppen, A.H. (2004). Wallerian degeneration: history and clinical significance. Journal of the neurological sciences *220*, 115-117.

Kosmaczewski, S.G., Han, S.M., Han, B., Meyer, B.I., Baig, H.S., Athar, W., Lin-Moore, A.T., Koelle, M.R., and Hammarlund, M. (2015). RNA ligation in neurons by RtcB inhibits axon regeneration. Proceedings of the National Academy of Sciences *112*, 8451-8456.

Kozol, R.A., Abrams, A.J., James, D.M., Buglo, E., Yan, Q., and Dallman, J.E. (2016). Function over form: modeling groups of inherited neurological conditions in zebrafish. Frontiers in molecular neuroscience *9*, 55.

Krarup-Hansen, A., Helweg-Larsen, S., Schmalbruch, H., Rørth, M., and Krarup, C. (2007). Neuronal involvement in cisplatin neuropathy: prospective clinical and neurophysiological studies. Brain *130*, 1076-1088.

Krivosheya, D., Tapia, L., Levinson, J.N., Huang, K., Kang, Y., Hines, R., Ting, A.K., Craig, A.M., Mei, L., and Bamji, S.X. (2008). ErbB4-neuregulin signaling modulates synapse development and dendritic arborization through distinct mechanisms. Journal of Biological Chemistry *283*, 32944-32956.

Kuan, C.-Y., Whitmarsh, A.J., Yang, D.D., Liao, G., Schloemer, A.J., Dong, C., Bao, J., Banasiak, K.J., Haddad, G.G., and Flavell, R.A. (2003). A critical role of neural-specific JNK3 for ischemic apoptosis. Proceedings of the National Academy of Sciences *100*, 15184-15189.

Kwan, K.M., Fujimoto, E., Grabher, C., Mangum, B.D., Hardy, M.E., Campbell, D.S., Parant, J.M., Yost, H.J., Kanki, J.P., and Chien, C.B. (2007). The Tol2kit: a multisite gateway ‐ based construction kit for Tol2 transposon transgenesis constructs. Developmental dynamics: an official publication of the American Association of Anatomists *236*, 3088-3099.

Lam, C.S., Korzh, V., and Strahle, U. (2005). Zebrafish embryos are susceptible to the dopaminergic neurotoxin MPTP. European Journal of Neuroscience *21*, 1758-1762.

Landrum, M.J., Lee, J.M., Riley, G.R., Jang, W., Rubinstein, W.S., Church, D.M., and Maglott, D.R. (2013). ClinVar: public archive of relationships among sequence variation and human phenotype. Nucleic acids research *42*, D980-D985.

Lecaudey, V., Cakan-Akdogan, G., Norton, W.H., and Gilmour, D. (2008). Dynamic Fgf signaling couples morphogenesis and migration in the zebrafish lateral line primordium. Development *135*, 2695-2705.

Li, M., Zhao, L., Page-McCaw, P.S., and Chen, W. (2016). Zebrafish genome engineering using the CRISPR–Cas9 system. Trends in Genetics *32*, 815-827.

Lin, M.-Y., Cheng, X.-T., Tammineni, P., Xie, Y., Zhou, B., Cai, Q., and Sheng, Z.-H. (2017). Releasing syntaphilin removes stressed mitochondria from axons independent of mitophagy under pathophysiological conditions. Neuron *94*, 595-610. e596.

Lisse, T.S., Middleton, L.J., Pellegrini, A.D., Martin, P.B., Spaulding, E.L., Lopes, O., Brochu, E.A., Carter, E.V., Waldron, A., and Rieger, S. (2016). Paclitaxel-induced epithelial damage and ectopic MMP-13 expression promotes neurotoxicity in zebrafish. Proceedings of the National Academy of Sciences *113*, E2189-E2198.

Liu, K., Lu, Y., Lee, J.K., Samara, R., Willenberg, R., Sears-Kraxberger, I., Tedeschi, A., Park, K.K., Jin, D., and Cai, B. (2010). PTEN deletion enhances the regenerative ability of adult corticospinal neurons. Nature neuroscience *13*, 1075.

López-Schier, H., and Hudspeth, A. (2005). Supernumerary neuromasts in the posterior lateral line of zebrafish lacking peripheral glia. Proceedings of the National Academy of Sciences *102*, 1496-1501.

Lopez-Schier, H., and Pujol-Martí, J. (2013). Developmental and architectural principles of the lateral-line neural map. Frontiers in neural circuits *7*, 47.

López-Schier, H., Starr, C.J., Kappler, J.A., Kollmar, R., and Hudspeth, A. (2004). Directional cell migration establishes the axes of planar polarity in the posterior lateral-line organ of the zebrafish. Developmental cell *7*, 401-412.

Loreto, A., Di Stefano, M., Gering, M., and Conforti, L. (2015). Wallerian degeneration is executed by an NMN-SARM1-dependent late Ca2+ influx but only modestly influenced by mitochondria. Cell reports *13*, 2539-2552.

Lovett-Barron, M., Andalman, A.S., Allen, W.E., Vesuna, S., Kauvar, I., Burns, V.M., and Deisseroth, K. (2017). Ancestral circuits for the coordinated modulation of brain state. Cell *171*, 1411-1423. e1417.

Luo, X., and Park, K.K. (2012). Neuron-intrinsic inhibitors of axon regeneration: PTEN and SOCS3. In International review of neurobiology (Elsevier), pp. 141-173.

Lutz, A.B., and Barres, B.A. (2014). Contrasting the glial response to axon injury in the central and peripheral nervous systems. Developmental cell *28*, 7-17.

Lyons, D.A., Pogoda, H.-M., Voas, M.G., Woods, I.G., Diamond, B., Nix, R., Arana, N., Jacobs, J., and Talbot, W.S. (2005). erbb3 and erbb2 are essential for schwann cell migration and myelination in zebrafish. Current Biology *15*, 513-524.

Lyons, D.A., and Talbot, W.S. (2015). Glial cell development and function in zebrafish. Cold Spring Harbor perspectives in biology *7*, a020586.

Ma, Y., Adjemian, S., Yang, H., Catani, J.P.P., Hannani, D., Martins, I., Michaud, M., Kepp, O., Sukkurwala, A.Q., and Vacchelli, E. (2013). ATP-dependent recruitment, survival and differentiation of dendritic cell precursors in the tumor bed after anticancer chemotherapy. Oncoimmunology *2*, e24568.

Mahar, M., and Cavalli, V. (2018). Intrinsic mechanisms of neuronal axon regeneration. Nature Reviews Neuroscience, 1.

Malapati, H., Millen, S.M., and Buchser, W.J. (2017). The axon degeneration gene SARM1 is evolutionarily distinct from other TIR domain-containing proteins. Molecular genetics and genomics *292*, 909-922.

Mandal, A., Pinter, K., and Drerup, C. (2018). Analyzing neuronal mitochondria in vivo using fluorescent reporters in zebrafish. Frontiers in cell and developmental biology *6*, 144.

Marin-Valencia, I., Novarino, G., Johansen, A., Rosti, B., Issa, M.Y., Musaev, D., Bhat, G., Scott, E., Silhavy, J.L., and Stanley, V. (2018). A homozygous founder mutation in TRAPPC6B associates with a neurodevelopmental disorder characterised by microcephaly, epilepsy and autistic features. Journal of medical genetics *55*, 48-54.

Martin, S.M., O'Brien, G.S., Portera-Cailliau, C., and Sagasti, A. (2010). Wallerian degeneration of zebrafish trigeminal axons in the skin is required for regeneration and developmental pruning. Development *137*, 3985-3994.

Martini, R., Fischer, S., López‐Vales, R., and David, S. (2008). Interactions between Schwann cells and macrophages in injury and inherited demyelinating disease. Glia *56*, 1566-1577.

Massoll, C., Mando, W., and Chintala, S.K. (2013). Excitotoxicity upregulates SARM1 protein expression and promotes Wallerian-like degeneration of retinal ganglion cells and their axons. Investigative ophthalmology & visual science *54*, 2771-2780.

Mathur, P., and Guo, S. (2010). Use of zebrafish as a model to understand mechanisms of addiction and complex neurobehavioral phenotypes. Neurobiology of disease *40*, 66-72.

Maurel, P., Einheber, S., Galinska, J., Thaker, P., Lam, I., Rubin, M.B., Scherer, S.S., Murakami, Y., Gutmann, D.H., and Salzer, J.L. (2007). Nectin-like proteins mediate axon–Schwann cell interactions along the internode and are essential for myelination. J Cell Biol *178*, 861-874.

McDonald, E.S., and Windebank, A.J. (2002). Cisplatin-Induced apoptosis of DRG neurons involves Bax redistribution and cytochrome cRelease but not fas receptor signaling. Neurobiology of disease *9*, 220-233.

McKee, A.C., and Daneshvar, D.H. (2015). The neuropathology of traumatic brain injury. In Handbook of clinical neurology (Elsevier), pp. 45-66.

McKinley, E.T., Baranowski, T.C., Blavo, D.O., Cato, C., Doan, T.N., and Rubinstein, A.L. (2005). Neuroprotection of MPTP-induced toxicity in zebrafish dopaminergic neurons. Molecular Brain Research *141*, 128-137.

Metcalfe, W.K., Kimmel, C.B., and Schabtach, E. (1985). Anatomy of the posterior lateral line system in young larvae of the zebrafish. Journal of Comparative Neurology *233*, 377-389.

Miller, J.C., Tan, S., Qiao, G., Barlow, K.A., Wang, J., Xia, D.F., Meng, X., Paschon, D.E., Leung, E., and Hinkley, S.J. (2011). A TALE nuclease architecture for efficient genome editing. Nature biotechnology *29*, 143.

Miller, V.M., Nelson, R.F., Gouvion, C.M., Williams, A., Rodriguez-Lebron, E., Harper, S.Q., Davidson, B.L., Rebagliati, M.R., and Paulson, H.L. (2005). CHIP suppresses polyglutamine aggregation and toxicity in vitro and in vivo. Journal of Neuroscience *25*, 9152-9161.

Mink, M., Fogelgren, B., Olszewski, K., Maroy, P., and Csiszar, K. (2001). A novel human gene (SARM) at chromosome 17q11 encodes a protein with a SAM motif and structural similarity to Armadillo/β-catenin that is conserved in mouse, Drosophila, and Caenorhabditis elegans. Genomics *74*, 234-244.

Moehle, E.A., Rock, J.M., Lee, Y.-L., Jouvenot, Y., DeKelver, R.C., Gregory, P.D., Urnov, F.D., and Holmes, M.C. (2007). Targeted gene addition into a specified location in the human genome using designed zinc finger nucleases. Proceedings of the National Academy of Sciences *104*, 3055-3060.

Mogha, A., Benesh, A.E., Patra, C., Engel, F.B., Schöneberg, T., Liebscher, I., and Monk, K.R. (2013). Gpr126 functions in Schwann cells to control differentiation and myelination via G-protein activation. Journal of Neuroscience *33*, 17976-17985.

Mols, F., van de Poll-Franse, L.V., Vreugdenhil, G., Beijers, A.J., Kieffer, J.M., Aaronson, N.K., and Husson, O. (2016). Reference data of the European Organisation for Research and Treatment of Cancer (EORTC) QLQ-CIPN20 Questionnaire in the general Dutch population. European Journal of Cancer *69*, 28-38.

Monk, K.R., Feltri, M.L., and Taveggia, C. (2015). New insights on Schwann cell development. Glia *63*, 1376-1393.

Morell, P., and Toews, A.D. (1996). Schwann cells as targets for neurotoxicants. Neurotoxicology *17*, 685-695.

Mukherjee, P., Winkler, C.W., Taylor, K.G., Woods, T.A., Nair, V., Khan, B.A., and Peterson, K.E. (2015). SARM1, not MyD88, mediates TLR7/TLR9-induced apoptosis in neurons. The Journal of Immunology *195*, 4913-4921.

Mukherjee, P., Woods, T.A., Moore, R.A., and Peterson, K.E. (2013). Activation of the innate signaling molecule MAVS by bunyavirus infection upregulates the adaptor protein SARM1, leading to neuronal death. Immunity *38*, 705-716.

Münzel, E.J., Schaefer, K., Obirei, B., Kremmer, E., Burton, E.A., Kuscha, V., Becker, C.G., Brösamle, C., Williams, A., and Becker, T. (2012). Claudin k is specifically expressed in cells that form myelin during development of the nervous system and regeneration of the optic nerve in adult zebrafish. Glia *60*, 253-270.

Murata, H., Khine, C.C., Nishikawa, A., Yamamoto, K.-i., Kinoshita, R., and Sakaguchi, M. (2018). c-Jun N-terminal kinase (JNK)-mediated phosphorylation of SARM1 regulates NAD+ cleavage activity to inhibit mitochondrial respiration. Journal of Biological Chemistry *293*, 18933-18943.

Murata, H., Sakaguchi, M., Kataoka, K., and Huh, N.-h. (2013). SARM1 and TRAF6 bind to and stabilize PINK1 on depolarized mitochondria. Molecular biology of the cell *24*, 2772-2784.

Muto, A., Ohkura, M., Abe, G., Nakai, J., and Kawakami, K. (2013). Real-time visualization of neuronal activity during perception. Current Biology *23*, 307-311.

Nave, K.-A., and Salzer, J.L. (2006). Axonal regulation of myelination by neuregulin 1. Current opinion in neurobiology *16*, 492-500.

Nechiporuk, A., and Raible, D.W. (2008). FGF-dependent mechanosensory organ patterning in zebrafish. Science *320*, 1774-1777.

Neumann, B., Coakley, S., Giordano-Santini, R., Linton, C., Lee, E.S., Nakagawa, A., Xue, D., and Hilliard, M.A. (2015). EFF-1-mediated regenerative axonal fusion requires components of the apoptotic pathway. Nature *517*, 219.

Norrmén, C., Figlia, G., Pfistner, P., Pereira, J.A., Bachofner, S., and Suter, U. (2018). mTORC1 is transiently reactivated in injured nerves to promote c-Jun elevation and Schwann cell dedifferentiation. Journal of Neuroscience *38*, 4811-4828.

Norsworthy, M.W., Bei, F., Kawaguchi, R., Wang, Q., Tran, N.M., Li, Y., Brommer, B., Zhang, Y., Wang, C., and Sanes, J.R. (2017). Sox11 expression promotes regeneration of some retinal ganglion cell types but kills others. Neuron *94*, 1112-1120. e1114.

O'Donnell, K.C., Vargas, M.E., and Sagasti, A. (2013). WldS and PGC-1α regulate mitochondrial transport and oxidation state after axonal injury. Journal of Neuroscience *33*, 14778-14790.

Osterloh, J.M., Yang, J., Rooney, T.M., Fox, A.N., Adalbert, R., Powell, E.H., Sheehan, A.E., Avery, M.A., Hackett, R., and Logan, M.A. (2012). dSarm/Sarm1 is required for activation of an injury-induced axon death pathway. Science *337*, 481-484.

Ota, S., Hisano, Y., Ikawa, Y., and Kawahara, A. (2014). Multiple genome modifications by the CRISPR/Cas9 system in zebrafish. Genes to Cells *19*, 555-564.

Oteiza, P., Odstrcil, I., Lauder, G., Portugues, R., and Engert, F. (2017). A novel mechanism for mechanosensory-based rheotaxis in larval zebrafish. Nature *547*, 445.

Ozaki, T., Yamashita, T., and Ishiguro, S.-i. (2009). Mitochondrial m-calpain plays a role in the release of truncated apoptosis-inducing factor from the mitochondria. Biochimica et Biophysica Acta (BBA)-Molecular Cell Research *1793*, 1848-1859.

Paavola, K.J., Sidik, H., Zuchero, J.B., Eckart, M., and Talbot, W.S. (2014). Type IV collagen is an activating ligand for the adhesion G protein–coupled receptor GPR126. Sci Signal *7*, ra76-ra76.

Pan, Z.-G., and An, X.-S. (2018). SARM1 deletion restrains NAFLD induced by high fat diet (HFD) through reducing inflammation, oxidative stress and lipid accumulation. Biochemical and biophysical research communications *498*, 416-423.

Park, J.Y., Jang, S.Y., Shin, Y.K., Suh, D.J., and Park, H.T. (2013a). Calcium-dependent proteasome activation is required for axonal neurofilament degradation. Neural regeneration research *8*, 3401.

Park, K.K., Liu, K., Hu, Y., Smith, P.D., Wang, C., Cai, B., Xu, B., Connolly, L., Kramvis, I., and Sahin, M. (2008). Promoting axon regeneration in the adult CNS by modulation of the PTEN/mTOR pathway. Science *322*, 963-966.

Park, S.B., Goldstein, D., Krishnan, A.V., Lin, C.S.Y., Friedlander, M.L., Cassidy, J., Koltzenburg, M., and Kiernan, M.C. (2013b). Chemotherapy‐induced peripheral neurotoxicity: a critical analysis. CA: a cancer journal for clinicians *63*, 419-437.

Parrinello, S., Napoli, I., Ribeiro, S., Digby, P.W., Fedorova, M., Parkinson, D.B., Doddrell, R.D., Nakayama, M., Adams, R.H., and Lloyd, A.C. (2010). EphB signaling directs peripheral nerve regeneration through Sox2-dependent Schwann cell sorting. Cell *143*, 145-155.

Patot, S., Imbert, P.R., Baude, J., Simões, P.M., Campergue, J.-B., Louche, A., Nijland, R., Bès, M., Tristan, A., and Laurent, F. (2017). The TIR homologue lies near resistance genes in Staphylococcus aureus, coupling modulation of virulence and antimicrobial susceptibility. PLoS pathogens *13*, e1006092.

Pereira, J.A., Lebrun-Julien, F., and Suter, U. (2012). Molecular mechanisms regulating myelination in the peripheral nervous system. Trends in neurosciences *35*, 123-134.

Pérez-Cadahía, B., Drobic, B., Espino, P.S., He, S., Mandal, S., Healy, S., and Davie, J.R. (2011). Role of MSK1 in the malignant phenotype of Ras-transformed mouse fibroblasts. Journal of Biological Chemistry *286*, 42-49.

Perlson, E., Hanz, S., Ben-Yaakov, K., Segal-Ruder, Y., Seger, R., and Fainzilber, M. (2005). Vimentin-dependent spatial translocation of an activated MAP kinase in injured nerve. Neuron *45*, 715-726.

Petersen, S.C., Luo, R., Liebscher, I., Giera, S., Jeong, S.-J., Mogha, A., Ghidinelli, M., Feltri, M.L., Schöneberg, T., and Piao, X. (2015). The adhesion GPCR GPR126 has distinct, domain-dependent functions in Schwann cell development mediated by interaction with laminin-211. Neuron *85*, 755-769.

Piirsoo, M., Kaljas, A., Tamm, K., and Timmusk, T. (2010). Expression of NGF and GDNF family members and their receptors during peripheral nerve development and differentiation of Schwann cells in vitro. Neuroscience letters *469*, 135-140.

Poruchynsky, M.S., Sackett, D.L., Robey, R.W., Ward, Y., Annunziata, C., and Fojo, T. (2008). Proteasome inhibitors increase tubulin polymerization and stabilization in tissue culture cells: a possible mechanism contributing to peripheral neuropathy and cellular toxicity following proteasome inhibition. Cell Cycle *7*, 940-949.

Postma, T., Benard, B., Huijgens, P., Ossenkoppele, G., and Heimans, J. (1993). Long term effects of vincristine on the peripheral nervous system. Journal of neuro-oncology *15*, 23-27.

Prober, D.A., Rihel, J., Onah, A.A., Sung, R.-J., and Schier, A.F. (2006). Hypocretin/orexin overexpression induces an insomnia-like phenotype in zebrafish. Journal of Neuroscience *26*, 13400-13410.

Procacci, P., Ballabio, M., Castelnovo, L.F., Mantovani, C.M., and Magnaghi, V. (2013). GABA-B receptors in the PNS have a role in Schwann cells differentiation? Frontiers in cellular neuroscience *6*, 68.

Pudla, M., Limposuwan, K., and Utaisincharoen, P. (2011). Burkholderia pseudomallei-induced expression of a negative regulator, sterile-α and Armadillo motif-containing protein, in mouse macrophages: a possible mechanism for suppression of the MYD88-independent pathway. Infection and immunity *79*, 2921-2927.

Pujol-Martí, J., and López-Schier, H. (2013). Developmental and architectural principles of the lateral-line neural map. Front. Neural Circuits 7:47.

Pujol-Martí, J., Faucherre, A., Aziz-Bose, R., Asgharsharghi, A., Colombelli, J., Trapani, J.G., and López-Schier, H. (2014). Converging axons collectively initiate and maintain synaptic selectivity in a constantly remodeling sensory organ. Current Biology *24*, 2968-2974.

Puttagunta, R., Tedeschi, A., Sória, M.G., Hervera, A., Lindner, R., Rathore, K.I., Gaub, P., Joshi, Y., Nguyen, T., and Schmandke, A. (2014). PCAF-dependent epigenetic changes promote axonal regeneration in the central nervous system. Nature communications *5*, 3527.

Raphael, A.R., and Talbot, W.S. (2011). New insights into signaling during myelination in zebrafish. In Current topics in developmental biology (Elsevier), pp. 1-19.

Rishal, I., and Fainzilber, M. (2014). Axon–soma communication in neuronal injury. Nature Reviews Neuroscience *15*, 32.

Rosenberg, A.F., Isaacman-Beck, J., Franzini-Armstrong, C., and Granato, M. (2014). Schwann cells and deleted in colorectal carcinoma direct regenerating motor axons towards their original path. Journal of Neuroscience *34*, 14668-14681.

Rotshenker, S. (2011). Wallerian degeneration: the innate-immune response to traumatic nerve injury. Journal of neuroinflammation *8*, 109.

Sahenk, Z., Barohn, R., New, P., and Mendell, J.R. (1994). Taxol neuropathy: electrodiagnostic and sural nerve biopsy findings. Archives of neurology *51*, 726-729.

Sahenk, Z., Oblinger, J., and Edwards, C. (2008). Neurotrophin-3 deficient Schwann cells impair nerve regeneration. Experimental neurology *212*, 552-556.

Sakowski, S.A., Lunn, J.S., Busta, A.S., Oh, S.S., Zamora-Berridi, G., Palmer, M., Rosenberg, A.A., Philip, S.G., Dowling, J.J., and Feldman, E.L. (2012). Neuromuscular effects of G93A-SOD1 expression in zebrafish. Molecular neurodegeneration *7*, 44.

Salzer, J.L. (2015). Schwann cell myelination. Cold Spring Harbor perspectives in biology *7*, a020529.

Sander, J.D., Cade, L., Khayter, C., Reyon, D., Peterson, R.T., Joung, J.K., and Yeh, J.-R.J. (2011). Targeted gene disruption in somatic zebrafish cells using engineered TALENs. Nature biotechnology *29*, 697.

Sasaki, Y., Hackett, A.R., Kim, S., Strickland, A., and Milbrandt, J. (2018). Dysregulation of NAD+ metabolism induces a Schwann cell dedifferentiation program. Journal of Neuroscience *38*, 6546-6562.

Sasaki, Y., Vohra, B.P., Baloh, R.H., and Milbrandt, J. (2009). Transgenic mice expressing the Nmnat1 protein manifest robust delay in axonal degeneration in vivo. Journal of Neuroscience *29*, 6526-6534.

Schiffer, N.W., Broadley, S.A., Hirschberger, T., Tavan, P., Kretzschmar, H.A., Giese, A., Haass, C., Hartl, F.U., and Schmid, B. (2007). Identification of anti-prion compounds as efficient inhibitors of polyglutamine protein aggregation in a zebrafish model. Journal of Biological Chemistry *282*, 9195-9203.

Schoonheim, P.J., Arrenberg, A.B., Del Bene, F., and Baier, H. (2010). Optogenetic localization and genetic perturbation of saccade-generating neurons in zebrafish. Journal of Neuroscience *30*, 7111-7120.

Schubert, J., Siekierska, A., Langlois, M., May, P., Huneau, C., Becker, F., Muhle, H., Suls, A., Lemke, J.R., and De Kovel, C.G. (2014). Mutations in STX1B, encoding a presynaptic protein, cause fever-associated epilepsy syndromes. Nature genetics *46*, 1327.

Schuster, K., Dambly-Chaudière, C., and Ghysen, A. (2010). Glial cell line-derived neurotrophic factor defines the path of developing and regenerating axons in the lateral line system of zebrafish. Proceedings of the National Academy of Sciences *107*, 19531-19536.

Schwab, M.E., and Strittmatter, S.M. (2014). Nogo limits neural plasticity and recovery from injury. Current opinion in neurobiology *27*, 53-60.

Schweitzer, J., Becker, T., Becker, C.G., and Schachner, M. (2003). Expression of protein zero is increased in lesioned axon pathways in the central nervous system of adult zebrafish. Glia *41*, 301-317.

Schweitzer, J., Gimnopoulos, D., Lieberoth, B.C., Pogoda, H.-M., Feldner, J., Ebert, A., Schachner, M., Becker, T., and Becker, C.G. (2007). Contactin1a expression is associated with oligodendrocyte differentiation and axonal regeneration in the central nervous system of zebrafish. Molecular and Cellular Neuroscience *35*, 194-207.

Seijffers, R., Mills, C.D., and Woolf, C.J. (2007). ATF3 increases the intrinsic growth state of DRG neurons to enhance peripheral nerve regeneration. Journal of Neuroscience *27*, 7911-7920.

Selvaraj, B.T., Frank, N., Bender, F.L., Asan, E., and Sendtner, M. (2012). Local axonal function of STAT3 rescues axon degeneration in the pmn model of motoneuron disease. J Cell Biol *199*, 437-451.

Seretny, M., Currie, G.L., Sena, E.S., Ramnarine, S., Grant, R., MacLeod, M.R., Colvin, L.A., and Fallon, M. (2014). Incidence, prevalence, and predictors of chemotherapy-induced peripheral neuropathy: a systematic review and meta-analysis. PAIN® *155*, 2461-2470.

Shin, J.E., Cho, Y., Beirowski, B., Milbrandt, J., Cavalli, V., and DiAntonio, A. (2012). Dual leucine zipper kinase is required for retrograde injury signaling and axonal regeneration. Neuron *74*, 1015-1022.

Simon, D.J., and Watkins, T.A. (2018). Therapeutic opportunities and pitfalls in the treatment of axon degeneration. Current opinion in neurology *31*, 693-701.

Song, Y., Sretavan, D., Salegio, E.A., Berg, J., Huang, X., Cheng, T., Xiong, X., Meltzer, S., Han, C., and Nguyen, T.-T. (2015). Regulation of axon regeneration by the RNA repair and splicing pathway. Nature neuroscience *18*, 817.

Soto, J., and Monje, P.V. (2017). Axon contact‐driven Schwann cell dedifferentiation. Glia *65*, 864-882.

Starobova, H., and Vetter, I. (2017). Pathophysiology of chemotherapy-induced peripheral neuropathy. Frontiers in molecular neuroscience *10*, 174.

Stern, S., Haverkamp, S., Sinske, D., Tedeschi, A., Naumann, U., Di Giovanni, S., Kochanek, S., Nordheim, A., and Knöll, B. (2013). The transcription factor serum response factor stimulates axon regeneration through cytoplasmic localization and cofilin interaction. Journal of Neuroscience *33*, 18836-18848.

Stewart, W.J., Cardenas, G.S., and McHenry, M.J. (2013). Zebrafish larvae evade predators by sensing water flow. Journal of Experimental Biology *216*, 388-398.

Streisinger, G., Coale, F., Taggart, C., Walker, C., and Grunwald, D.J. (1989). Clonal origins of cells in the pigmented retina of the zebrafish eye. Developmental biology *131*, 60-69.

Streisinger, G., Walker, C., Dower, N., Knauber, D., and Singer, F. (1981). Production of clones of homozygous diploid zebra fish (Brachydanio rerio). Nature *291*, 293.

Strumberg, D., Brügge, S., Korn, M., Koeppen, S., Ranft, J., Scheiber, G., Reiners, C., Möckel, C., Seeber, S., and Scheulen, M. (2002). Evaluation of long-term toxicity in patients after cisplatin-based chemotherapy for non-seminomatous testicular cancer. Annals of oncology *13*, 229-236.

Suchánková, T., Kubíček, K., Kašpárková, J., Brabec, V., and Kozelka, J. (2012). Platinum–DNA interstrand crosslinks: Molecular determinants of bending and unwinding of the double helix. Journal of inorganic biochemistry *108*, 69-79.

Summers, D.W., DiAntonio, A., and Milbrandt, J. (2014). Mitochondrial dysfunction induces Sarm1-dependent cell death in sensory neurons. Journal of Neuroscience *34*, 9338-9350.

Suster, M.L., Kikuta, H., Urasaki, A., Asakawa, K., and Kawakami, K. (2009). Transgenesis in zebrafish with the tol2 transposon system. In Transgenesis techniques (Springer), pp. 41-63.

Sztal, T.E., Ruparelia, A.A., Williams, C., and Bryson-Richardson, R.J. (2016). Using touch-evoked response and locomotion assays to assess muscle performance and function in zebrafish. JoVE (Journal of Visualized Experiments), e54431.

Tomasiewicz, H.G., Flaherty, D.B., Soria, J., and Wood, J.G. (2002). Transgenic zebrafish model of neurodegeneration. Journal of neuroscience research *70*, 734-745.

Tian, W., Asgharsharghi, A., Valera, G., Czopka, T., Haehnel-Taguchi, M., López-Schier, H. (2018). Systemic loss of Sarm1 is glioprotective after neurotrauma. bioRxiv 493163; doi: https://doi.org/10.1101/493163.

Tian, W., Czopka, T. & López-Schier, H. (2020). Systemic loss of Sarm1 protects Schwann cells from chemotoxicity by delaying axon degeneration. Commun Biol 3, 49.

Trimarco, A., Forese, M.G., Alfieri, V., Lucente, A., Brambilla, P., Dina, G., Pieragostino, D., Sacchetta, P., Urade, Y., and Boizet-Bonhoure, B. (2014). Prostaglandin D2 synthase/GPR44: a signaling axis in PNS myelination. Nature neuroscience *17*, 1682.

Turkiew, E., Falconer, D., Reed, N., and Höke, A. (2017). Deletion of Sarm1 gene is neuroprotective in two models of peripheral neuropathy. Journal of the Peripheral Nervous System *22*, 162-171.

Urnov, F.D., Miller, J.C., Lee, Y.-L., Beausejour, C.M., Rock, J.M., Augustus, S., Jamieson, A.C., Porteus, M.H., Gregory, P.D., and Holmes, M.C. (2005). Highly efficient endogenous human gene correction using designed zinc-finger nucleases. Nature *435*, 646.

Valentin, G., Haas, P., and Gilmour, D. (2007). The chemokine SDF1a coordinates tissue migration through the spatially restricted activation of Cxcr7 and Cxcr4b. Current Biology *17*, 1026-1031.

Van Hoecke, A., Schoonaert, L., Lemmens, R., Timmers, M., Staats, K.A., Laird, A.S., Peeters, E., Philips, T., Goris, A., and Dubois, B. (2012). EPHA4 is a disease modifier of amyotrophic lateral sclerosis in animal models and in humans. Nature medicine *18*, 1418.

Vargas, M.E., Yamagishi, Y., Tessier-Lavigne, M., and Sagasti, A. (2015). Live imaging of calcium dynamics during axon degeneration reveals two functionally distinct phases of calcium influx. Journal of Neuroscience *35*, 15026-15038.

Varshney, G.K., Pei, W., LaFave, M.C., Idol, J., Xu, L., Gallardo, V., Carrington, B., Bishop, K., Jones, M., and Li, M. (2015). High-throughput gene targeting and phenotyping in zebrafish using CRISPR/Cas9. Genome research *25*, 1030-1042.

Vérièpe, J., Fossouo, L., and Parker, J.A. (2015). Neurodegeneration in C. elegans models of ALS requires TIR-1/Sarm1 immune pathway activation in neurons. Nature communications *6*, 7319.

Verma, N.K., Dourlat, J., Davies, A.M., Long, A., Liu, W.-Q., Garbay, C., Kelleher, D., and Volkov, Y. (2009). STAT3-stathmin interactions control microtubule dynamics in migrating T-cells. Journal of Biological Chemistry *284*, 12349-12362.

Villegas, R., Martin, S.M., O'Donnell, K.C., Carrillo, S.A., Sagasti, A., and Allende, M.L. (2012). Dynamics of degeneration and regeneration in developing zebrafish peripheral axons reveals a requirement for extrinsic cell types. Neural development *7*, 19.

Villegas, R., Martinez, N.W., Lillo, J., Pihan, P., Hernandez, D., and Twiss, J.L. (2014). Calcium release from intra-axonal endoplasmic reticulum leads to axon degeneration through mitochondrial dysfunction. Journal of Neuroscience *34*, 7179-7189.

Wakatsuki, Y., Noda, K., Wada, Y., Toyabe, T., and Matsushige, K. (2011). Molecular doping effect in bottom-gate, bottom-contact pentacene thin-film transistors. Journal of Applied Physics *110*, 054505.

Waller, A.V. (1850). XX. Experiments on the section of the glossopharyngeal and hypoglossal nerves of the frog, and observations of the alterations produced thereby in the structure of their primitive fibres. Philosophical Transactions of the Royal Society of London, 423-429.

Walton, E.M., Cronan, M.R., Beerman, R.W., and Tobin, D.M. (2015). The macrophage-specific promoter mfap4 allows live, long-term analysis of macrophage behavior during mycobacterial infection in zebrafish. PloS one *10*, e0138949.

Wang, J., Zhai, Q., Chen, Y., Lin, E., Gu, W., McBurney, M.W., and He, Z. (2005). A local mechanism mediates NAD-dependent protection of axon degeneration. J Cell Biol *170*, 349-355.

Wang, J.T., Medress, Z.A., and Barres, B.A. (2012). Axon degeneration: molecular mechanisms of a self-destruction pathway. J Cell Biol *196*, 7-18.

Wang, M.-S., Wu, Y., Culver, D.G., and Glass, J.D. (2001). The gene for slow Wallerian degeneration (WldS) is also protective against vincristine neuropathy. Neurobiology of disease *8*, 155-161.

Wang, Q., Zhang, S., Liu, T., Wang, H., Liu, K., Wang, Q., and Zeng, W. (2018). Sarm1/Myd88-5 regulates neuronal intrinsic immune response to traumatic axonal injuries. Cell reports *23*, 716-724.

Weng, Y.-L., Joseph, J., An, R., Song, H., and Ming, G.-l. (2016). Epigenetic regulation of axonal regenerative capacity. Epigenomics *8*, 1429-1442.

Williams, C.H., and Hong, C.C. (2011). Multi-step usage of in vivo models during rational drug design and discovery. International Journal of Molecular Sciences *12*, 2262-2274.

Wong, K.M., Babetto, E., and Beirowski, B. (2017). Axon degeneration: make the Schwann cell great again. Neural regeneration research *12*, 518.

Woodhoo, A., Alonso, M.B.D., Droggiti, A., Turmaine, M., D'antonio, M., Parkinson, D.B., Wilton, D.K., Al-Shawi, R., Simons, P., and Shen, J. (2009). Notch controls embryonic Schwann cell differentiation, postnatal myelination and adult plasticity. Nature neuroscience *12*, 839.

Wright, D.A., Thibodeau-Beganny, S., Sander, J.D., Winfrey, R.J., Hirsh, A.S., Eichtinger, M., Fu, F., Porteus, M.H., Dobbs, D., and Voytas, D.F. (2006). Standardized reagents and protocols for engineering zinc finger nucleases by modular assembly. Nature protocols *1*, 1637.

Wyman, C., and Kanaar, R. (2006). DNA double-strand break repair: all's well that ends well. Annu Rev Genet *40*, 363-383.

Xiao, Y., Faucherre, A., Pola-Morell, L., Heddleston, J.M., Liu, T.-L., Chew, T.-L., Sato, F., Sehara-Fujisawa, A., Kawakami, K., and López-Schier, H. (2015a). High-resolution live imaging reveals axon-glia interactions during peripheral nerve injury and repair in zebrafish. Disease models & mechanisms *8*, 553-564.

Xiao, Y., and López-Schier, H. (2016). Studying Axonal Regeneration by Laser Microsurgery and High-Resolution Videomicroscopy. In Zebrafish (Springer), pp. 271-280.

Xiao, Y., Tian, W., and López-Schier, H. (2015b). Optogenetic stimulation of neuronal repair. Current Biology *25*, R1068-R1069.

Yamamoto, M., Hikosaka, K., Mahmood, A., Tobe, K., Shojaku, H., Inohara, H., and Nakagawa, T. (2016). Nmnat3 is dispensable in mitochondrial NAD level maintenance in vivo. PloS one *11*, e0147037.

Yang, J., Wu, Z., Renier, N., Simon, D.J., Uryu, K., Park, D.S., Greer, P.A., Tournier, C., Davis, R.J., and Tessier-Lavigne, M. (2015a). Pathological axonal death through a MAPK cascade that triggers a local energy deficit. Cell *160*, 161-176.

Yang, Y., Yao, K., Ma, X., Shi, W., Yuan, L., and Yang, Y. (2015b). Variation in Bordetella pertussis susceptibility to erythromycin and virulence-related genotype changes in China (1970-2014). PLoS One *10*, e0138941.

Yang, Z., Fujii, H., Mohan, S.V., Goronzy, J.J., and Weyand, C.M. (2013). Phosphofructokinase deficiency impairs ATP generation, autophagy, and redox balance in rheumatoid arthritis T cells. Journal of Experimental Medicine *210*, 2119-2134.

Yant, S.R., Wu, X., Huang, Y., Garrison, B., Burgess, S.M., and Kay, M.A. (2005). High-resolution genome-wide mapping of transposon integration in mammals. Molecular and cellular biology *25*, 2085-2094.

Yiu, G., and He, Z. (2006). Glial inhibition of CNS axon regeneration. Nature Reviews Neuroscience *7*, 617.

Zhang, J.-c., Yao, W., and Hashimoto, K. (2016). Brain-derived neurotrophic factor (BDNF)-TrkB signaling in inflammation-related depression and potential therapeutic targets. Current neuropharmacology *14*, 721-731.

Zhang, Q., Zmasek, C.M., Cai, X., and Godzik, A. (2011). TIR domain-containing adaptor SARM is a late addition to the ongoing microbe–host dialog. Developmental & Comparative Immunology *35*, 461-468.

Zhang, Z., Huang, J., Shen, Y., and Li, R. (2017). BACE1-Dependent Neuregulin-1 Signaling: An Implication for Schizophrenia. Frontiers in molecular neuroscience *10*, 302.

Zou, H., Ho, C., Wong, K., and Tessier-Lavigne, M. (2009). Axotomy-induced Smad1 activation promotes axonal growth in adult sensory neurons. Journal of Neuroscience *29*, 7116-7123.

7. Acknowledgements

First and foremost, I would like to give the sincere gratitude to my supervisor, Dr. Hernán López-Schier. He gave me the chance to study in neuroscience with zebrafish in his lab. He is full of scientific enthusiasm which influences me in the whole PhD study. His motivation, patience and encouragement support me to finish the PhD project.

I would like to express my gratitude to my co-supervisor Prof. Dr. Barbara Conradt for her valuable guidance and efficient discussion with my project. I am also thankful to my thesis advisory committee Prof. Dr. Michael Kiebler for his valuable advice and comments. They helped me to think critically and to resolve the questions during the project. Thank you very much.

I am sincerely thankful to Prof. Dr. Anja Horn-Bochtler, Prof. Dr. Christof Osman and Prof. Dr. Claude Becker for being my thesis examiners and reviewing my thesis. Thanks also go to Prof. Dr. Leonhardt Heinrich and Prof. Dr. Oliver Behrend for reviewing my thesis. Thanks to your time and dedication.

I would like to thank my collaborators, Dr. Tim Czopka, for sharing the chemogenetic constructs and myelin labeling lines; Dr. Melanie Haehnel-Taguchi, for her help of the electrophysiological tests. I also thanks to their great scientific exchange in this project.

I would like to thank all the staff in the fish facilities. Thanks for taking care of the animals.

I would also like to thank my friends in Helmholtz center and Munich. Thanks to all the friends in my life.

My most sincere thanks go to the wonderful members of the lab: Laura Pola-Morell, for her technical assistance and suggestions for the protocol of experiments; Petra Hammerl, for her kindly help to deal with the non-academic issues; Dr. Chapouton Prisca, for her discussion of some experiments and results and for the comments on my thesis; Yan Xiao, for her help me to involve in the lab fast and for teaching me to do some experiments; Amir Asgharsharghi Bonab, for his help with the behavioral experiments; Dr. Jesús Pujol-Martí,

8. Curriculum Vitae

Personal information

Name: Weili Tian   **Date of birth:** 03-12-1986

Nationality: Chinese   **Gender:** Male

Education

2014.11–present   PhD candidate, Helmholtz center of Munich and University of
Munich

2009.09–2012.07   M.S., Cell biology, Nankai University

2005.09–2009.07   B.S., Biotechnology, Fourth Military Medical University

Working experience

2012.09 – 2014.09   Research assistant, Affiliated Hospital of Guangdong Medical
College

Publications

1. **Tian, W.**, Czopka, T. & López-Schier, H. Systemic loss of Sarm1 protects Schwann cells from chemotoxicity by delaying axon degeneration. Commun Biol 3, 49 (2020)

2. **Weili Tian**, Amir Asgharsharghi, Gema Valera, Tim Czopka, Melanie Haehnel-Taguchi, Hernán López-Schier. Systemic loss of Sarm1 is glioprotective after neurotrauma. bioRxiv 493163; doi: https://doi.org/10.1101/493163 (2018)

3. Xiao Y, **Tian W**, López-Schier H. "Optogenetic stimulation of neuronal repair". Current Biology. 16:25(22): R1068-9, 2015.

4. **Tian W**#, Li W#, Chen Y, Yan Z, et al. "Phosphorylation of ULK1 by AMPK regulates translocation of ULK1 to mitochondria and mitophagy". FEBS Lett. 2015 Jul 8;589(15):1847-54. (# Co-first author)

5. Wu WenXian#, **Tian Weili**#, Zhe Hu, Guo Chen, et al. "ULK1 translocates to mitochondria and phosphorylates FUNDC1 to regulate mitophagy". EMBO Rep. 2014 May; 15(5): 566–575. (# Co-first author)

6. Li W, Zhang X, Zhuang H, Chen HG, Chen Y, **Tian W**, et al. "MicroRNA-137 is a Novel Hypoxia-responsive MicroRNA that Inhibits Mitophagy via Regulation of Two Mitophagy Receptors FUNDC1 and NIX". J Biol Chem. 2014 Apr 11; 289(15): 10691–10701

7. Du L, Rao G, Wang H, Li B, **Tian W**, et al. "CD44-positive cancer stem cells expressing cellular prion protein contribute to metastatic capacity in colorectal cancer". Cancer Res. 2013 Apr 15;73(8):2682-94.

8. Zhao L, He F, Liu H, Zhu Y, **Tian W**, et al. "Natural diterpenoid compound elevates expression of Bim protein, which interacts with antiapoptotic protein Bcl-2, converting it to proapoptotic Bax-like molecule". J Biol Chem. 2012 Jan 6; 287(2): 1054–1065.

9. Wang H, Song P, Du L, **Tian W**, et al. "Parkin ubiquitinates Drp1 for proteasome-dependent degradation: implication of dysregulated mitochondrial dynamics in Parkinson disease". J Biol Chem. 2011 Apr 1;286(13):11649-58.

10. Yushan Zhu, Lixia Zhao, Lei Liu, Ping Gao, **Weili Tian**, et al. "Beclin 1 cleavage by caspase-3 inactivates autophagy and promotes apoptosis". Protein & Cell. 2010 May; 1(5): 468–477.

Eidesstattliche Erklärung

Ich versichere hiermit an Eides statt, dass die vorgelegte Dissertation von mir selbständig und ohne unerlaubte Hilfe angefertigt ist.

München, den .... 18.03.2020 .... Weili Tian ....

<center>(Unterschrift)</center>

Erklärung

Hiermit erkläre ich, *

[X] dass die Dissertation nicht ganz oder in wesentlichen Teilen einer anderen Prüfungskommission vorgelegt worden ist.

[X] dass ich mich anderweitig einer Doktorprüfung ohne Erfolg **nicht** unterzogen habe.

[ ] dass ich mich mit Erfolg der Doktorprüfung im Hauptfach ....

und in den Nebenfächern ....

bei der Fakultät für .... der ....

<center>(Hochschule/Universität)</center>

unterzogen habe.

[ ] dass ich ohne Erfolg versucht habe, eine Dissertation einzureichen oder mich der Doktorprüfung zu unterziehen.

München, den.......... 18. 03. 2020 .... Weili Tian ....

<center>(Unterschrift)</center>